

**ISTANBUL TECHNICAL UNIVERSITY ★ GRADUATE SCHOOL OF SCIENCE**  
**ENGINEERING AND TECHNOLOGY**

**SPECTROSCOPIC, MORPHOLOGIC, AND ELECTROCHEMICAL  
IMPEDANCE CHARACTERIZATIONS OF DNA FUNCTIONALIZED  
SILICA COATED  $\gamma$ -Fe<sub>2</sub>O<sub>3</sub> MAGNETIC NANOPARTICLES**

**M.Sc. THESIS**

**Burcu SAYINLI**

**Department of Nanoscience and Nanoengineering**

**Nano Science and Nano Engineering Programme**

**Anabilim Dalı : Herhangi Mühendislik, Bilim**

**Programı : Herhangi Program**

**DECEMBER 2015**



**ISTANBUL TECHNICAL UNIVERSITY ★ GRADUATE SCHOOL OF SCIENCE**  
**ENGINEERING AND TECHNOLOGY**

**SPECTROSCOPIC, MORPHOLOGIC, AND ELECTROCHEMICAL  
IMPEDANCE CHARACTERIZATIONS OF DNA FUNCTIONALIZED  
SILICA COATED  $\gamma$ -Fe<sub>2</sub>O<sub>3</sub> MAGNETIC NANOPARTICLES**

**M.Sc. THESIS**

**Burcu SAYINLI  
(513131012)**

**Department of Nanoscience and Nanoengineering**

**Nano Science and Nano Engineering Programme**

**Thesis Advisor: Prof. Dr. A. Sezai SARAC  
Anabilim Dalı : Herhangi Mühendislik, Bilim  
Programı : Herhangi Program**

**DECEMBER 2015**



**İSTANBUL TEKNİK ÜNİVERSİTESİ ★ FEN BİLİMLERİ ENSTİTÜSÜ**

**DNA İLE FONKSİYONELLENDİRİLMİŞ SİLİKA KAPLI  $\gamma$ -Fe<sub>2</sub>O<sub>3</sub>  
MANYETİK NANOPARTİKÜLLERİN SPEKTROSKOPİK, MORFOLOJİK  
VE ELEKTROKİMYASAL EMPEDANS İLE KARAKTERİZASYONU**

**YÜKSEK LİSANS TEZİ**

**Burcu SAYINLI  
(513131012)**

**Nano Bilim ve Nano Mühendislik Anabilim Dalı**

**Nano Bilim ve Nano Mühendislik Programı**

**Tez Danışmanı: Prof. Dr. A. Sezai SARAC  
Anabilim Dalı : Herhangi Mühendislik, Bilim  
Programı : Herhangi Program**

**ARALIK 2015**



**Burcu SAYINLI**, a **M.Sc.** student of **ITU Graduate School of Science Engineering and Technology** student ID **513131012**, successfully defended the thesis entitled “**SPECTROSCOPIC, MORPHOLOGIC, AND ELECTROCHEMICAL IMPEDANCE CHARACTERIZATIONS OF DNA FUNCTIONALIZED SILICA COATED  $\gamma$ -Fe<sub>2</sub>O<sub>3</sub> MAGNETIC NANOPARTICLES**”, which she prepared after fulfilling the requirements specified in the associated legislations, before the jury whose signatures are below.

**Thesis Advisor :**      **Prof. Dr. A. Sezai SARAÇ** .....  
Istanbul Technical University

**Jury Members :**      **Assoc.Prof.Dr. Fatma Neşe KÖK** .....  
Istanbul Technical University

**Prof. Dr. Cemal ÖZEROĞLU** .....  
Istanbul University

**Date of Submission : 27 November 2015**  
**Date of Defence : 22 December 2015**





*To my family,*



## **FOREWORD**

I would like to express my sincere appreciation and thanks to my supervisor, Prof. Dr. A.Sezai SARAÇ for his continuous encouragement, guidance, motivation and immense knowledge.

I would like to thanks to Sentromer DNA Technologies Company for all support, and especially to Pınar AKALIN for her helpful and motivated behavior and giving opportunities to do experiment at her laboratory.

I am also thankful to my colleagues Selin GÜMRÜKÇÜ, Uğur DAĞLI, Samin DASTJERD, İlknur GERGIN, Zeliha GÜLER, Timuçin BALKAN, Ezgi İŞMAR, Rana GOLSHAEI, Mehmet Tolga SATICI, Havva BAŞKAN, Fatma Zehra ENGİN, Deniz GÜLERCAN, and Aslı GENÇTÜRK for their collaborative and friendly manner.

I would especially like to thank my friend Dilek KAÇMAZ for constant encouragement and for always being there.

Lastly, and most importantly, I wish to thank my family to whom I dedicate this thesis as a token of my gratitude.

December 2015

Burcu SAYINLI  
(Chemist)



## TABLE OF CONTENTS

	<u>Page</u>
<b>FOREWORD</b> .....	<b>ix</b>
<b>TABLE OF CONTENTS</b> .....	<b>xi</b>
<b>ABBREVIATIONS</b> .....	<b>xiii</b>
<b>LIST OF TABLES</b> .....	<b>xv</b>
<b>LIST OF FIGURES</b> .....	<b>xvii</b>
<b>SUMMARY</b> .....	<b>xxi</b>
<b>ÖZET</b> .....	<b>xxiii</b>
<b>1. INTRODUCTION</b> .....	<b>1</b>
<b>2. THEORETICAL PART</b> .....	<b>11</b>
2.1 Iron Oxide Nanoparticles .....	11
2.2 $\gamma$ -Fe <sub>2</sub> O <sub>3</sub> Nanoparticles .....	11
2.3 Electrochemical Impedance Spectroscopy (EIS) .....	12
2.4 Basic Principles and Terms in Impedance Spectroscopy .....	13
<b>3. EXPERIMENTAL PART</b> .....	<b>15</b>
3.1 Materials .....	15
3.2 Synthesis of Fe <sub>3</sub> O <sub>4</sub> Nanoparticles .....	15
3.3 Synthesis of Fe <sub>2</sub> O <sub>3</sub> Nanoparticles .....	17
3.4 Synthesis of Fe <sub>2</sub> O <sub>3</sub> @SiO <sub>2</sub> Nanoparticles .....	17
3.5 Binding Process of DNA Oligonucleotides to Fe <sub>2</sub> O <sub>3</sub> @SiO <sub>2</sub> Nanoparticles ....	17
3.6 Structural, Morphological and Electrochemical Characterization .....	19
<b>4. RESULTS AND DISCUSSION</b> .....	<b>21</b>
4.1 FTIR-ATR Spectroscopic Characterization of Synthesized and Commercial Magnetic Nanoparticles .....	21
4.2 Raman Spectroscopic Characterization of Synthesized and Commercial Magnetic Nanoparticles .....	23
4.3 Uv-Vis Spectrophotometric Analyses of ttr4 DNA Oligonucleotide .....	27
4.4 Uv-Vis Spectrophotometric Analyses of Iron Oxide Magnetic Nanoparticles .....	28
4.5 Electrochemical Impedance Spectroscopy (EIS) Analyses of ttr4 and dT20 DNA Oligonucleotides .....	31
4.6 Electrochemical Impedance Spectroscopy (EIS) Analyses of Iron Oxide Magnetic Nanoparticles .....	34
4.7 Interaction Amongst UV Absorbance/Impedance/Concentration .....	41
4.8 Comparative EIS Results of Magnetic Nanoparticles .....	49
4.9 Morphological Characterization of Magnetic Nanoparticles .....	51
<b>5. CONCLUSION</b> .....	<b>59</b>
<b>REFERENCES</b> .....	<b>61</b>
<b>CURRICULUM VITAE</b> .....	<b>71</b>



## **ABBREVIATIONS**

<b>AFM</b>	: Atomic Force Microscope
<b>DEG</b>	: Diethylene glycol
<b>EIS</b>	: Electrochemical Impedance Spectroscopy
<b>FTIR</b>	: Fourier Transform Infrared Spectroscopy
<b>MNP</b>	: Magnetic Nanoparticle
<b>NP</b>	: Nanoparticle
<b>PBS</b>	: Phosphate Buffer Saline
<b>SEM</b>	: Scanning Electron Microscope
<b>SiMAG</b>	: Silica coated magnetic nanoparticle
<b>UV-Vis</b>	: Ultraviolet Visible Spectrophotometer
<b>TEOS</b>	: Tetraethyl orthosilicate





## LIST OF TABLES

	<u>Page</u>
<b>Table 1.1 :</b> Name of the DNA oligonucleotides used in study and their base sequences and numbers.....	9
<b>Table 3.1 :</b> Name of the samples used in study and their base sequences and numbers.....	19
<b>Table 4.1 :</b> Impedance and Capacitance values obtaining from Nyquist and Bode-Magnitude plots and belonging to SiMAG without DNA binding, SiMAG-Cola, SiMAG-3C-Cola, SiMAG-6C-Cola, and SiMAG-30T at %0.06, %0.10, and %0.14 (v/v) dilution ratios.....	40
<b>Table 4.2 :</b> Roughness values of SiMAG without DNA binding, SiMAG-Cola, SiMAG-3C-Cola, SiMAG-6C-Cola, and SiMAG-30T nanoparticles.....	51
<b>Table 4.3:</b> Measured granule diameters from SEM images belonging to SiMAG without DNA binding, SiMAG-Cola, SiMAG-3C-Cola, and SiMAG-6C-Cola nanoparticles and ttr4 and dT20 DNA oligonucleotides.....	57



## LIST OF FIGURES

	<u>Page</u>
<b>Figure 1.1</b> : Physicochemical mechanism for modifying the silane agents on the surface of iron oxide NPs.....	4
<b>Figure 2.1</b> : Crystal structures of iron oxide nanoparticles [99]..	12
<b>Figure 2.2</b> : Impedance expressed as the modulus $ Z $ and the phase angle $\phi$ , or specified by the real ( $Z_{re}$ ) and imaginary ( $Z_{im}$ ) parts.....	13
<b>Figure 2.3</b> : Randles' equivalent circuit for an electrode in contact with an electrolyte.....	14
<b>Figure 3.1</b> : Photograph shows synthesis of $Fe_3O_4$ nanoparticles inside the three-neck glass flask .....	16
<b>Figure 3.2</b> : Photograph shows the dispersion of $Fe_3O_4$ nanoparticles in centrifuge tube before and after centrifuge .....	16
<b>Figure 3.3</b> : Photograph shows the $Fe_2O_3$ nanoparticles after calcination process...	17
<b>Figure 3.4</b> : Photographs show the magnetic nanoparticles in microcentrifuge tube before and after placed on magnet.. .....	18
<b>Figure 4.1</b> : FTIR-ATR spectra of $\gamma$ - $Fe_2O_3$ (maghemite) nanoparticle produced by calcination of commercial $Fe_3O_4$ and synthesized $Fe_3O_4$ nanoparticles. ....	21
<b>Figure 4.2</b> : FTIR-ATR spectra of SiMAG nanoparticles and synthesized $\gamma$ - $Fe_2O_3$ @ $SiO_2$ nanoparticles.. .....	22
<b>Figure 4.3</b> : FTIR-ATR spectra of synthesized $\gamma$ - $Fe_2O_3$ nanoparticles and synthesized $\gamma$ - $Fe_2O_3$ @ $SiO_2$ nanoparticles. ....	23
<b>Figure 4.4</b> : Raman spectra of $\gamma$ - $Fe_2O_3$ (maghemite) nanoparticle produced by calcination of synthesized $Fe_3O_4$ nanoparticles. ....	24
<b>Figure 4.5</b> : Raman spectra of $\gamma$ - $Fe_2O_3$ (maghemite) nanoparticle produced by calcination of commercial $Fe_3O_4$ nanoparticles. ....	25
<b>Figure 4.6</b> : Raman spectra of SiMAG nanoparticles obtained from Chemicell Company.....	25
<b>Figure 4.7</b> : Raman spectra of synthesized $\gamma$ - $Fe_2O_3$ @ $SiO_2$ nanoparticles by coating of $\gamma$ - $Fe_2O_3$ nanoparticles with silica.....	26
<b>Figure 4.8</b> : Raman spectra of SiMAG nanoparticles obtained from Chemicell Company and synthesized $\gamma$ - $Fe_2O_3$ @ $SiO_2$ nanoparticles by coating of $\gamma$ - $Fe_2O_3$ nanoparticles with silica. ....	26
<b>Figure 4.9</b> : UV-Vis spectrum of ttr4 DNA oligonucleotide at 6nM, 20nM, 30nM, and 40nM concentration values a) 200-900nm range b) 200-320nm range.....	27
<b>Figure 4.10</b> : UV-Vis spectrum of SiMAG nanoparticles at %0.06, %0.10, and %0.14 (v/v) dilution ratios .....	29
<b>Figure 4.11</b> : UV-Vis spectrum of SiMAG-Cola nanoparticles at %0.06, %0.10, and %0.14 (v/v) dilution ratios. ....	29

<b>Figure 4.12</b> : UV-Vis spectrum of SiMAG-3C Cola nanoparticles at %0.06, %0.10, and %0.14 (v/v) dilution ratios. ....	30
<b>Figure 4.13</b> : UV-Vis spectrum of SiMAG-6C-Cola nanoparticles at %0.06, %0.10, and %0.14 (v/v) dilution ratios. ....	30
<b>Figure 4.14</b> : UV-Vis spectrum of SiMAG-30T nanoparticles at %0.06, %0.10, and %0.14 (v/v) dilution ratios.. ....	31
<b>Figure 4.15</b> : Nyquist (a) and Bode-Magnitude (b) plots of ttr4 DNA oligonucleotide at 6nM, 20nM, 30nM, and 40nM concentration values .....	33
<b>Figure 4.16</b> : Nyquist (a) and Bode-Magnitude (b) plots of dT20 DNA oligonucleotide at 6nM, 20nM, 30nM, and 40nM concentration values .....	34
<b>Figure 4.17</b> : Nyquist (a) and Bode-Magnitude (b) plots of SiMAG nanoparticle at %0.06, %0.10, and %0.14 (v/v) dilution ratios.....	35
<b>Figure 4.18</b> : Nyquist (a) and Bode-Magnitude (b) plots of SiMAG-Cola nanoparticle at %0.06, %0.10, and %0.14 (v/v) dilution ratios.....	36
<b>Figure 4.19</b> : Nyquist (a) and Bode-Magnitude (b) plots of SiMAG-3C-Cola nanoparticle at %0.06, %0.10, and %0.14 (v/v) dilution ratios. ....	37
<b>Figure 4.20</b> : Nyquist (a) and Bode-Magnitude (b) plots of SiMAG-6C-Cola nanoparticle at %0.06, %0.10, and %0.14 (v/v) dilution ratios. ....	38
<b>Figure 4.21</b> : Nyquist (a) and Bode-Magnitude (b) plots of SiMAG-30T nanoparticle at %0.06, %0.10, and %0.14 (v/v) dilution ratios .....	39
<b>Figure 4.22</b> : $ Z $ -Concentration % (v/v) & Absorbance-Concentration % (v/v) plot for ttr4 DNA oligonucleotide.....	41
<b>Figure 4.23</b> : $C_{dl}$ -Concentration % (v/v), $C_{LF}$ -Concentration % (v/v) & Absorbance-Concentration % (v/v) plot for ttr4 DNA oligonucleotide.....	41
<b>Figure 4.24</b> : $ Z $ -Concentration % (v/v), $C_{LF}$ -Concentration % (v/v), & $C_{dl}$ Concentration % (v/v) plot for dT20 DNA oligonucleotide .....	42
<b>Figure 4.25</b> : $ Z $ -Concentration % (v/v) & Absorbance-Concentration % (v/v) plot for SiMAG nanoparticle. ....	43
<b>Figure 4.26</b> : $C_{dl}$ -Concentration % (v/v), $C_{LF}$ -Concentration % (v/v) & Absorbance-Concentration % (v/v) plot for SiMAG nanoparticle.. ....	43
<b>Figure 4.27</b> : $ Z $ -Concentration % (v/v) & Absorbance-Concentration % (v/v) plot for SiMAG-Cola nanoparticle. ....	44
<b>Figure 4.28</b> : $C_{dl}$ -Concentration % (v/v), $C_{LF}$ -Concentration % (v/v) & Absorbance-Concentration % (v/v) plot for SiMAG-Cola nanoparticle.....	44
<b>Figure 4.29</b> : $ Z $ -Concentration % (v/v) & Absorbance-Concentration % (v/v) plot for SiMAG-3C-Cola nanoparticle. ....	45
<b>Figure 4.30</b> : $C_{dl}$ -Concentration % (v/v), $C_{LF}$ -Concentration % (v/v) & Absorbance-Concentration % (v/v) plot for SiMAG-3C-Cola nanoparticle.....	45
<b>Figure 4.31</b> : $ Z $ -Concentration % (v/v) & Absorbance-Concentration % (v/v) plot for SiMAG-6C-Cola nanoparticle. ....	46
<b>Figure 4.32</b> : $C_{dl}$ -Concentration % (v/v), $C_{LF}$ -Concentration % (v/v) & Absorbance-Concentration % (v/v) plot for SiMAG-6C-Cola nanoparticle.....	46
<b>Figure 4.33</b> : $ Z $ -Concentration % (v/v) & Absorbance-Concentration % (v/v) plot for SiMAG-30T nanoparticle .....	47
<b>Figure 4.34</b> : $C_{dl}$ -Concentration % (v/v), $C_{LF}$ -Concentration % (v/v) & Absorbance-Concentration % (v/v) plot for SiMAG-30T nanoparticle.....	47

<b>Figure 4.35</b> : $ Z $ -Concentration % (v/v) plot for SiMAG without DNA binding, SiMAG-Cola, SiMAG-3C-Cola, SiMAG-6C-Cola, and SiMAG-30T at %0.06, %0.10, and %0.14 (v/v) dilution ratios.....	50
<b>Figure 4.36</b> : $C_{dl}$ -Concentration % (v/v) plot for SiMAG without DNA binding, SiMAG-Cola, SiMAG-3C-Cola, SiMAG-6C-Cola, and SiMAG-30T at %0.06, %0.10, and %0.14 (v/v) dilution ratios.....	50
<b>Figure 4.37</b> : $C_{LF}$ -Concentration % (v/v) plot for SiMAG without DNA binding, SiMAG-Cola, SiMAG-3C-Cola, SiMAG-6C-Cola, and SiMAG-30T at %0.06, %0.10, and %0.14 (v/v) dilution ratios.....	51
<b>Figure 4.38</b> : AFM images of SiMAG without DNA binding, SiMAG-Cola, SiMAG-3C-Cola, SiMAG-6C-Cola, and SiMAG-30T nanoparticles on two dimensional (2D)....	52
<b>Figure 4.39</b> : AFM images of SiMAG without DNA binding, SiMAG-Cola, SiMAG-3C-Cola, SiMAG-6C-Cola, and SiMAG-30T nanoparticles on three dimensional (3D).....	53
<b>Figure 4.40</b> : AFM images of ttr4 DNA oligonucleotide at 1 $\mu$ m and 500nm scales, and on 2D and 3D.....	54
<b>Figure 4.41</b> : SEM images of ttr4 DNA oligonucleotide at 40 $\mu$ m, 5 $\mu$ m, and 1 $\mu$ m scales.....	55
<b>Figure 4.42</b> : SEM images of dT20 DNA oligonucleotide at 400nm scale .....	55
<b>Figure 4.43</b> : SEM images of a) SiMAG without DNA binding, b) SiMAG-Cola, c) SiMAG-3C-Cola, d) SiMAG-6C-Cola, and e) SiMAG-30T nanoparticles at 500nm scale. ....	56
<b>Figure 4.44</b> : Roughness- $ Z $ relationship amongst samples which were enumerated as 1) ttr4 DNA oligonucleotide, 2) SiMAG, 3) SiMAG-3C-Cola, 4) SiMAG-6C-Cola, 5) SiMAG-30T.....	57
<b>Figure 4.45</b> : Roughness- $C_{dl}$ relationship amongst samples which were enumerated as 1) ttr4 DNA oligonucleotide, 2) SiMAG, 3) SiMAG-3C-Cola, 4) SiMAG-6C-Cola, 5) SiMAG-30T.....	58



# **SPECTROSCOPIC, MORPHOLOGIC, AND ELECTROCHEMICAL IMPEDANCE CHARACTERIZATIONS OF DNA FUNCTIONALIZED SILICA COATED $\gamma$ -Fe<sub>2</sub>O<sub>3</sub> MAGNETIC NANOPARTICLES**

## **SUMMARY**

Silica coated magnetic iron oxide nanoparticles (SiMAG, special name of the product) at maghemite form ( $\gamma$ -Fe<sub>2</sub>O<sub>3</sub> NPs) were obtained from Chemicell Company (Belgium). Different DNA oligonucleotides (Cola, 3C-Cola, and 6C-Cola) were bound to the surface of silica coated magnetic iron oxide NPs (SiMAG) by Sentromer DNA Technologies Company. Additionally, magnetic iron oxide nanoparticles on magnetite form (Fe<sub>3</sub>O<sub>4</sub>) was also synthesized. Then, magnetite iron oxide nanoparticles were converted to maghemite form ( $\gamma$ -Fe<sub>2</sub>O<sub>3</sub>) by calcination process at 300°C. After that,  $\gamma$ -Fe<sub>2</sub>O<sub>3</sub> NPs were coated with silica. Therefore, silica coated  $\gamma$ -Fe<sub>2</sub>O<sub>3</sub> NPs that have same structural form as SiMAG were obtained. Both synthesized silica coated  $\gamma$ -Fe<sub>2</sub>O<sub>3</sub> NPs and SiMAG nanoparticles were characterized spectroscopically with Fourier Transform Infrared - Attenuated Total Reflectance (FTIR-ATR), Raman Spectrophotometer, and UV-Vis spectrophotometer. Analysis results were compared in each other. It was observed that both of magnetic nanoparticles had same structure and formation owing to exhibition same characteristic bands from the analyses. In addition, DNA oligonucleotides (ttr4, and dT20) and magnetic nanoparticles with and without DNA binding (SiMAG, SiMAG-Cola, SiMAG-3C-Cola, SiMAG-6C-Cola, and SiMAG-30T) were investigated spectroscopically (UV-Vis Spectrophotometer), morphologically (AFM and SEM), and electrochemically (Electrochemical Impedance Spectroscopy (EIS)). The effect of parameters such as concentration, presence of bound DNA, length of DNA on impedance, capacitance, UV absorbance and granule size were investigated. As a result of the measurements, it was observed that when the concentration was increased,  $C_{dl}$  (double layer capacitance) and  $C_{LF}$  (Low frequency capacitance) values decreased while  $|Z|$  (impedance) and UV absorbance values increased. Moreover, when the DNA oligonucleotide was bound to the magnetic nanoparticle and the length of DNA oligonucleotide was elongated from 12 base to 30 base, it was observed that granule diameters were expanded, the  $|Z|$  values diminished,  $C_{dl}$  and  $C_{LF}$  values increased for each concentration value.





# **DNA İLE FONKSİYONELLENDİRİLMİŞ SİLİKA KAPLI $\gamma$ -Fe<sub>2</sub>O<sub>3</sub> MANYETİK NANOPARTİKÜLLERİN SPEKTROSKOPİK, MORFOLOJİK VE ELEKTROKİMYASAL EMPEDANS İLE KARAKTERİZASYONU**

## **ÖZET**

Manyetik nanopartiküller süperparamanyetizm, yüksek koersivite (artık mıknatıslanım) ve yüksek manyetik duyarlılık gibi çeşitli spesifik manyetik özelliklere sahip partiküllerdir. Pek çok farklı disiplinlerden araştırmacılar manyetik nanopartiküllere ve onların manyetik akışkanlar, veri depolama, kataliz ve biyolojik uygulamaları alanlarına karşı önemli ilgi göstermektedir. Günümüzde manyetik nanopartiküller yaygın olarak manyetik biyolojik ayırım, hücre, protein, nükleik asit, enzim, bakteri ve virüs gibi biyolojik varlıkların tespiti, klinik tanı ve tedavi (manyetik rezonans görüntüleme), hedefe yönelik ilaç salınımı, biyolojik etiketleme, RNA ve DNA saflaştırması, enzim ve protein immobilizasyonu ve kataliz gibi önemli biyolojik uygulamalarda kullanılmaktadır. Son dönemlerde manyetik nanopartiküllerle ilgili yapılan çalışmalar artmış olup, özellikle çalışmalar magnetit (Fe<sub>3</sub>O<sub>4</sub>), hematit ( $\alpha$ -Fe<sub>2</sub>O<sub>3</sub>), magemit ( $\gamma$ -Fe<sub>2</sub>O<sub>3</sub>), vüstit (FeO),  $\epsilon$ -Fe<sub>2</sub>O<sub>3</sub>, and  $\beta$ -Fe<sub>2</sub>O<sub>3</sub> gibi demir oksit nanopartiküllerinin farklı türlerine yoğunlaştırılmıştır.

Demir oksit nanopartikülleri arasından magnetit ve magemit formundaki nanopartiküller biyoyumluluk, toksik olmama, biyo-çözünürlük, geniş yüzey alanı, küçük partikül boyutu ve uygun manyetik özelliklerinden dolayı biyolojik, biyomedikal uygulamalarda oldukça yaygın olarak kullanılmaktadır. Manyetik demir oksit nanopartikülleri yüzey-hacim oranının yüksek olmasından dolayı fazla miktarda enerjiyi yüzeyinde barındırır. Bu sebeple, hem nanopartiküller arasındaki hidrofobik etkileşimleri hem de yüzey enerjisini azaltma isteği, manyetik nanopartiküllerin agregre olmasına (bir araya toplanma), partikül boyutunun büyümesine neden olur. Demir oksit nanopartikülleri yüksek kimyasal aktiviteye sahiptir ve havaya maruz kaldıklarında kolaylıkla okside olabilirler. Bu durum genellikle demir oksit nanopartiküllerinin manyetizm ve dağılıbilirlik özelliklerinin azalmasına neden olmaktadır. Tüm bu sorunların üstesinden gelmek, manyetik nanopartiküllere stabilite ve fonksiyonallite kazandırmanın yolu, demir oksit nanopartiküllerinin yüzeyinin modifiye edilmesidir. Manyetik nanopartiküllerin yüzeyi organik moleküller, yüzey aktif maddeler, polimerler, biyomoleküller, metal ya da metal olmayan maddeler, metal oksit, metal sülfid veya silika ile kaplanarak modifiye edilebilir.

Organik yapılarla kaplı demir oksit nanopartikülleri, nanopartiküllerin yüzeyini çevreleyen fonksiyonel gruplar sayesinde çeşitli alanlarda uygulama imkanı sunmaktadır. Organik moleküllerin nanopartiküllere sunduğu bu fonksiyonel gruplara aldehid, hidroksil, karboksil ve amino grubu örnek gösterilebilir. Bu gruplar çeşitli uygulamalar kapsamında antikor, protein, DNA, enzim gibi biyolojik moleküllere bağlanabilirler.

Manyetik nanopartiküllerin silika ile kaplanması partiküllere stabilite kazandırır ve partiküller arası etkileşimden meydana gelen aglomerasyonun oluşmasını önler.

Bununla birlikte, silika kaplı demir oksit nanopartikülleri daha iyi biyoyumluluk, hidrofilisite ve stabilite özellikleri göstermektedir. Ayrıca silika ile kaplama kalınlığı diğer kaplama maddelerine göre daha kolay kontrol edilebilmektedir. Silika kaplı manyetik nanopartiküller enzim immobilizasyonu, ilaç salınımı, çevresel teknoloji, biyolojik ayırım gibi özellikle biyolojik uygulamarda yaygın olarak kullanılmaktadır. Silika kaplamanın bir başka avantajı ise farklı biyomoleküllerin silika yüzeyine bağlanabilmesine olanak sağlamasıdır. Demir oksit nanopartikülleri, yüzeyine farklı biyolojik moleküller bağlanarak fonksiyonellendirilebilir. Protein, polipeptid, antikor, biyotin ve avidin gibi biyolojik moleküller kimyasal olarak demir oksit nanopartikülüne bağlanır. Bu modifikasyon demir oksit nanopartikülüne fonksiyonel gruplarından dolayı hem hedef özelliği hem de biyoyumluluk kazandırır.

İlgili çalışmaya manyetik demir oksit nanopartikülleri ve bu nanopartiküllerin biyoyumluluk, toksik olmama, biyo-çözünürlük, geniş yüzey alanı ve düşük partikül boyutu gibi üstün özellikleri ve biyolojik, biyomedikal uygulamalarda oldukça yaygın olarak kullanılmasından ilham alınarak başlanmıştır. Kaplanmamış manyetik demir oksit nanopartiküllerinin partiküller arası etkileşim ve hidrofobisite sonucu oluşan aglomerasyonuna karşılık nanopartiküllerin seçilen uygun yöntemlerle modifiye edilmesi planlanmıştır. Bu sebeple aglomerasyonu engellemek adına demir oksit nanopartikülleri silika ile kaplanmıştır. Silika kaplama demir oksit nanopartiküllerinde aglomerasyonu önlemenin yanı sıra nanopartiküllerin biyoyumluluk, hidrofilisite ve stabilite özelliklerini iyileştirmiş, ayrıca farklı uygulamalara yönelik nanopartikül yüzeyine çeşitli biyolojik grupların bağlanmasına da olumlu yönde katkı sağlamıştır.

Bu çalışmada, silika kaplı magemit ( $\gamma$ -Fe<sub>2</sub>O<sub>3</sub>) yapısındaki demir oksit nanopartikülleri kullanılmıştır. Bu nanopartiküller hem sentezlenmiş hem de ticari olarak Chemicell firmasından alınmıştır. Alınan ve özel adı SiMAG olan bu nanopartiküllere Sentromer DNA Teknolojileri firması tarafından özel adı Cola, 3C-Cola ve 6C-Cola olmak üzere farklı DNA oligonükleotidleri bağlanmıştır. Silika kaplı magemit ( $\gamma$ -Fe<sub>2</sub>O<sub>3</sub>) yapısındaki demir oksit nanopartikülü sentezi için ilk olarak FeCl<sub>2</sub>.4H<sub>2</sub>O (demir (II) klörür tetrahidrat) ve FeCl<sub>3</sub>.6H<sub>2</sub>O (demir (III) klörür hekzahidrat) kimyasallarından magnetit (Fe<sub>3</sub>O<sub>4</sub>) sentezlenmesiyle başlanmıştır. Sentezlenen magnetit nanopartikülü 300°C’de kül fırınında kalsine edilerek magemit yapısında dönüştürülmüştür. Ardından magemit nanopartikülleri TEOS (tetraetil ortosilikat) kimyasalı varlığında silika ile kaplanmış ve silika kaplı magemit yapısındaki demir oksit nanopartikülleri elde edilmiştir. Hem sentezlenen hem de ticari olarak alınan (SiMAG) silika kaplı magemit yapısındaki demir oksit nanopartikülleri spektroskopik olarak FTIR-ATR (Fourier Transform Infrared - Attenuated Total Reflectance), Raman ve UV-Vis Spektrofotometre cihazlarıyla karakterize edilmiştir. Analiz sonuçları karşılaştırıldığında iki numunenin de aynı karakteristik pikleri/bandları verdiği, analiz sonuçlarının örtüştüğü, dolayısıyla sentez yoluyla elde edilen silika kaplı magemit yapısındaki demir oksit nanopartikülünün ticari olarak alınan nanopartikül ile içerik ve yapı bakımından aynı olduğu görülmüştür.

DNA oligonükleotidleri (ttr4 ve dT20), SiMAG, SiMAG nanopartikülüne farklı DNA oligonükleotidleri bağlanmış olan SiMAG-Cola, SiMAG-3C-Cola, SiMAG-6C-Cola ve ticari olarak Chemicell firmasından alınan SiMAG-30T nanopartikülleri spektroskopik (UV-Vis Spektrofotometre), morfolojik (AFM (Atomik Kuvvet Mikroskobu) ve SEM (Taramalı Elektron Mikroskobu)) ve elektrokimyasal (Elektrokimyasal Empedans Spektroskopisi (EIS)) ile incelenmiş, karakterize edilmiştir. Konsantrasyon, DNA bağlanması, bağlanan DNA uzunluğu gibi

parametrelerin empedans, kapasitans, UV absorbans ve tanecik büyüklüğüne etkileri araştırılmıştır.

Ölçümler sonucunda konsantrasyonun artmasıyla  $C_{dl}$  (çift tabaka kapasitansı) ve  $C_{LF}$  (düşük frekans kapasitansı) değerlerinin azaldığı, empedans ( $|Z|$ ) ve UV absorbans değerlerinin arttığı gözlemlenmiştir. Ayrıca, DNA oligonükleotidinin manyetik nanopartiküle bağlanması ve DNA oligonucleotid uzunluğunun 12 bazdan 30 baza arttırılması sonucunda granül çapının ve pürüzlülüğün arttığı, empedans değerinin azaldığı ve  $C_{dl}$  ve  $C_{LF}$  değerlerinin arttığı görülmektedir.



## 1. INTRODUCTION

Nanotechnology can be described as the controlling of matter in atomic, molecular, and supramolecular range. Nanoparticle research is currently an area of intense scientific research, due to their potential technological importance, which results from their unique physical properties [1,2].

Magnetic nanoparticles (MNPs) have numerous specific magnetic properties such as superparamagnetic, high coercivity, low Curie temperature, high magnetic susceptibility, etc. Researchers from a broad range of disciplines are in outstanding interest about MNPs and their application fields including magnetic fluids, data storage, catalysis, and bioapplications [3-7].

Currently, MNPs are widely used in significant bioapplications, including magnetic bioseparation [8] and detection of biological entities (cell, protein, nucleic acids, enzyme, bacteria, virus, etc.), clinic diagnosis and therapy (such as MRI (magnetic resonance image) and MFH (magnetic fluid hyperthermia)), targeted drug delivery [9], biological labels, RNA and DNA purification, enzyme and protein immobilization [10], and catalysis [11].

In the last decade, investigations related to MNPs have been increased, especially researches have been focused on several types of iron oxide nanoparticles such as magnetite ( $\text{Fe}_3\text{O}_4$ ), hematite ( $\alpha\text{-Fe}_2\text{O}_3$ ), maghemite ( $\gamma\text{-Fe}_2\text{O}_3$ ), wüstite ( $\text{FeO}$ ),  $\epsilon\text{-Fe}_2\text{O}_3$ , and  $\beta\text{-Fe}_2\text{O}_3$ . Among iron oxide nanoparticles, magnetite and maghemite forms have very extensive use particularly in biological and biomedical applications due to their biocompatibility, nontoxicity, biodegradability, large surface area, low particle dimensions, and suitable magnetic properties [12]. Magnetic iron oxide NPs keep high surface energy because they have large surface-to volume ratio. Therefore, due to both hydrophobic interactions between the NPs and the desire to decrease the surface energies, MNPs tend to aggregate and form large clusters, resulting in increased particle size [13]. Moreover, the naked iron oxide NPs have high chemical

activity, and they are easily oxidized in air (especially magnetite). That situation mostly leads to decrease of magnetism and dispersibility.

Consequently, the key to overcome these problems, to stabilize and to be gained further functionalizations to the MNP is to apply proper surface modification to iron oxide nanoparticles. These surface modification techniques which can be applied to MNPs can be collocated as coating with organic molecules, including small organic molecules or surfactants, polymers, and biomolecules, or coating with an inorganic layer, such as silica, metal or nonmetal elementary substance, metal oxide or metal sulfide [14].

Organic compounds coated on iron oxide NPs offer a high potential application in several areas under favour of functional groups covering the surface of MNP. Organic molecules can provide the ensemble functional reactive group such as aldehyde groups, hydroxyl groups, carboxyl groups, amino groups, etc. It is very critical that their groups can attach to the active biosubstance such as antibody, protein, DNA, enzyme, etc., for the further application. Guo et al. [15] have reported the carboxyl functioned magnetic nanoparticles (CMNPs) magnetic  $\text{Fe}_3\text{O}_4$  nanoparticles were synthesized, then glucoamylase was direct bonded onto the carboxyl magnetic nanoparticles. In conclusion, it was observed that the immobilized glucoamylase exhibits various activities in wider ranges of temperature and pH, compared with its free form.

Another surface modification technique basically dividing into three types as oil-soluble, water-soluble, and amphiphilic is functionalization of iron nanoparticles with small molecules or surfactants. Oleic acid is a widely used long chain substance which has a C18 tail with a cis-double-bond in the middle, for oil-soluble type functionalization of iron oxide nanoparticles, especially in ferrite nanoparticles. The mystery of precedence on oleic acid can be explained that highly uniform and monodisperse particles can be produced because oleic acid can form a dense protective monolayer around iron oxide nanoparticle. Sun et al. [16] have reported that they achieved uniform iron oxide nanoparticles which were prepared by thermal decomposition of  $\text{Fe}(\text{acac})_3$  in the presence of surfactants, oleylamine, and oleic acid.

The mainly researches focus on the synthesis of water-soluble functionalized iron oxide NPs which can be widely utilized in bioseparation and biodetection. There are

number of methods to produce the water-soluble functionalized iron oxide NPs. One of them is to directly add the biocompatible small organic molecules such as amino acid [17], citric acid [18, 19], vitamin [20,21], cyclodextrin [22–24], etc. during the synthesis procedure. Xia et al. [25] reported that they prepared water-soluble  $\text{Fe}_3\text{O}_4$  NPs with a surrounded layer by use of polyethylene glycol nonylphenyl ether (NP5) and cyclodextrin (CD) in aqueous medium.

Different from the first method, that method includes transforming of the oil-soluble type into water-soluble type functionalized iron oxide NPs, and the ligand-exchange reaction [26]. Lattuada and Hatton [27] reported that the oleic groups initially present on the above nanoparticle surfaces were replaced via ligand-exchange reaction with various capping agents bearing reactive hydroxyl moieties.

Nevertheless, ligand-exchange reaction frequently results to the complicated operations and difficulty of control exchange rate. The solution to overcome these undesired situations is to utilize silane agent which has outstanding properties as biocompatibility, high density of surface functional endgroups, and allowing for connecting to other metal, polymer or biomolecules for modifying on the surface of iron oxide NPs directly [28,29]. Can et al. [30] have reported that firstly surface of magnetite nanoparticle was modified by the aminosilane agent of aminopropyltriethoxysilane (APTES), then after albumin which is a model protein was immobilized to surface of modified  $\text{Fe}_3\text{O}_4$  NPs. According to the report, the product can find preciousness for magnetic applications in diverse bioprocesses, biomedical devices and biomedicine.

According to Arkles, the physicochemical mechanism of the silane agent modifying on the surface of iron oxide NPs is depicted in Figure 1.1 [31]. The mechanism expresses that the hydroxyl groups on the iron oxide NPs surface reacted with the methoxy groups of the silane molecules. It leads to the formation of Si–O bonds and leaving the terminal functional groups available for immobilization the other substance.

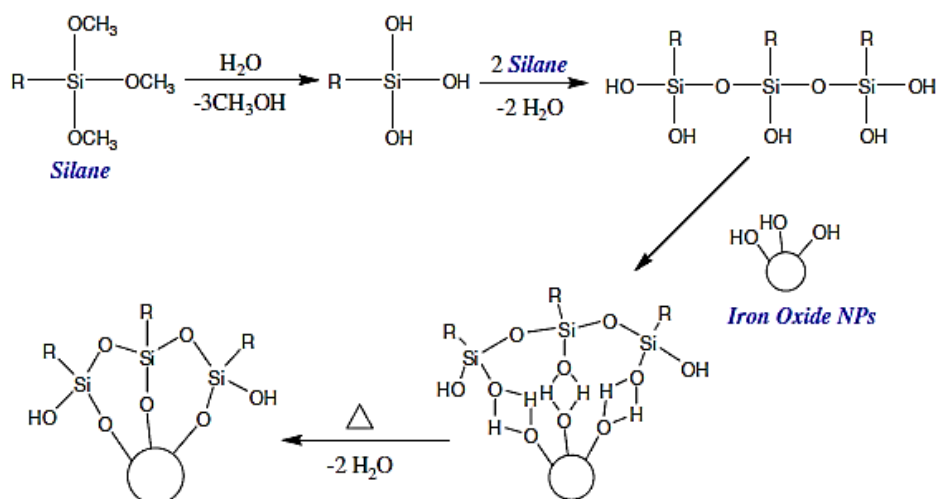


**Figure 1.1 :** Physicochemical mechanism for modifying the silane agents on the surface of iron oxide NPs.

Functionalized iron oxide NPs with polymers is a prevalent method to modify the magnetic nanoparticles. Polymer coating submits some benefits to the iron oxide NPs system causing to high repulsive forces which balance the magnetic and the van der Waals attractive forces acting on the NPs.

Polymer coated and functionalized iron oxide NPs provide a high potential in the application of several fields. Polymer coating materials can be classified into synthetic and natural. Dextran is a natural polymer which enables optimum polar interactions with iron oxide surfaces and has stability and biocompatibility properties [32,33]. Starch which improves the biocompatibility and drug target delivery [34] and gelatin which is used as biocompatible gelling agent [35] are other natural polymers for functionalization of iron oxide NPS. Moreover, chitosan is the another favorite natural polymer which is non-toxic, alkaline, hydrophilic, biocompatible, and widely used as non-viral gene delivery system [36,37]. Hereaa et al. [38] have synthesized MNPs coated with glucose-derived polymer which can be used in magnetic hyperthermia due to its physical properties and biocompatibility.

Synthetic polymers have a particular importance for functionalizing of iron oxide NPs. Alginate [39,40] and Polyacrylic acid (PAA) [41,42] improve stability and biocompatibility. Moreover, Poly(lactide acid) (PLA) which has low toxicity in human body develops the biodegradability of iron oxide NPs when the coated with these polymers as well as stability and biocompatibility [43]. Poly(vinyl alcohol)



(PVA) is a convenient polymer so as to prevent agglomeration and to bring on monodispersibility [44,45]. For thermosensitive drug delivery and cell separation applications, Polymethylmethacrylate (PMMA) is a polymer which is commonly used [46,47]. Demchenko et al. [48] have synthesized  $\gamma$ -Fe<sub>2</sub>O<sub>3</sub> nanoparticles surrounded with a COOH- poly(NVP)-MP (Poly-N-vinyl pyrrolidone)-(peroxide group)) shell by using surface-active polyfunctional oligoperoxides which were used as the nanoreactors for the controlled formation and modification of  $\gamma$ -Fe<sub>2</sub>O<sub>3</sub> particle shells. These nanoparticles are promising potential medical application such as anticancer magnetic hyperthermia.

Poly(ethyleneglycol) (PEG) is widely used polymer since their long polymeric chains are highly soluble in water and nontoxic in the blood, also they enhance the hydrophilicity and improve the biocompatibility of iron oxide NPs [49]. Yanga et al. [50] have synthesized PEG-Fe<sub>3</sub>O<sub>4</sub> NPs via a simple coprecipitation way at 60°C under different external condition. In recent researches, PEG coated iron oxide nanoparticles have taken place on applications related to drugs. Some of these applications can be exemplified as synthesis of doxorubicin loaded PEG-b-poly(4-vinylbenzylphosphonate) coated magnetic iron oxide nanoparticles NPs (PEG-PIONs/DOX) as drug nanocarrier for magnetically mediated targeted anticancer therapy [51] and Polylysine coated iron oxide nanoparticles (PLL/PEG-SPIONs) as transporting cargo-loaded SPIONs to cells [52]. Consequently, it may prompt the excellent utility of PEG-Fe<sub>3</sub>O<sub>4</sub> NPs in biomedical applications including bioseparation, drug targeting and diagnostic analysis.

As an alternative to these mentioned techniques, inorganic compounds can be used to functionalize the iron oxide NPs especially owing to enhance the antioxidation properties for naked iron oxide NPs. Inorganic materials such as metal, nonmetal, metal oxides, sulfides, and silica can be utilized coating of iron oxide NPs.

Single-metal functionalized iron oxide NPs are generally synthesized by reducing the single-metal ions on the surface of iron oxide NPs. These type of iron oxide NPs are employed as catalysts, such as Au/Fe<sub>2</sub>O<sub>3</sub> catalyst for CO oxidation [53], Au/ $\alpha$ -Fe<sub>2</sub>O<sub>3</sub> catalyst for water-gas shift reaction [54,55], Fe<sub>3</sub>O<sub>4</sub>/Pd nanoparticle-based catalyst for the cross-coupling of acrylic acid with iodobenzene [56] and decarboxylative coupling reaction in aqueous media [57], Ag-Fe<sub>3</sub>O<sub>4</sub> catalyst for epoxidation of styrene [58], etc.

On the other side, non-metal functionalized iron oxide NPs can be produced by reduction of the single-metal ion on the surface of the small molecule, polymer or SiO<sub>2</sub> functionalized iron oxide NPs. Wang et al. [59] reported that they synthesized Fe<sub>3</sub>O<sub>4</sub>/C nanocomposite by heating the aqueous solution of glucose and oleic acid-stabilized magnetite NPs. As a result of these modifications, the iron oxide NPs were protected from rapidly degraded by environment and were prevented from agglomeration caused by van der Waals attraction.

Metal oxides or metal sulfides functionalized iron oxide NPs have unique physical or chemical properties. In general, researches principally focus on common materials (ZnO, MgO, CaO, SnO<sub>2</sub>, Al<sub>2</sub>O<sub>3</sub> etc.) [60-62], magnetic materials (iron oxides, CoO, NiO, CoFe<sub>2</sub>O<sub>4</sub>, etc.) [63], optical and electrical functional materials (TiO<sub>2</sub>, ZnS, Y<sub>2</sub>O<sub>3</sub>, etc.) [64,65]. Metal oxides or metal sulfides functionalized iron oxide NPs have various applications in bioanalytical, biomedical, and bioseparation. Chen et al. [66] have reported that synthesized functional Fe<sub>3</sub>O<sub>4</sub>/TiO<sub>2</sub> core-shell magnetic NPs can be employed as photokilling agents for pathogenic bacteria. Another research, Habibi et al. [67] have reported that Fe<sub>2</sub>O<sub>3</sub> nanoparticles were coated with ZnO nanolayer. Then S-layer proteins from *C. Crescentus* bacteria were immobilized on zincite-coated Fe<sub>2</sub>O<sub>3</sub> nanoparticles by hydroxyl groups of zinc oxide shell. This synthesis has high importance due to further improvement on immobilization of macromolecules and development of new biosensors.

Silica (SiO<sub>2</sub>) coated iron oxide NPs have attracted increased attention in recent years owing to the fact that silica coating gives stability to iron oxide NPs in solution and it prevents agglomeration reasoning from interparticle interactions. Besides silica coated iron oxide NPs exhibit good biocompatibility, hydrophilicity and stability properties, and additionally the shell thickness of silica coating can be easily controlled unlike the other coating compounds.

Mesoporous silicas which have large surface area and narrow particle size distribution are especially promising materials with potential applications in heterogeneous catalysis [68], enzyme immobilization [69], drug delivery [70], environmental technology [71], bioseparations [72], and many other fields.

Fellenza et al. [73] synthesized maghemite nanoparticles coated with MCM-41 (mesoporous ordered silica structure). It was observed that these nanoparticles can

adsorb Cr (VI) and Cu (II) metals, and they are promising for potential applications in different important fields such as pollutants adsorption from aqueous matrix, biomolecules separation, and drug delivery. In another research, it was reported that Cu (II) in aqueous media adsorbed by chrysin-based silica core-shell MNPs,  $\text{Fe}_3\text{O}_4@\text{SiO}_2\text{-N-chrysin}$  [74]. Ma et al. [75] reported a synthesis of  $\text{Fe}_x\text{O}_y@\text{SiO}_2$  core-shell NPs. Firstly they synthesized silica coated iron oxide NPs. Afterwards, they doped the dye molecules inside a second silica shell owing to improving photostability and allowing for miscellaneous surface functionalities.

Moreover, silica-coating has advantage to bind the different biological or the other ligands at the NPs surface for various applications. Ashtari et al. [76] have reported an effective method for recovery of target ssDNA based on aminomodified silica-coated  $\text{Fe}_3\text{O}_4$  NPs. Chen et al. [77] reported that they synthesized mesoporous  $\text{SiO}_2$  microspheres with superparamagnetic  $\gamma\text{-Fe}_2\text{O}_3$  particles embedded in the walls and demonstrate their applications in magnetic extraction of genomic DNA for amplification-based analysis. Similar researches were accomplished related to DNA isolation, extraction, and retrieving such as isolation of plasma DNA by synthesized  $\gamma\text{-Fe}_2\text{O}_3$ /alginate/silica microspheres [78], adsorption of DNA for extraction and purification by the magnetite-loaded silica microspheres [79], and retrieval of double stranded DNA molecules from aqueous solutions by Pani-modified  $\gamma\text{-Fe}_2\text{O}_3$  NPs [80].

Iron oxide nanoparticles can be functionalized by binding various biological molecules to the surface of iron oxide NPs. These biological molecules such as protein [81,82], polypeptide [83], antibody [84, 85], biotin and avidin [86] can be bound chemically to the surface of iron oxide NPs directly or indirectly. The modification leads to that iron oxide nanoparticles gain not only target facility but also biocompatibility due to the functional endgroups on their surface.

When the suitable chemical route is applied to iron oxide NPs so as to functionalize, biomolecules can immobilize on iron oxide NPs. At one of the research, Penicillin G acylase (PGA) which is one of the important pharmaceutical enzymes during the production of  $\beta$ -lactam antibiotic was immobilized onto the magnetic silica nanoparticles *via* physical adsorption [87]. At another immobilization application, cholesterol oxidase (COD) was bound to silica-coated maghemite NPs functionalized with amino silane organic molecules for the purpose protein immobilization [88].

Zhang et al. [89] have reported that they synthesized a human serum albumin (HAS)-coated  $\text{Fe}_3\text{O}_4$  NPs which is a radioisotope carrier labeled with  $^{188}\text{Re}$  so as to use on regional target therapy field.

MRS technology can be used to detect different types of molecular interactions (DNA-DNA, protein-protein, protein-small molecule, and enzyme reactions) with high efficiency and sensitivity using magnetic relaxation measurements MRI. Perez et al. [90] have developed biocompatible magnetic nanosensors that act as MRS to detect molecular interactions in the reversible self-assembly of disperse magnetic particles into stable nano assemblies.

Recently, Lee and colleagues [91] developed a method for binding the  $\gamma\text{-Fe}_2\text{O}_3$  NPs with single strand oligonucleotides. At first, the water-soluble magnetic NPs with carboxyl groups on their surfaces were prepared, and then they successfully modified a protein, streptavidin, on the surface of  $\gamma\text{-Fe}_2\text{O}_3$  NPs by using 1-ethyl-3-(3-dimethylaminopropyl) carbodiimide hydrochloride (EDC) as a linker reagent. Streptavidin functionalized  $\gamma\text{-Fe}_2\text{O}_3$  can catch a biotin-labeled single strand oligonucleotides through the strong affinity between streptavidin and biotin.

In this study, we started to our research inspiring from magnetic iron oxide nanoparticle, its great facilities such as biocompatibility, nontoxicity, biodegradability, large surface area, low particle dimensions, and suitable magnetic properties, and employability on biological and biomedical applications. However naked magnetic iron oxide nanoparticles exhibit agglomeration reasoning from interparticle interactions and hydrophobicity. For that reason, coating of magnetic iron oxide NPs with silica is a very effective route so as to prevent agglomeration. Silica coating provides superiority to magnetic iron oxide NPs by not only it prevents agglomeration, but also it gains good biocompatibility, hydrophilicity, stability, and advantage availability to bind the different biological or the other ligands at the NPs surface for various applications.

In this study, we purchased silica coated magnetic iron oxide NPs (SiMAG, special name of the product) at maghemite form ( $\gamma\text{-Fe}_2\text{O}_3$  NPs) from Chemicell Company (Belgium). Then, different DNA oligonucleotides (Cola, 3C-Cola, and 6C-Cola) listed on Table 1.1 were bound to the surface of silica coated magnetic iron oxide NPs (SiMAG) by Sentromer DNA Technologies Company.

**Table 1.1** : Name of the DNA oligonucleotides used in study and their base sequences and numbers.

Name of DNA Oligonucleotides	Base Sequence	Number of Base
Cola	CGC ACT TAG GTC	12
3C-Cola	CCC CGC ACT TAG GTC	15
6C-Cola	CCC CCC CGC ACT TAG GTC	18
30T	TTT TTT TTT TTT TTT TTT TTT TTT TTT TTT	30
ttr4	AGC TCA GAC CAA AAG TGA CCA TC	23
dT20	TTT TTT TTT TTT TTT TTT TT	20

Besides, on the other hand, we synthesized magnetic iron oxide nanoparticles on maghemite form ( $\gamma\text{-Fe}_2\text{O}_3$  NPs) by transforming synthesized magnetic NPs at magnetite form ( $\text{Fe}_3\text{O}_4$ ) with calcination on oven at  $300^\circ\text{C}$ . After that,  $\gamma\text{-Fe}_2\text{O}_3$  NPs were coated with silica. Therefore, silica coated  $\gamma\text{-Fe}_2\text{O}_3$  NPs were synthesized by following that procedure.

Both synthesized silica coated  $\gamma\text{-Fe}_2\text{O}_3$  NPs and SiMAG nanoparticles were characterized spectroscopically with Fourier Transform Infrared - Attenuated Total Reflectance (FTIR-ATR), Raman Spectrophotometer, and UV-Vis spectrophotometer. Analysis results were compared in each other. It was observed that both of magnetic nanoparticles had same structure and formation owing to exhibition same characteristic bands from the analyses. In additional, DNA oligonucleotides (ttr4, and dT20) and magnetic nanoparticles with and without DNA binding (SiMAG, SiMAG-Cola, SiMAG-3C-Cola, SiMAG-6C-Cola, and SiMAG-30T) were investigated spectroscopically (UV-Vis Spectrophotometer), morphologically (AFM and SEM), and electrochemically (Electrochemical Impedance Spectroscopy (EIS)). The effect of parameters such as concentration, presence of bound DNA, length of DNA on impedance, capacitance, UV absorbance and granule size were investigated.

As a result of the measurements, it was observed that when the concentration was increased,  $C_{dl}$  (double layer capacitance) and  $C_{LF}$  (Low frequency capacitance) values decreased while  $|Z|$  (impedance) and UV absorbance values increased. Moreover, when the DNA oligonucleotide was bound to the magnetic nanoparticle and the length of DNA oligonucleotide was elongated from 12 base to 30 base, it was observed that granule diameters were expanded, the  $|Z|$  values diminished,  $C_{dl}$  and  $C_{LF}$  values increased, and for each concentration value.



## 2. THEORETICAL PART

### 2.1 Iron Oxide Nanoparticles

Iron oxides are chemical compounds composed of iron and oxygen. There exist various iron oxides such as hematite ( $\alpha\text{-Fe}_2\text{O}_3$ ), magnetite ( $\text{Fe}_3\text{O}_4$ ), maghemite ( $\gamma\text{-Fe}_2\text{O}_3$ ),  $\beta\text{-Fe}_2\text{O}_3$ ,  $\varepsilon\text{-Fe}_2\text{O}_3$ , and Wüstite ( $\text{FeO}$ ) (Figure 2.1) [92]. The iron oxide at  $\text{Fe}_2\text{O}_3$  form which is the most common oxide of iron has four polymorphs as alpha, beta, gamma and epsilon. The most frequent polymorphs structure alpha (hematite,  $\alpha\text{-Fe}_2\text{O}_3$ ), is the oldest known Fe oxide mineral. It is extremely stable and is often the final stage of transformations of other iron oxides. It has a rhombohedral-hexagonal, prototype corundum structures and also has strongly antiferromagnetic properties [93]. Generally, the semiconductor properties of the hematite are extremely useful in solar energy conversion, photocatalyse, water splitting. Beta  $\text{Fe}_2\text{O}_3$  ( $\beta\text{-Fe}_2\text{O}_3$ ) has cubic bixbyite structure and it exhibits paramagnetic properties while epsilon  $\text{Fe}_2\text{O}_3$  ( $\varepsilon\text{-Fe}_2\text{O}_3$ ) which is a transition phase between hematite and maghemite has orthorhombic structure and ferromagnetic properties. Maghemite ( $\gamma\text{-Fe}_2\text{O}_3$ ) has cubic spinel structure, and it is a ferromagnetic mineral isostructural with magnetite ( $\text{Fe}_3\text{O}_4$ ) which is also a ferromagnetic mineral containing both Fe (II) and Fe (III). It differs from the inverse spinel structure of magnetite through vacancies on the cation sublattice.

### 2.2 $\gamma\text{-Fe}_2\text{O}_3$ Nanoparticles

$\gamma\text{-Fe}_2\text{O}_3$  (maghemite) which is a technologically important magnetic material possess a wide range of applications in the production of permanent magnetic materials [94], magnetic refrigeration, information storage, controlled drug delivery, bioprocessing and ferrofluids [95,96]. At nanoscale, these composite materials have attracted great interest for widely usage as electromagnetic shielding, biosensors, electrochromism,

and corrosion resistance due to their excellent electrical conductivity, processability, magnetic, mechanical, and environmental sensitivity, as well [97,98].

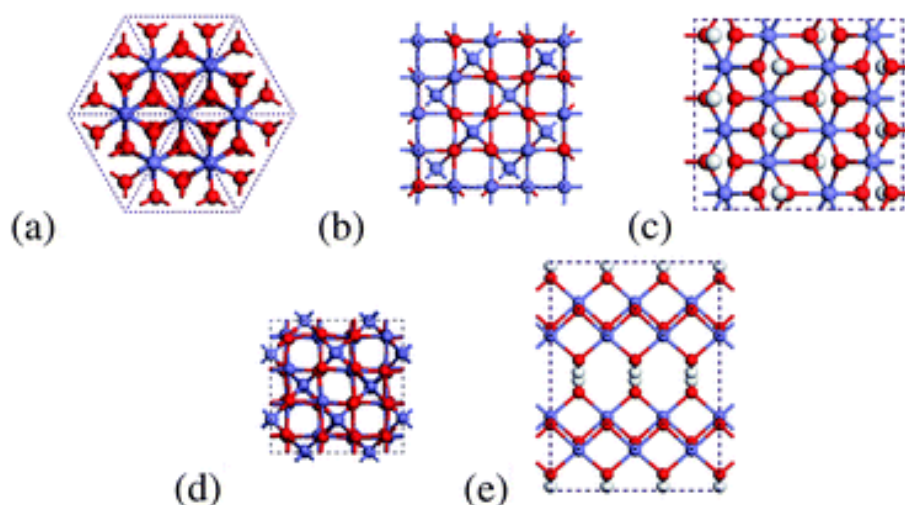


**Figure 2.1** : Crystal structures of iron oxide nanoparticles [99].

Moreover, maghemite  $\gamma\text{-Fe}_2\text{O}_3$  is biocompatible and therefore is one of the most extensively used biomaterials for different applications like cell separation, drug delivery in cancer therapy, magnetic induced hyperthermia, MRI contrast agent, immunomagnetic separation IMC and others.

Unfortunately, it is very difficult to synthesize a single-phase nanocrystalline  $\gamma\text{-Fe}_2\text{O}_3$  via both conventional and chemistry-based processing routes, due to the fact that the nanocrystallites tend to aggregate and coarsen at the calcination temperatures [100]. To prevent the formation of unwanted crystallite coarsening and particle aggregation and to stabilize the maghemite phase, several attempts have been conducted to disperse the maghemite phase in a variety of matrix materials such as silica [101,102], porous glass [103], polymers [104], and biomolecules [105].

### 2.3 Electrochemical Impedance Spectroscopy (EIS)

Electrochemical impedance spectroscopy is a powerful tool in biosensor applications, both in fabrication and detection processes. This technique analyzes the changes in interfacial properties of modified electrodes, resulting from the biorecognition process taking place at the surfaces. Formation of a recognition complex between the biological recognition element and the analyte molecule at the conductive or semiconductive transducer interface results in changes in electrical properties, such as capacitance or resistance. Measured impedance is the total result



of each individual contribution from the solution, the support material, the sensing biomolecule, the working electrode and the counter electrode. Therefore, besides the consequent detection through the biorecognition process, a step-by-step analysis can reveal the effects of every single stage of surface modification process, such as the effect of biomolecule immobilization on the transducer. Therefore, this makes electrochemical impedance spectroscopy an indispensable tool not only for detection, but for sensor optimization process as well, which is crucial for attaining high reactivity, stability, and avoidance of nonspecific interactions.

## 2.4 Basic Principles and Terms in Impedance Spectroscopy

The impedance of a system ( $Z$ ) is measured by detecting the current response for an applied voltage perturbation of a small amplitude. It is a complex value because the change in current can occur both in terms of amplitude, and in terms of phase angle ( $\phi$ ) as well. Therefore, the impedance value can be expressed either by the modulus  $|Z|$  with the phase shift  $\phi$ , or by giving the real ( $Z_{re}$ ) and imaginary ( $Z_{im}$ ) parts of the impedance (Figure 2.2). The plot displaying  $\log|Z|$  and  $\phi$  as a function of logarithm of frequency ( $\log f$ ) is termed as a Bode plot, and the plot displaying  $Z_{re}$  and  $Z_{im}$  is called a Nyquist plot.

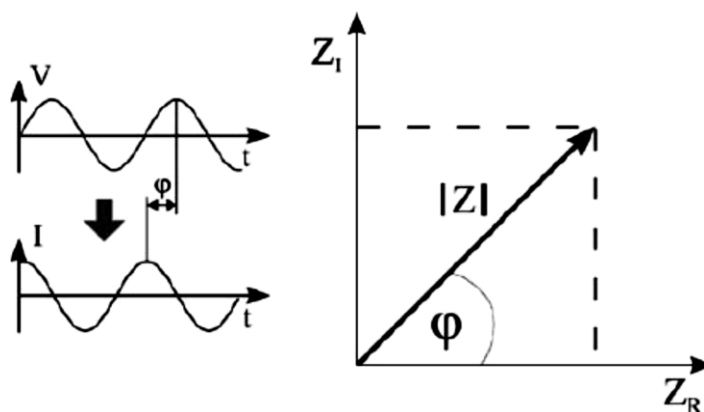


**Figure 2.2 :** Impedance expressed as the modulus  $|Z|$  and the phase angle  $\phi$ , or specified by the real ( $Z_{re}$ ) and imaginary ( $Z_{im}$ ) parts.

Impedance measurements are not performed at a single frequency value, it rather covers a wide frequency spectrum, so it is called spectroscopy. And this impedance spectrum allows the characterization of surfaces and layers, also giving information on exchange and diffusion processes. Furthermore, it simplifies the analytical

comparison between different systems through detecting the frequency interval where the relative changes are the most noticeable.

To define the impedance behaviour of an electrolyte solution, usually four elements are referred. These are ohmic resistance, capacitance, constant phase element and Warburg impedance. These ideal or distributed impedance elements, in the arrangements of series and/or parallel circuits, are employed in modelling equivalent circuits to approximate the experimental data with a fitting circuit model. This procedure allows for an in-depth analysis of the impedance behaviour for electrochemical systems.

Figure 2.3 displays a common equivalent circuit called Randles circuit which is applicable in the case of an electrode immersed in an electrolyte. This circuit consists of the solution resistance ( $R_s$ ), the charge transfer resistance ( $R_{ct}$ ), the double layer capacitance ( $C_{dl}$ ), and the Warburg impedance ( $W$ ).

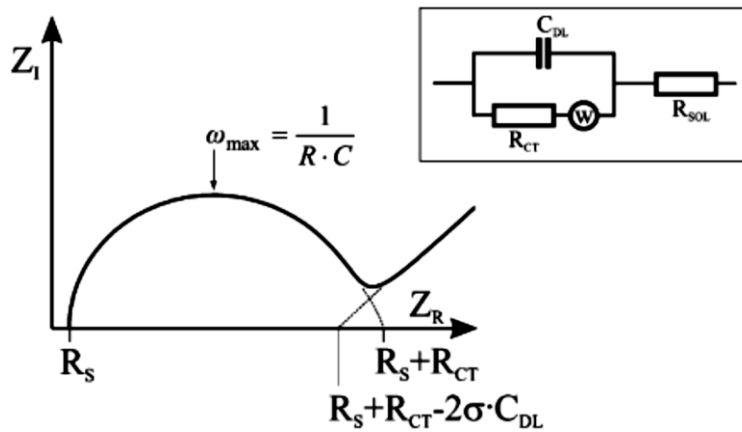


**Figure 2.3 :** Randles' equivalent circuit for an electrode in contact with an electrolyte.

$R_s$  is correlated with the ion concentration and the cell geometry.  $R_{ct}$  arises from the current flow generated by redox reactions at the interface.  $C_{dl}$  refers to charge that is stored in the double layer at the interface and  $W$  comes from the impedance of the current as a result of diffusion from the bulk solution to the interface.  $R_s$  and  $R_{ct}$  values can be determined from the Nyquist plot, and using the frequency at the maximum of the semicircle,  $C_{dl}$  can also be calculated from the formula  $\omega = 2\pi f = 1/R_{ct}C_{dl}$ . The intercept obtained when the 45° line expressing Warburg-limited behaviour is extrapolated to the real axis equals to  $R_s + R_{ct} - 2\sigma C_{dl}$ , from which  $\sigma$ , hence the diffusion coefficients, can be derived.

### **3. EXPERIMENTAL PART**

#### **3.1 Materials**

Iron (II) Chloride Tetrahydrate ( $\text{FeCl}_2 \cdot 4\text{H}_2\text{O}$ ) and Iron (III) Chloride Hexahydrate ( $\text{FeCl}_3 \cdot 6\text{H}_2\text{O}$ ) were purchased by Sigma Aldrich. Diethyleneglycol (DEG) and ammonia ( $\text{NH}_3$ ) were bought from Merck. Oleic acid and tetraethyl orthosilicate (TEOS) were obtained from Fisher Chemical. Sodium hydroxide (NaOH) was bought from Carlo Erba. Iron (II, III) oxide  $\text{Fe}_3\text{O}_4$  nanoparticle was supplied from Sigma Aldrich. Magnetic nanoparticles (SiMAG-Carboxyl and SiMAG-30T) purchased from Chemicell Company (Germany). Magnetic nanoparticles with DNA binding which are called as SiMAG-Cola, SiMAG-3C-Cola, and SiMAG-6C-Cola were provided from Sentromer DNA Technologies Company. Moreover, special synthesized DNA oligonucleotides called as ttr4 and dT20 were also obtained from Sentromer DNA Technologies Company. Phosphate buffer solution was bought from Sigma Aldrich. Ethanol and methanol being of analytical grade were also purchased by Merck. Distilled water was used.

#### **3.2 Synthesis of $\text{Fe}_3\text{O}_4$ Nanoparticles**

Firstly 2mmol  $\text{FeCl}_2 \cdot 4\text{H}_2\text{O}$  and 4mmol  $\text{FeCl}_3 \cdot 6\text{H}_2\text{O}$  were dissolved in 40g diethyleneglycol (DEG). Then  $\text{N}_2$  gas was circulated in reaction flask during 20 minutes. Separately 16 mmol NaOH was dissolved in 40g DEG. Then it was added to the metal chloride solution. After that the solution was stirred on magnetic stirrer in room temperature during 30 minutes (Figure 3.1). Oil bath was heated to  $220^\circ\text{C}$ . After it reached to that heat, the reaction flask was taken place inside of the oil bath and it was stirred on the that heat approximately 1-1,5 hours.



**Figure 3.1 :** Photograph shows synthesis of  $\text{Fe}_3\text{O}_4$  nanoparticles inside the three-neck glass flask.

After that time, the reaction flask was taken out from the oil bath. Then it was cooled to the room temperature without any interference. It took nearly 1,5 hour. The magnetic stirrer was taken out from the cooled down reaction flask. Afterwards the reaction was terminated by adding 2,6mmol oleic acid dissolved in 20g DEG. Precipitation started in the course of the addition. It was allowed for precipitation to mixture nearly 12 hours.

After precipitation, the product in reaction flask was transferred to tubes, and the tubes were centrifuged (Figure 3.2). At the end of the centrifugation, the liquid part was decanted, and the solid part, the product was separated. The product was lay down to filter paper. Then it was washed with methanol 3 or 4 times. After washing process, the product on to the filter paper was dried inside the oven at  $50^\circ\text{C}$  during 12 hours. Finally, as a result of that process the product,  $\text{Fe}_3\text{O}_4$  nanoparticles were synthesized [106].

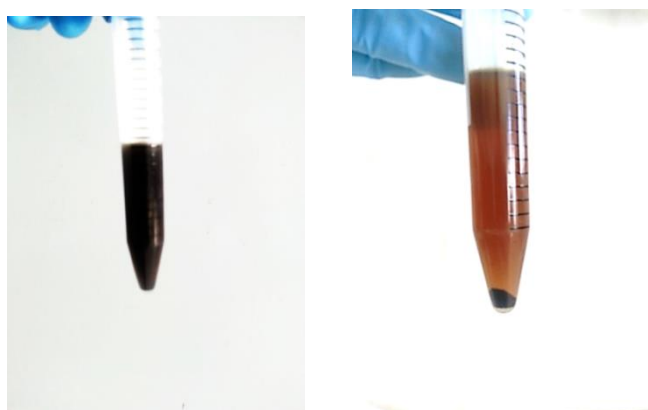


**Figure 3.2 :** Photograph shows the dispersion of  $\text{Fe}_3\text{O}_4$  nanoparticles in centrifuge tube before and after centrifuge.

### 3.3 Synthesis of Fe<sub>2</sub>O<sub>3</sub> Nanoparticles

M. Aliahmad et al [107] has reported that  $\gamma$ -Fe<sub>2</sub>O<sub>3</sub> nanoparticles can be produced while Fe<sub>3</sub>O<sub>4</sub> nanoparticles are calcinated at 300°C during 3 hours. In this way, Fe<sub>3</sub>O<sub>4</sub> nanoparticles were calcinated in the oven at 300°C during 3 hours while the temperature of oven were increased 5°C per one minute. At the end of the procedure,  $\gamma$ -Fe<sub>2</sub>O<sub>3</sub> nanoparticles were obtained (Figure 3.3).



**Figure 3.3 :** Photograph shows the Fe<sub>2</sub>O<sub>3</sub> nanoparticles after calcination process.

### 3.4 Synthesis of Fe<sub>2</sub>O<sub>3</sub>@SiO<sub>2</sub> Nanoparticles

0,25g Fe<sub>2</sub>O<sub>3</sub> nanoparticles were dissolved in 40mL ethanol. Then it was dispersed in solution during 1 hour using ultrasonic bath. After dispersion, 3mL concentrated NH<sub>4</sub>OH was added to mixture, and then with high stirring rate 0,5mL TEOS was added. The solution was stirred during 12 hours. After that time, it was centrifuged, and washed three times with ethanol. The particles were dried. As a result of the procedure, Fe<sub>2</sub>O<sub>3</sub>@SiO<sub>2</sub> nanoparticles were obtained [108].

### 3.5 Binding Process of DNA Oligonucleotides to Fe<sub>2</sub>O<sub>3</sub>@SiO<sub>2</sub> Nanoparticles

SiMAG-Cola, SiMAG-3C-Cola, and SiMAG-6C-Cola magnetic nanoparticles were synthesized by binding DNA chains to the SiMAG-DNA silica beads. That synthesis was performed by Sentromer DNA Technology Company. The protocol was followed [109].

100  $\mu$ l SiMAG-DNA silica beads was added to the 1mL DNA solution (ex. Cola) which was inside of 1.5 ml microcentrifuge tube. Then it was vortexed and incubated

for 5 minutes at room temperature. After that, the tube was taken place on a magnetic separator for 30 seconds and the bead/DNA-pellet was collected. Then the supernatant was removed and discarded.

1 ml Wash Buffer I, which consists of chemicals such as guanidine hydrochloride and chaotropic salts was added to the tube consisting of bead/DNA-pellet. It was vortexed at room temperature. Then bead/DNA-pellet was collected for 30 seconds with magnet (Figure 3.4). After that, the supernatant was removed and discarded. Washing step was repeated once.

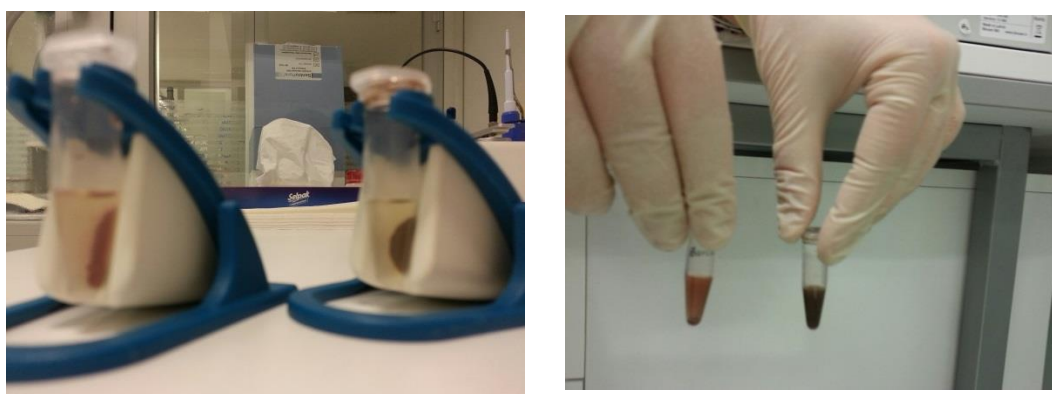


**Figure 3.4:** Photographs show the magnetic nanoparticles in microcentrifuge tube before and after placed on magnet.

1 ml Wash Buffer II which included 70% ethanol was added to the tube consisting of bead/DNA-pellet. It was vortexed for 5 seconds. Then bead/DNA-pellet was collected for 30 seconds with magnet. After that, the supernatant was removed and discarded. That washing step was repeated once with Wash Buffer III consisting with ddH<sub>2</sub>O (double distilled water).

100 Elution Buffer (ddH<sub>2</sub>O) was added to the tube consisting of bead/DNA-pellet. Then it was vortexed and incubated for 10 minutes at 65 °C in a thermo-mixer. After 10 minutes, the tube was vortexed from time to time for the complete resuspension of the pellet. Then beads were collected with the magnet and the solution was transferred with the eluted DNA to a new clean tube. If the solution is not clear, the step is repeated to remove remaining magnetic beads. The isolated DNA can be stored at 2-8 °C in a refrigerator, but for long term storage - 20 °C is recommended.

Table 3.1 shows that the list of the DNA oligonucleotides (ttr4 and dT20) and DNA functionalized SiMAG nanoparticles which were used in study and their base sequences and base numbers.

**Table 3.1 :** Name of the samples used in study and their base sequences and numbers.

<b>Name of Samples</b>	<b>Base Sequence</b>	<b>Number of Base</b>
SiMAG-Cola	CGC ACT TAG GTC	12
SiMAG-3C-Cola	CCC CGC ACT TAG GTC	15
SiMAG-6C-Cola	CCC CCC CGC ACT TAG GTC	18
SiMAG-30T	TTT TTT TTT TTT TTT TTT TTT TTT TTT TTT	30
ttr4	AGC TCA GAC CAA AAG TGA CCA TC	23
dT20	TTT TTT TTT TTT TTT TTT TT	20

### 3.6 Structural, Morphological and Electrochemical Characterization

The structural properties of magnetic nanoparticles, which were synthesized and purchased commercially, were investigated by FTIR-ATR spectrophotometer (Perkin Elmer, Spectrum One, with a universal ATR attachment with a diamond and a ZnSe crystal). Magnetic nanoparticles with and without DNA binding (SiMAG-Carboxyl, SiMAG-Cola, SiMAG-3C-Cola, SiMAG-6C-Cola, and SiMAG-30T) and DNA oligonucleotides (ttr4 and dT20) were analyzed by UV-Vis spectrophotometer. The structure, composition, and morphology of magnetic nanoparticles and DNA oligonucleotides were analyzed with SEM (Scanning Electron Microscopy) (QUANTA 400 F), with 10kV accelerating voltage after samples were coated with gold by Ion Sputter Metal Coating Device (MCM-100 Model) and AFM (Atomic Force Microscopy) (Nanosurf EasyScan2 STM). Electrochemical measurements were performed in 0.1 M PBS with 7 pH using potentiostat 2263 Electrochemical Analyser (Princeton Applied Research, USA) with frequency range between 0.01 Hz and 100 kHz and AC voltage of 10 mV. Three-electrode system, one of platinum wires as working electrode, the other platinum wire as counter electrode, and silver wire as pseudo reference electrode, was used.

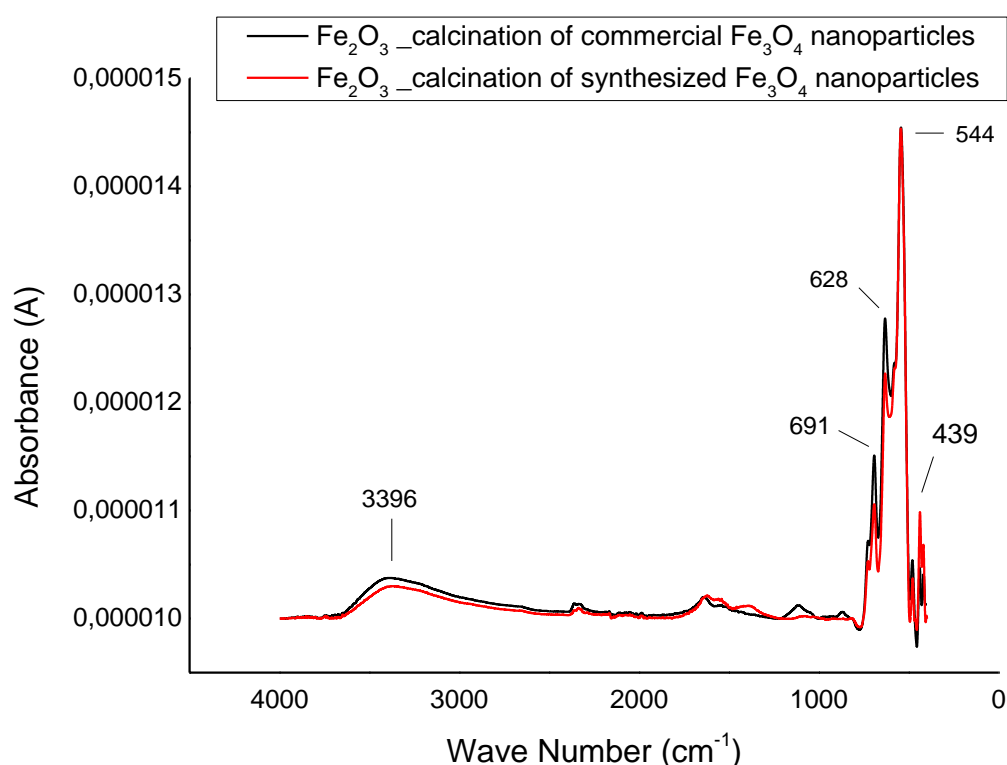




## 4. RESULTS AND DISCUSSION

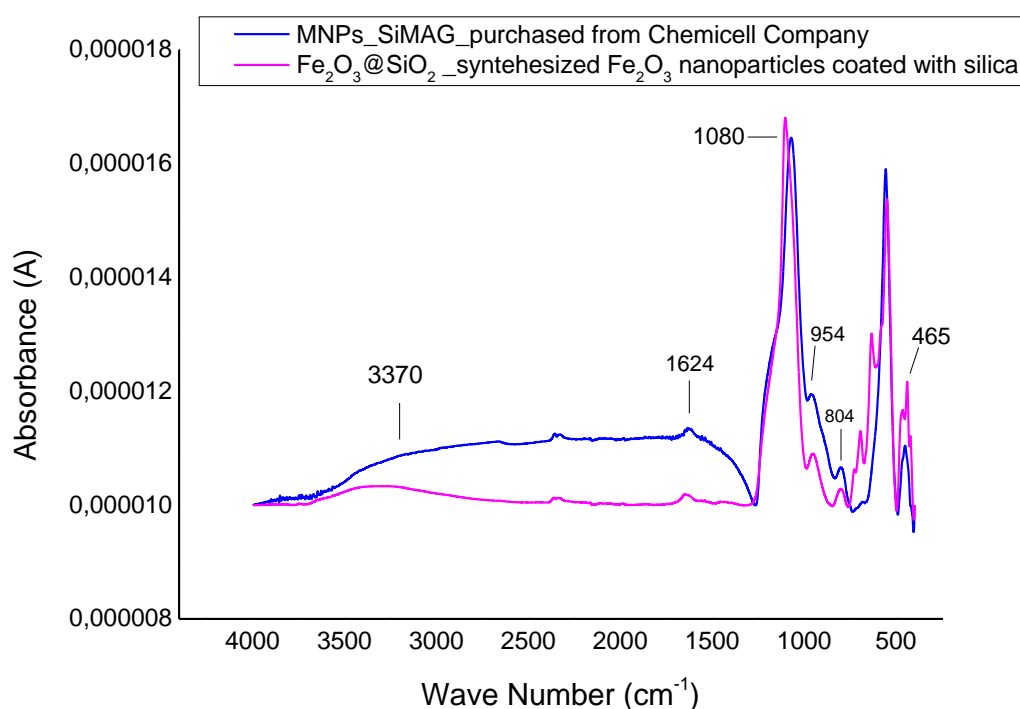
### 4.1 FTIR-ATR Spectroscopic Characterization of Synthesized and Commercial Magnetic Nanoparticles

$\gamma$ -Fe<sub>2</sub>O<sub>3</sub> (maghemite) nanoparticles were obtained from after Fe<sub>3</sub>O<sub>4</sub> nanoparticles were synthesized and calcinated in suitable conditions. FTIR-ATR measurement of the obtained nanoparticles is shown on the Figure 4.1. The bands at 628cm<sup>-1</sup>, 544cm<sup>-1</sup>, and 439cm<sup>-1</sup> are the characteristic Fe-O vibration bands which belong to  $\gamma$ -Fe<sub>2</sub>O<sub>3</sub> crystal form of Fe<sub>2</sub>O<sub>3</sub> nanoparticles. The broad band at 3396cm<sup>-1</sup> results from O-H stretching vibrations belonging to hydroxyl groups which is situated on the surface of nanoparticles [110,111].

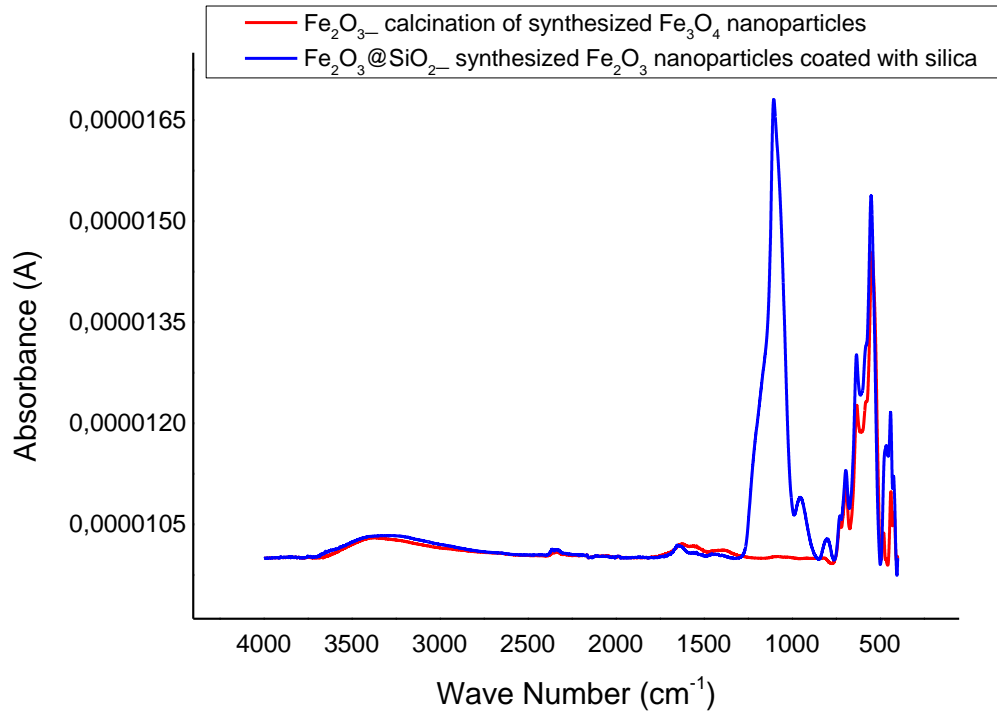


**Figure 4.1 :** FTIR-ATR spectra of  $\gamma$ -Fe<sub>2</sub>O<sub>3</sub> (maghemite) nanoparticle produced by calcination of commercial Fe<sub>3</sub>O<sub>4</sub> and synthesized Fe<sub>3</sub>O<sub>4</sub> nanoparticles.

$\gamma$ -Fe<sub>2</sub>O<sub>3</sub> (maghemite) nanoparticles which are obtained from after Fe<sub>3</sub>O<sub>4</sub> nanoparticles are calcinated are coated with silica. FTIR-ATR results of the magnetic nanoparticles which are both synthesized as  $\gamma$ -Fe<sub>2</sub>O<sub>3</sub>@SiO<sub>2</sub> and taken commercially from Chemicell Company are analyzed and are compared in same figure (Figure 4.2). The band shown at 1080cm<sup>-1</sup> arises from Si-O-Si asymmetric stretching band. Si-OH stretching band (954cm<sup>-1</sup>), Si-O-Si symmetric stretching band (804cm<sup>-1</sup>), and Si-O-Si bending vibrations (465cm<sup>-1</sup>) are the other bands belonging to SiO<sub>2</sub>. The broad band at 3370cm<sup>-1</sup> stems from H bonding because of H<sub>2</sub>O or Si-OH. H-O-H bending vibration is observed at 1624cm<sup>-1</sup> by reason of adsorbed water on silica surface [111]. As a result of the measurements, it is seemed that FTIR-ATR spectra of these two magnetic nanoparticles, synthesized and taken commercially, overlap. FTIR-ATR results of  $\gamma$ -Fe<sub>2</sub>O<sub>3</sub> nanoparticles with and without coated by silica are compared at Figure 4.3.



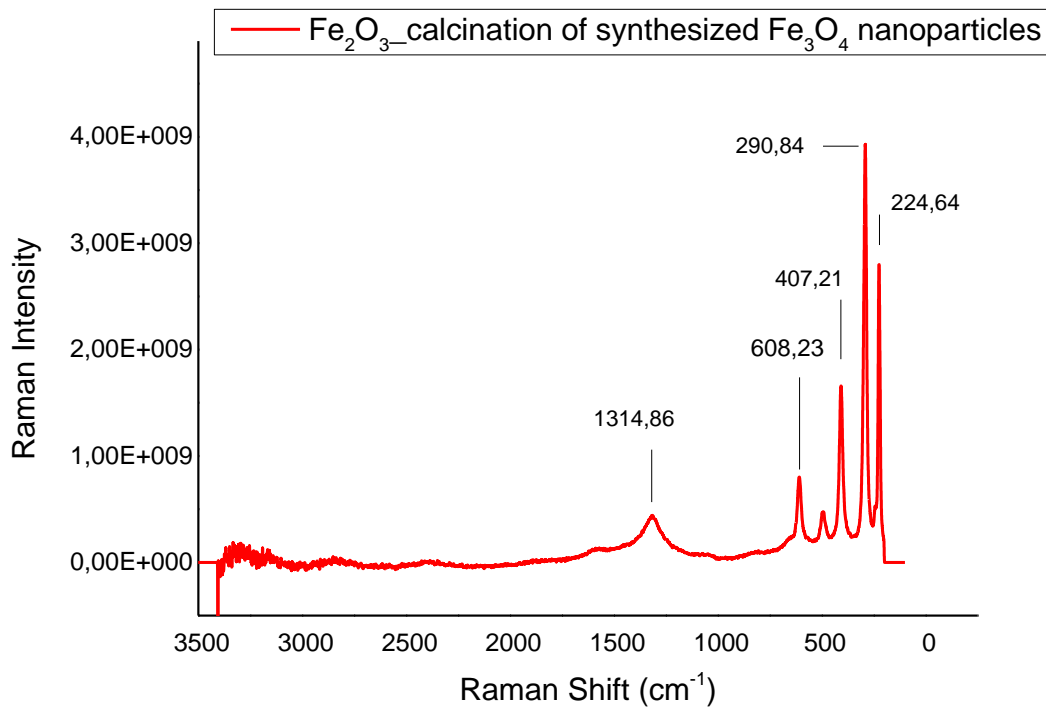
**Figure 4.2 :** FTIR-ATR spectra of SiMAG nanoparticles and synthesized  $\gamma$ -Fe<sub>2</sub>O<sub>3</sub>@SiO<sub>2</sub> nanoparticles.



**Figure 4.3 :** FTIR-ATR spectra of synthesized  $\gamma$ -Fe<sub>2</sub>O<sub>3</sub> nanoparticles and synthesized  $\gamma$ -Fe<sub>2</sub>O<sub>3</sub>@SiO<sub>2</sub> nanoparticles.

#### 4.2 Raman Spectroscopic Characterization of Synthesized and Commercial Magnetic Nanoparticles

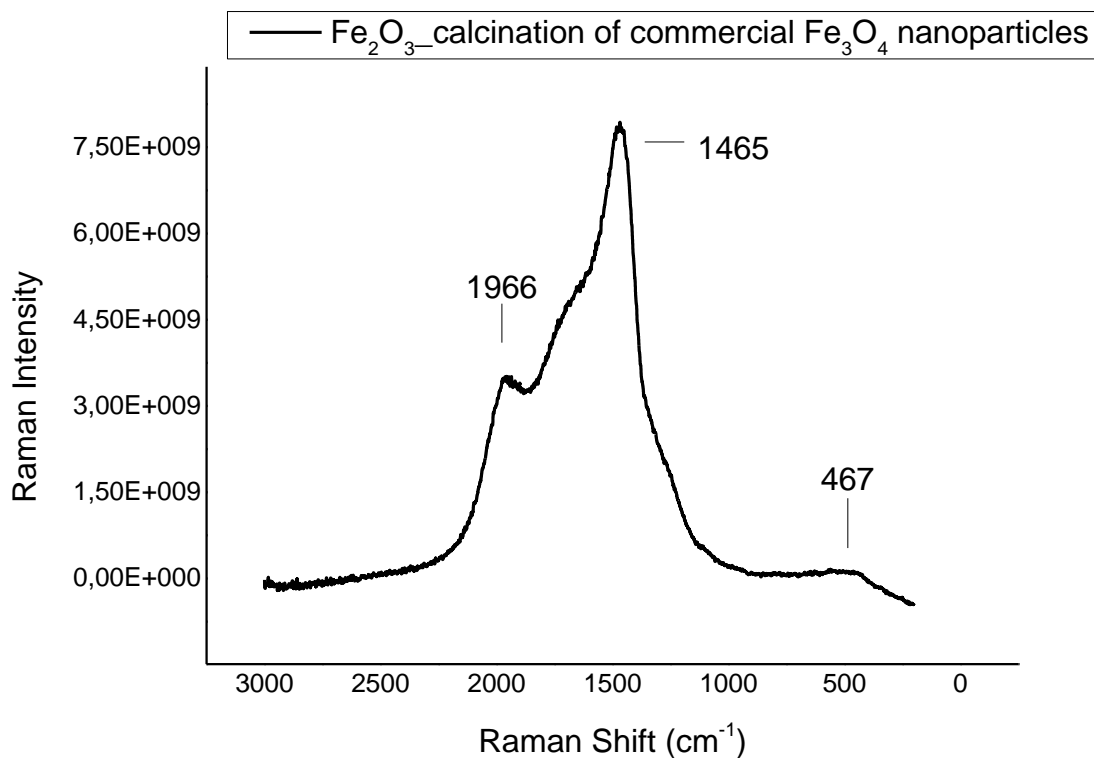
Iron oxide nanoparticles have characteristic band regions on Raman spectra. Peaks ingenerated by symmetric stretching of Fe-O bond are observed between 400-700 cm<sup>-1</sup> range while peaks ingenerated by bending of Fe-O bond at lower energy are observed between 400-500 cm<sup>-1</sup> range. Bands between 1000 and 1500 cm<sup>-1</sup> arise from the interaction between electronic (and magnetic) levels and the light because the laser beam wavelength interacts with the electronic levels [112]. Figure 4.4 shows Raman spectra belonging to  $\gamma$ -Fe<sub>2</sub>O<sub>3</sub> (maghemite) nanoparticles which were obtained from after Fe<sub>3</sub>O<sub>4</sub> nanoparticles were synthesized and calcinated in suitable conditions. Maghemite nanoparticle has characteristic peaks at 350, 500, 700, and 1400cm<sup>-1</sup>; however, 224, 290, 407, 608, and 1314 cm<sup>-1</sup> peaks which belong to hematite ( $\alpha$ -Fe<sub>2</sub>O<sub>3</sub>) nanoparticle are seen from the Figure 4.4 [112, 113]. The reason that laser irradiation at higher powers can easily convert maghemite into hematite form of Fe<sub>2</sub>O<sub>3</sub> [114].



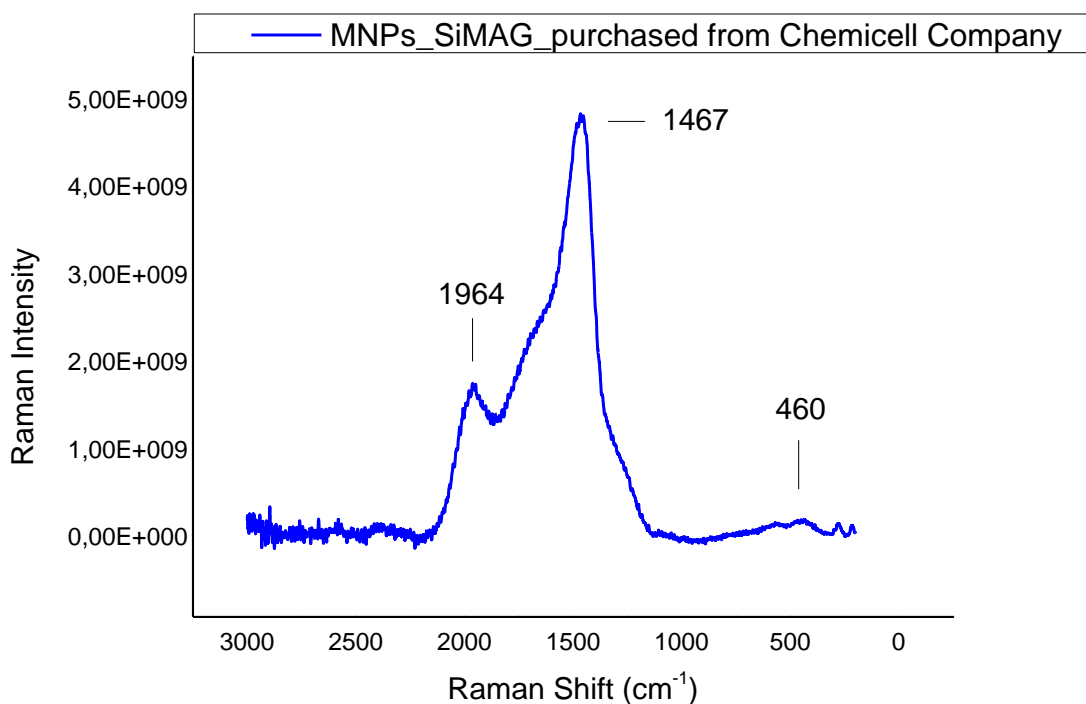
**Figure 4.4 :** Raman spectra of  $\gamma$ -Fe<sub>2</sub>O<sub>3</sub> (maghemite) nanoparticle produced by calcination of synthesized Fe<sub>3</sub>O<sub>4</sub> nanoparticles.

Figure 4.5 shows Raman spectra of  $\gamma$ -Fe<sub>2</sub>O<sub>3</sub> (maghemite) nanoparticle produced by calcination of commercial Fe<sub>3</sub>O<sub>4</sub> nanoparticles. Although the nanoparticles characterized on Figure 4.4 and Figure 4.5 are the same nanoparticles which were obtained by starting from same nanoparticle (magnetite) and following the same processing step to synthesise meghemite nanoparticle, the spectra results of these nanoparticles are different from each other.

Figure 4.6 and Figure 4.7 show Raman spectra of SiMAG nanoparticles obtained from Chemicell Company and synthesized  $\gamma$ -Fe<sub>2</sub>O<sub>3</sub>@SiO<sub>2</sub> nanoparticles by coating of  $\gamma$ -Fe<sub>2</sub>O<sub>3</sub> nanoparticles with silica, respectively. On spectra, there are three bands as 460, 1467, and 1964 cm<sup>-1</sup>. According to the literature, Si-O-Si symmetrical stretching band appears between 450-550 cm<sup>-1</sup> range [115]. Bands between 1400–1600 cm<sup>-1</sup> and 1800–2000 cm<sup>-1</sup> ranges originate from 3TO and 4TO (transversion of optical phonon owing to long wavelength) scattering belonging to silica. Moreover, the band nearly 2030cm<sup>-1</sup> results from hydrogen terminated surface of silica, S-H bond [116]. Figure 4.8 shows Raman spectra of SiMAG nanoparticles obtained from Chemicell Company and synthesized  $\gamma$ -Fe<sub>2</sub>O<sub>3</sub>@SiO<sub>2</sub> nanoparticles by coating of  $\gamma$ -Fe<sub>2</sub>O<sub>3</sub> nanoparticles with silica.



**Figure 4.5 :** Raman spectra of  $\gamma$ -Fe<sub>2</sub>O<sub>3</sub> (maghemite) nanoparticle produced by calcination of commercial Fe<sub>3</sub>O<sub>4</sub> nanoparticles.



**Figure 4.6 :** Raman spectra of SiMAG nanoparticles obtained from Chemicell Company.

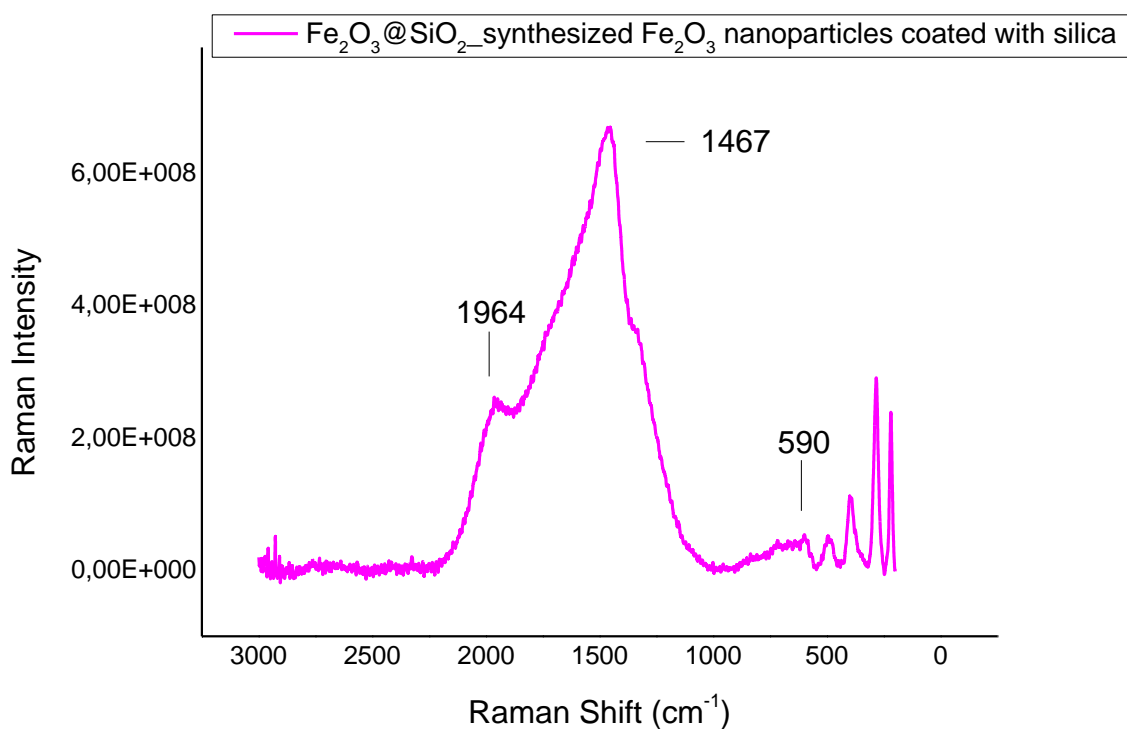


**Figure 4.7 :** Raman spectra of synthesized  $\gamma\text{-Fe}_2\text{O}_3@SiO_2$  nanoparticles by coating of  $\gamma\text{-Fe}_2\text{O}_3$  nanoparticles with silica.

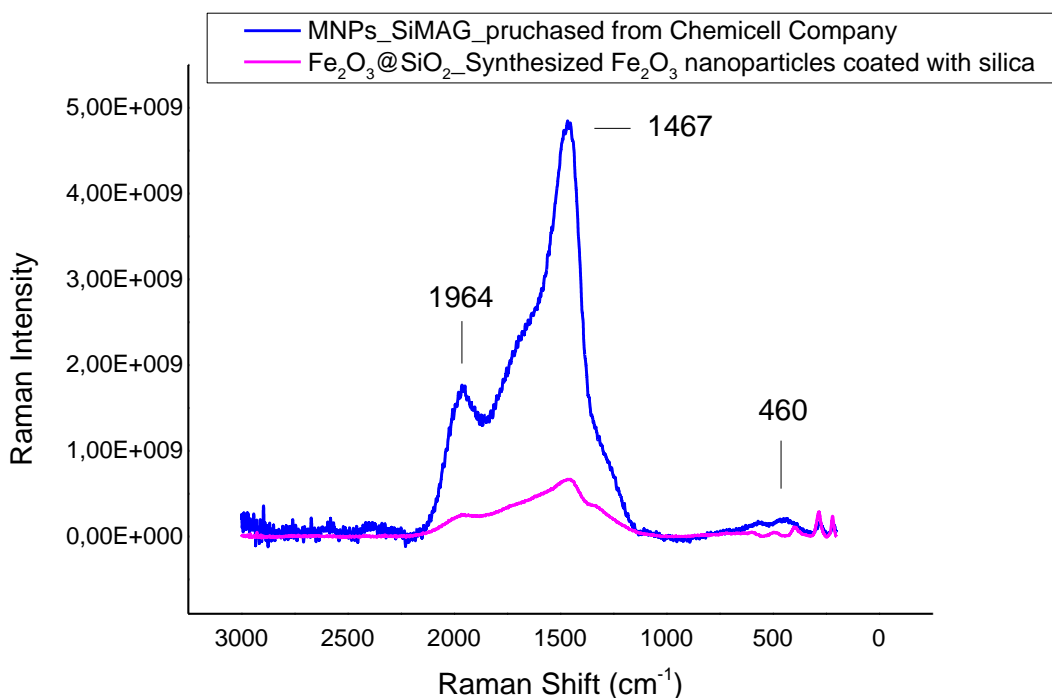


**Figure 4.8 :** Raman spectra of SiMAG nanoparticles obtained from Chemicell Company and synthesized  $\gamma\text{-Fe}_2\text{O}_3@SiO_2$  nanoparticles by coating of  $\gamma\text{-Fe}_2\text{O}_3$  nanoparticles with silica.

### 4.3 UV-Vis Spectrophotometric Analyses of ttr4 DNA Oligonucleotide

At Figure 4.9, it can be seen UV absorbance measurements of a DNA chain which is called with a special name as ttr4. ttr4 DNA oligonucleotide was measured at different concentration (6, 20, 30, and 40nM) at between 200-900nm ranges.

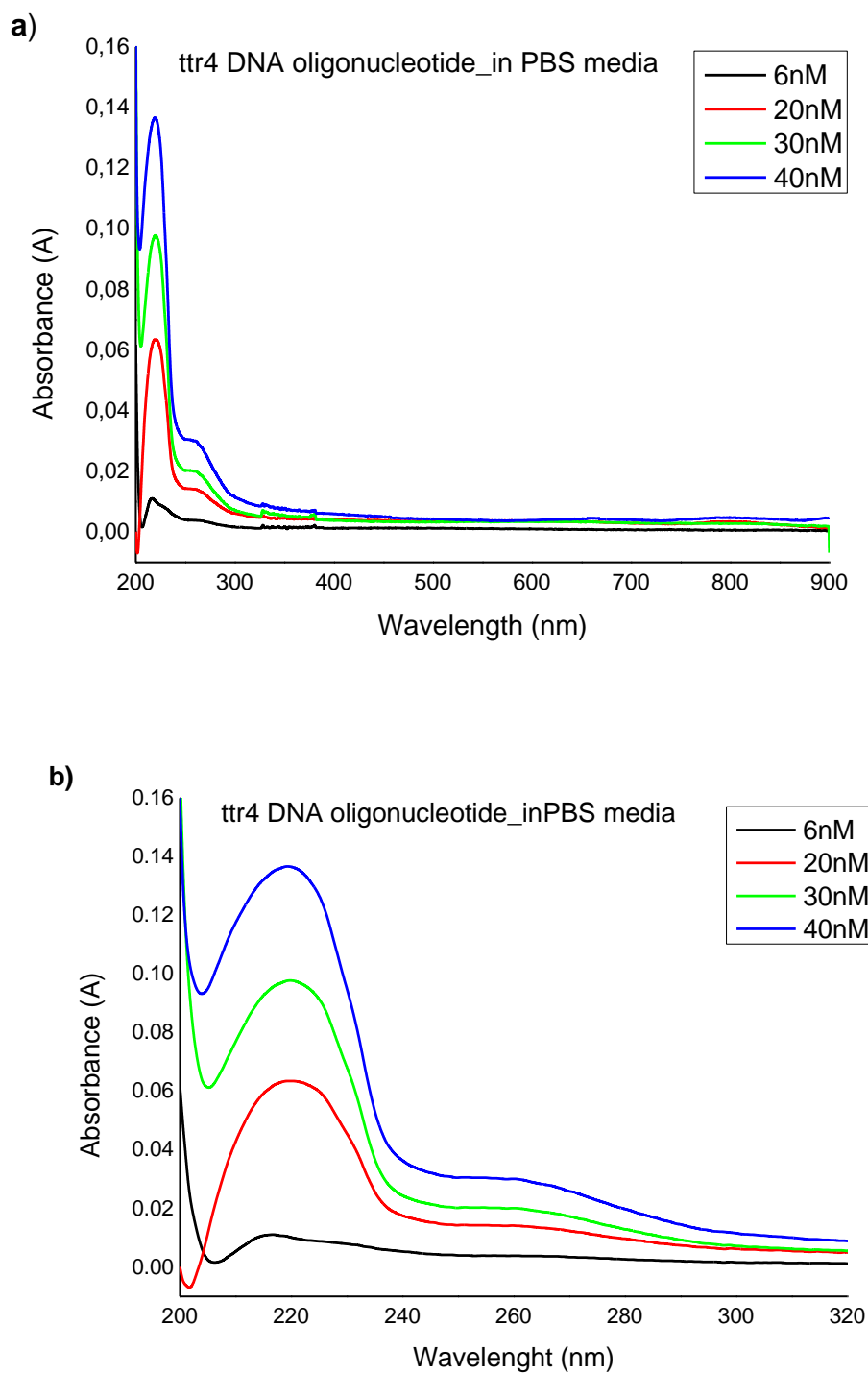


**Figure 4.9:** UV-Vis spectrum of ttr4 DNA oligonucleotide at 6nM, 20nM, 30nM, and 40nM concentration values a) 200-900nm range b) 200-320nm range.

On Figure 4.9, there are two broad bands one of them is around 220 nm, and the other one is between 260 to 280nm. According to the literature, it is known that DNA absorbs the UV light at 260 nm. Moreover, the other known information is that protein also absorbs the UV light at 230nm and 280 nm. While the band at 230nm is because of the absorbance by the peptide bonds, the band at 280 nm is because of by the rings of aromatic acids such as tryptophan, tyrosine, and phenylalanine [117]. Because of the presence of protein with DNA oligonucleotide, it can be seen two broad bands as well as the band belonging to DNA at 260nm from Figure 4.9.

#### **4.4 Uv-Vis Spectrophotometric Analyses of Iron Oxide Magnetic Nanoparticles**

Silica coated iron oxide Magnetic Nanoparticles (SiMAG) and 30 Thymine base bound to SiMAG (SiMAG-30T) were obtained commercially from Chemicell Company. Different DNA oligonucleotides with various longness and order were bound to SiMAG which were by Sentromer DNA Technology Company.

The UV absorbance values of SiMAG with and without binding DNA oligonucleotides (SiMAG, SiMAG-Cola, SiMAG-3C-Cola, SiMAG-6C-Cola, and SiMAG-30T) were measured at different dilution ratios (%0.06, %0.10, and %0.14 (v/v)) diluted with 0.1M phosphate buffer solution (PBS) with 7 pH. The absorption results which belong to each synthesized magnetic nanoparticle were compared in Figures 4.10, Figure 4.11, Figure 4.12, Figure 4.13, and Figure 4.14). The  $\gamma$ -Fe<sub>2</sub>O<sub>3</sub> showed two broad adsorption bands in 250-350 nm and 370-600 nm wavelengths. Absorption bands near 290-310, 360-380, and 430 nm correspond to ligand field transitions of Fe<sup>3+</sup>. A feature near 485-550 nm is assigned to excitation of an Fe-Fe pair. Higher energy features, at wavelengths below 270 nm, are assigned to ligand-to-metal charge-transfer transitions [118].

While concentration of whole magnetic nanoparticles with or without DNA binding increase, the UV absorbance values indicated presence of iron oxide nanoparticles increase in direct proportion to the concentrations. UV spectroscopy is a distinctive method to analysis iron oxide nanoparticles in different concentrations. However, UV spectroscopy is not a suitable method to detect DNA oligonucleotides which attach to the magnetic nanoparticles because of very broad band of the iron oxide. Therefore, difference in base sequence and length of the oligonucleotide cannot be analyzed properly by that method.



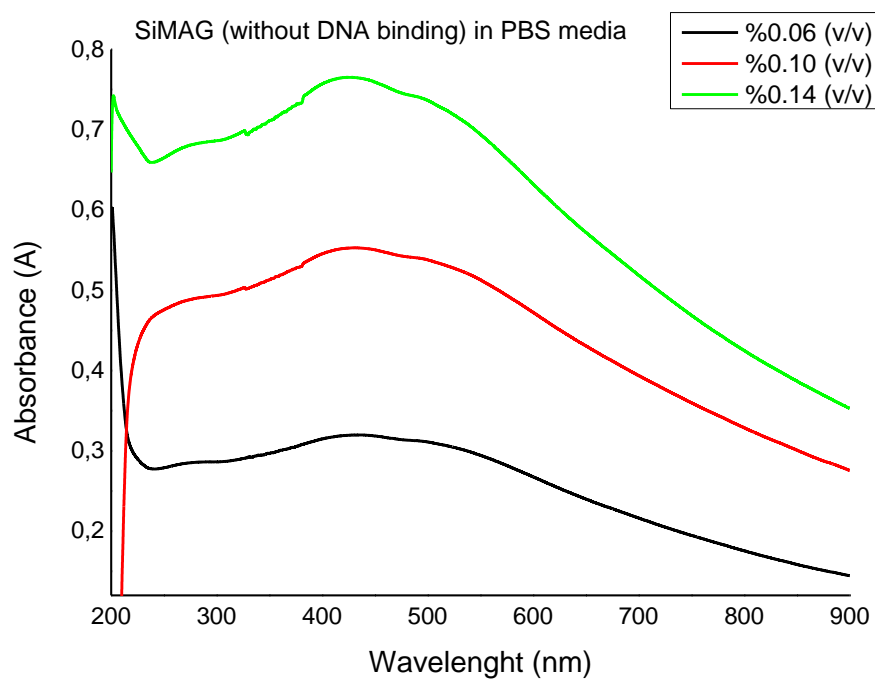


**Figure 4.10 :** UV-Vis spectrum of SiMAG nanoparticles at %0.06, %0.10, and %0.14 (v/v) dilution ratios.

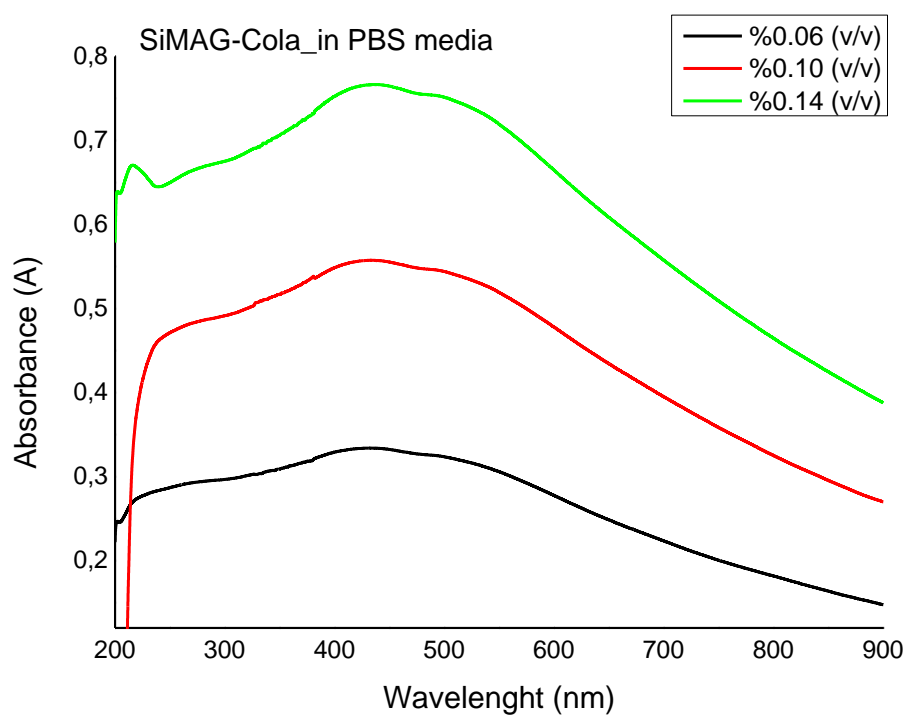


**Figure 4.11 :** UV-Vis spectrum of SiMAG-Cola nanoparticles at %0.06, %0.10, and %0.14 (v/v) dilution ratios.

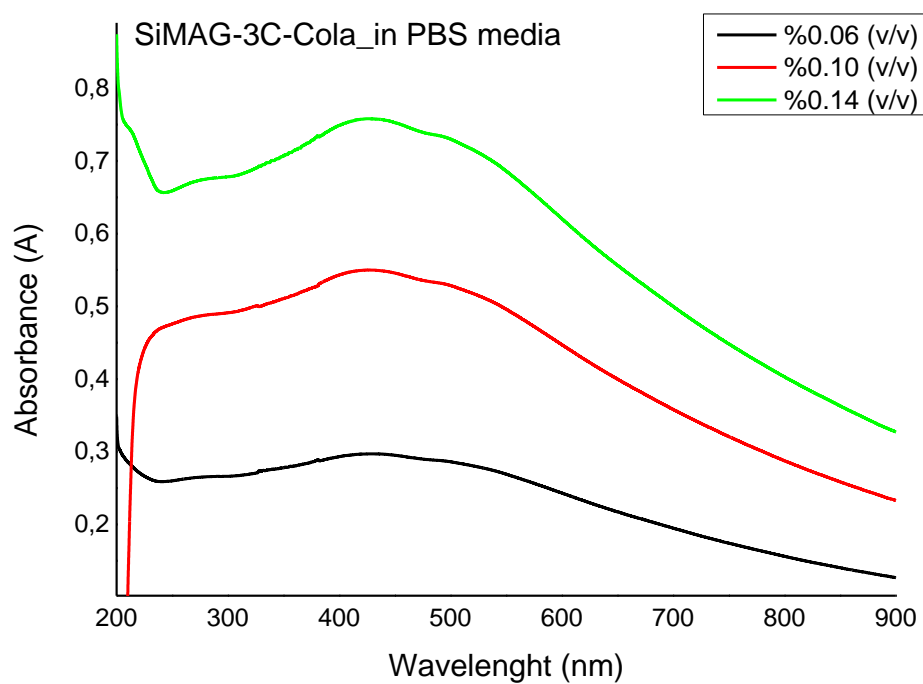


**Figure 4.12 :** UV-Vis spectrum of SiMAG-3C-Cola nanoparticles at %0.06, %0.10 and %0.14 (v/v) dilution ratios.

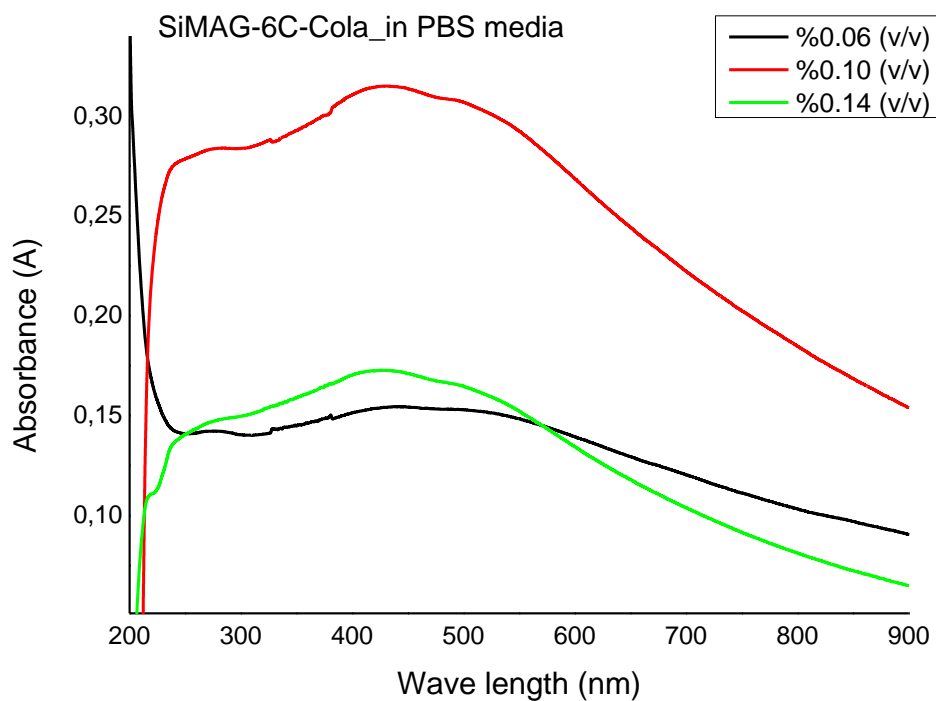


**Figure 4.13 :** UV-Vis spectrum of SiMAG-6C-Cola nanoparticles at %0.06, %0.10, and %0.14 (v/v) dilution ratios.

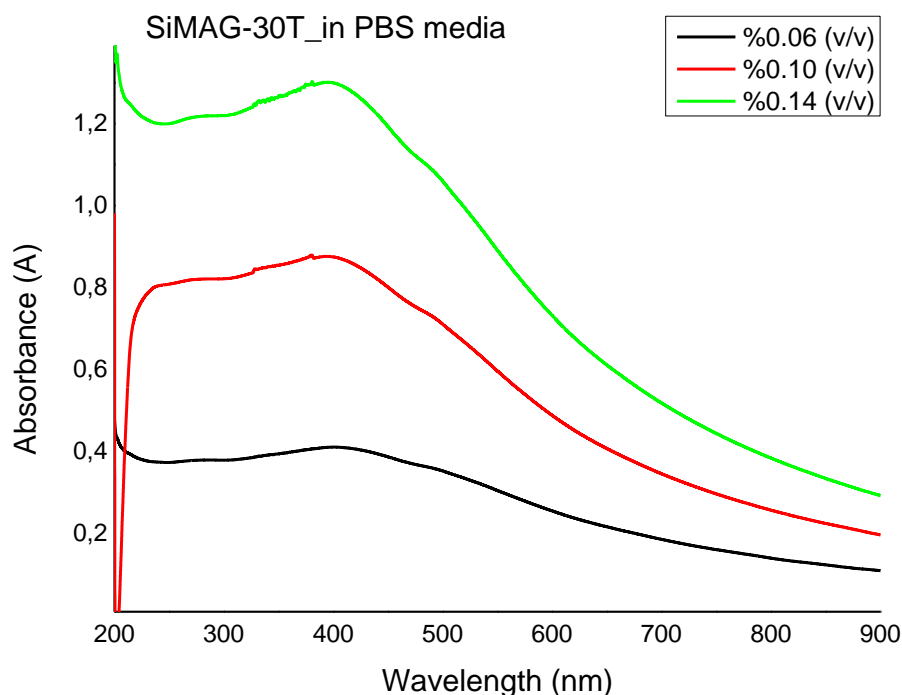


**Figure 4.14 :** UV-Vis spectrum of SiMAG-30T nanoparticles at %0.06, %0.10, and %0.14 (v/v) dilution ratios.

#### 4.5 Electrochemical Impedance Spectroscopy (EIS) Analyses of ttr4 and dT20 DNA Oligonucleotides

In order to obtain additional information of the electrochemical properties of the electrolyte-MNPs(DNA)/electrode system and the electrolyte-DNA/electrode system, EIS measurements of the systems were carried out in electrolyte-MNPs(DNA) or electrolyte-DNA solutions. 0.1M PBS with 7 pH was selected as electrolyte solution. Nyquist plot and Bode-Magnitude plot were obtained from EIS measurements. These plots, especially Nyquist, is given information us about the capacitive or resistive behavior of the system.

To evaluate each electrolyte conditions, low frequency capacitance ( $C_{LF}$ -Low Frequency capacitance) value was calculated from the related Nyquist graph by using the followed equation.

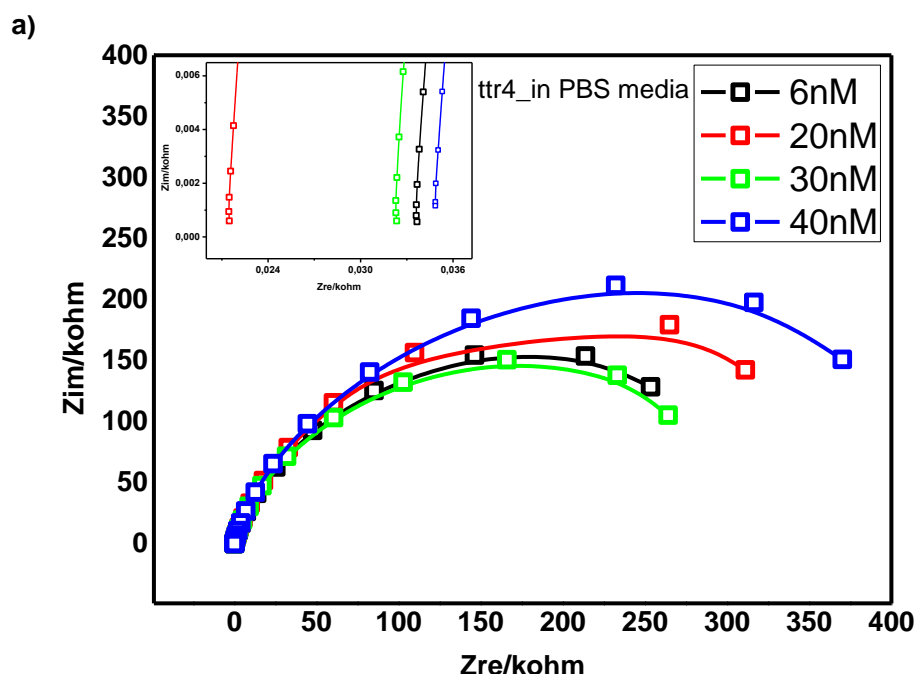
$$C_{LF} = \frac{1}{2\pi f Z_{im}}$$

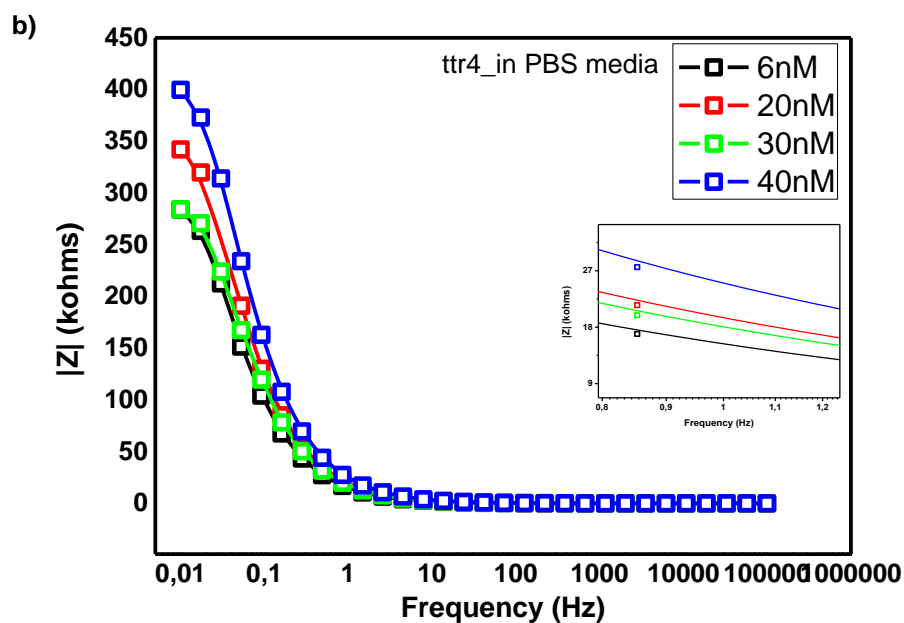
For various concentrations (6nM, 20nM, 30nM, and 40nM) of ttr4,  $C_{LF}$  values at 0.01 Hz were calculated. It was observed that the  $C_{LF}$  values diminished while the ttr4 concentration of the solution was increased.

Bode-Magnitude graph expresses if the sample exhibits resistance or conductive behavior. If the  $|Z|$  value increases at the lowest frequency 0,01Hz, it means that the sample has resistive character.

Double layer capacitance ( $C_{dl}$ ) values were calculated by using average of  $Z$  ( $|Z|$ ) which is obtained from Bode-Magnitude plot.  $C_{dl}$  is proportional to  $1/|Z|$ .

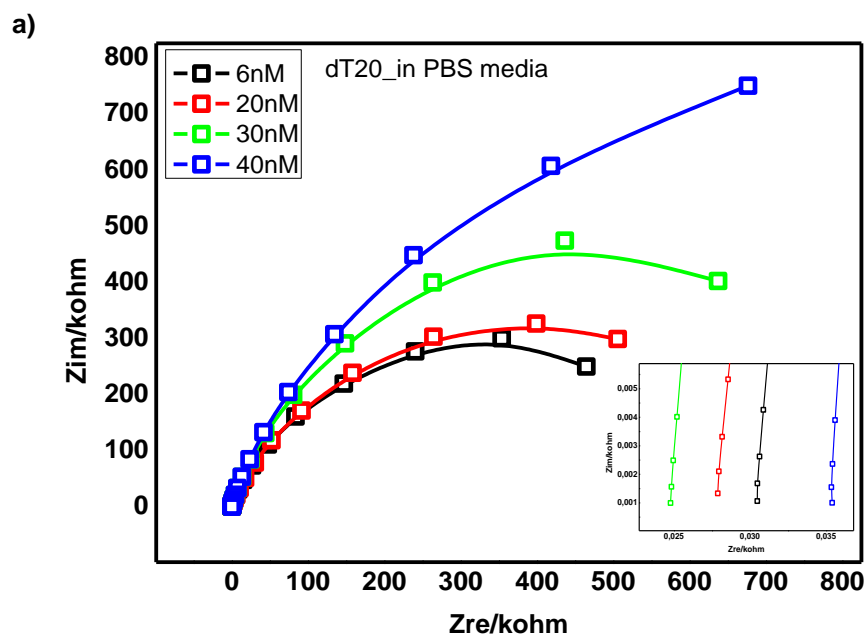
DNA is a negatively charged molecule. Additionally, the electrolyte media consisting of phosphate buffer solution has negatively charged due to  $PO_4^{-3}$  ions. Therefore, the interaction between DNA and the negatively charged ions leads to increase on resistivity [119]. According to the obtained values from Figure 4.15, while the ttr4 concentration of the solution was increased, the  $C_{dl}$  values diminished as well as  $C_{LF}$  values. However,  $|Z|$  values increased while the DNA concentration of the solution was increased.





**Figure 4.15 :** Nyquist (a) and Bode-Magnitude (b) plots of ttr4 DNA oligonucleotide at 6nM, 20nM, 30nM, and 40nM concentration values.

In addition to impedance measurements of ttr4 DNA oligonucleotide, another DNA oligonucleotide which is called as dT20 was evaluated in terms of impedance behavior. Figure 4.16 illustrated the Nyquist and Bode-Magnitude graphs of dT20 DNA oligonucleotide solution system.



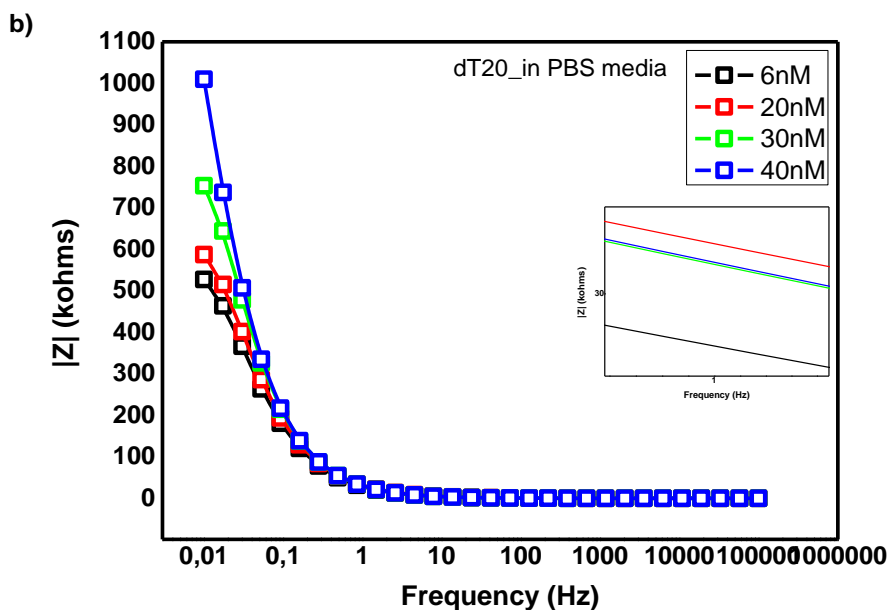


**Figure 4.16 :** Nyquist (a) and Bode-Magnitude (b) plots of dT20 DNA oligonucleotide at 6nM, 20nM, 30nM, and 40nM concentration values.

When the results were compared with that of ttr4 DNA oligonucleotides, it was seen clearly that while the DNA concentration was increased,  $|Z|$  values increased; however,  $C_{dl}$  and  $C_{LF}$  values diminished similar with impedance behavior of ttr4.

#### 4.6 Electrochemical Impedance Spectroscopy (EIS) Analyses of Iron Oxide Magnetic Nanoparticles

The impedance results of magnetic nanoparticles which are SiMAG without DNA binding, SiMAG-Cola, SiMAG-3C-Cola, SiMAG-6C-Cola, and SiMAG-30T were measured by Electrochemical Impedance Spectroscopy. Magnetic nanoparticles samples were diluted at same volume percentage (%0.06, %0.10 and %0.14 (v/v)) in 0.1M PBS with 7 pH media. After impedance measurements of samples, Nyquist and Bode-Magnitude graphs were plotted for each magnetic nanoparticles as SiMAG without DNA binding (Figure 4.17), SiMAG-Cola (Figure 4.18), SiMAG-3C-Cola (Figure 4.19), SiMAG-6C-Cola (Figure 4.20), and SiMAG-30T (Figure 4.21).

The  $|Z|$  values for 0.01Hz,  $C_{dl}$  values for 1Hz, and  $C_{LF}$  values for 0.01Hz belonging to MNP samples which are SiMAG without DNA binding, SiMAG-Cola, SiMAG-3C-Cola, SiMAG-6C-Cola, and SiMAG-30T were calculated from obtained Nyquist and Bode Magnitude graphs.

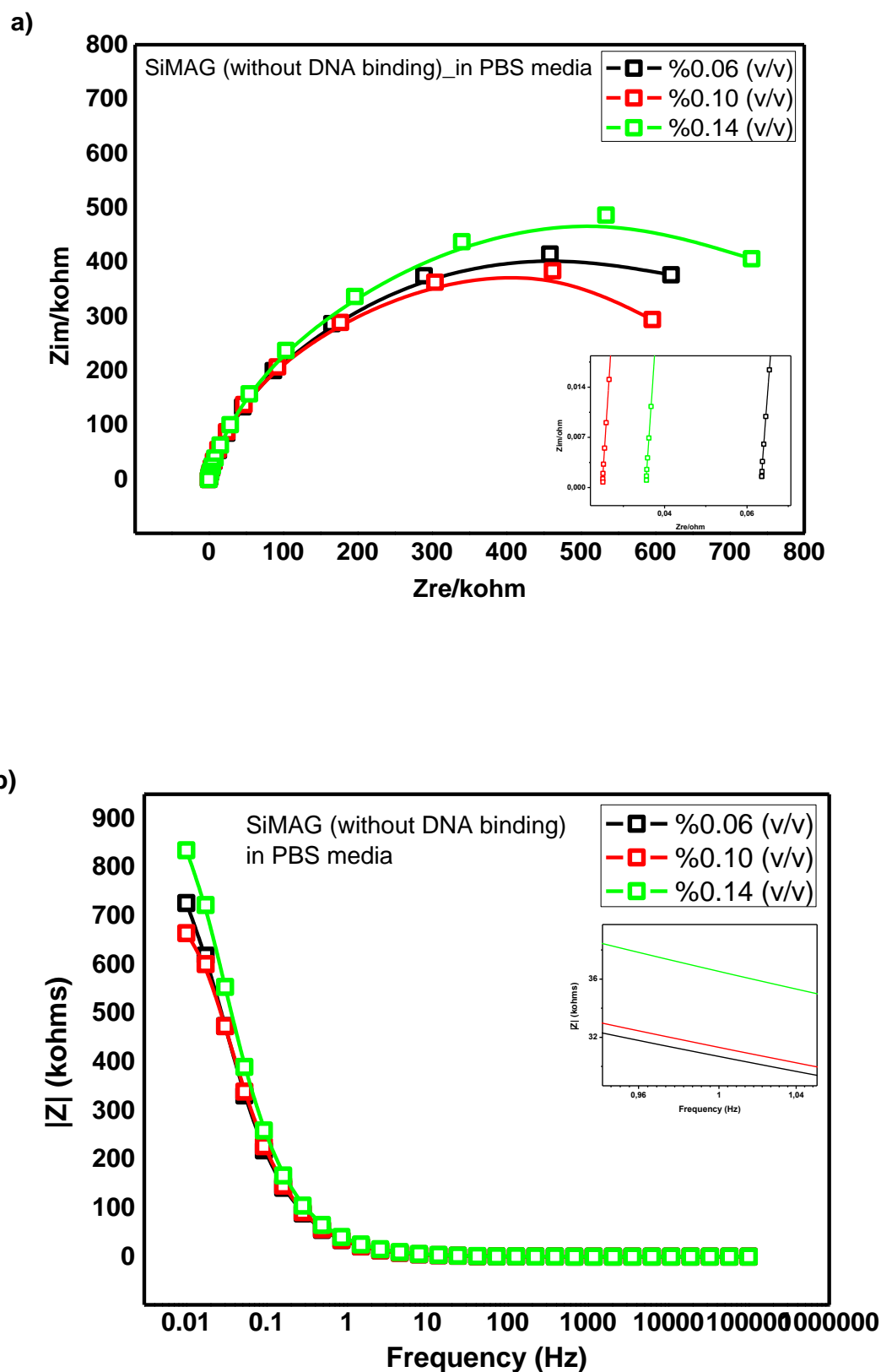


**Figure 4.17** : Nyquist (a) and Bode-Magnitude (b) plots of SiMAG nanoparticle at %0.06, %0.10, and %0.14 (v/v) dilution ratios.

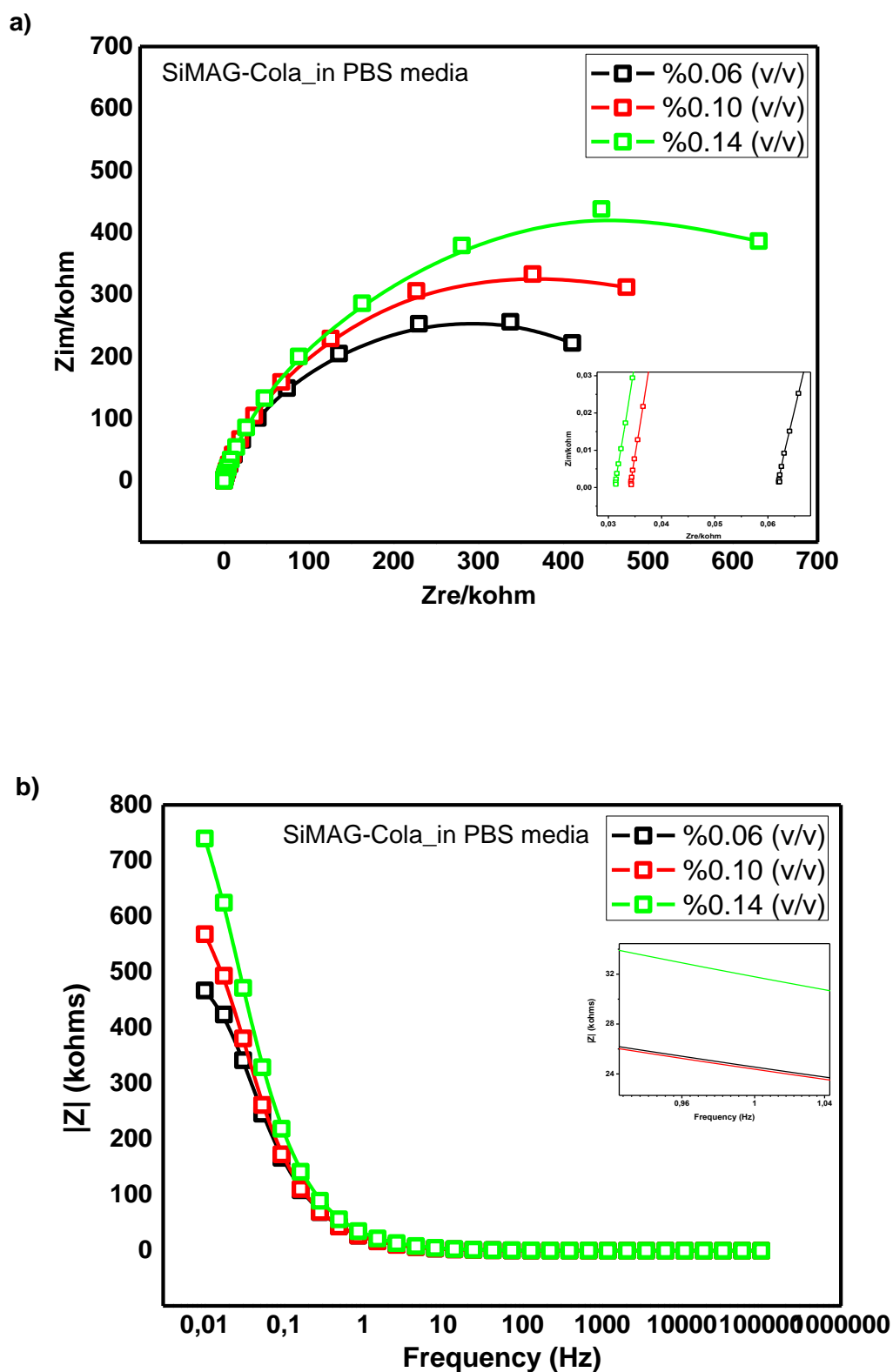


**Figure 4.18 :** Nyquist (a) and Bode-Magnitude (b) plots of SiMAG-Cola nanoparticle at %0.06, %0.10, and %0.14 (v/v) dilution ratios.



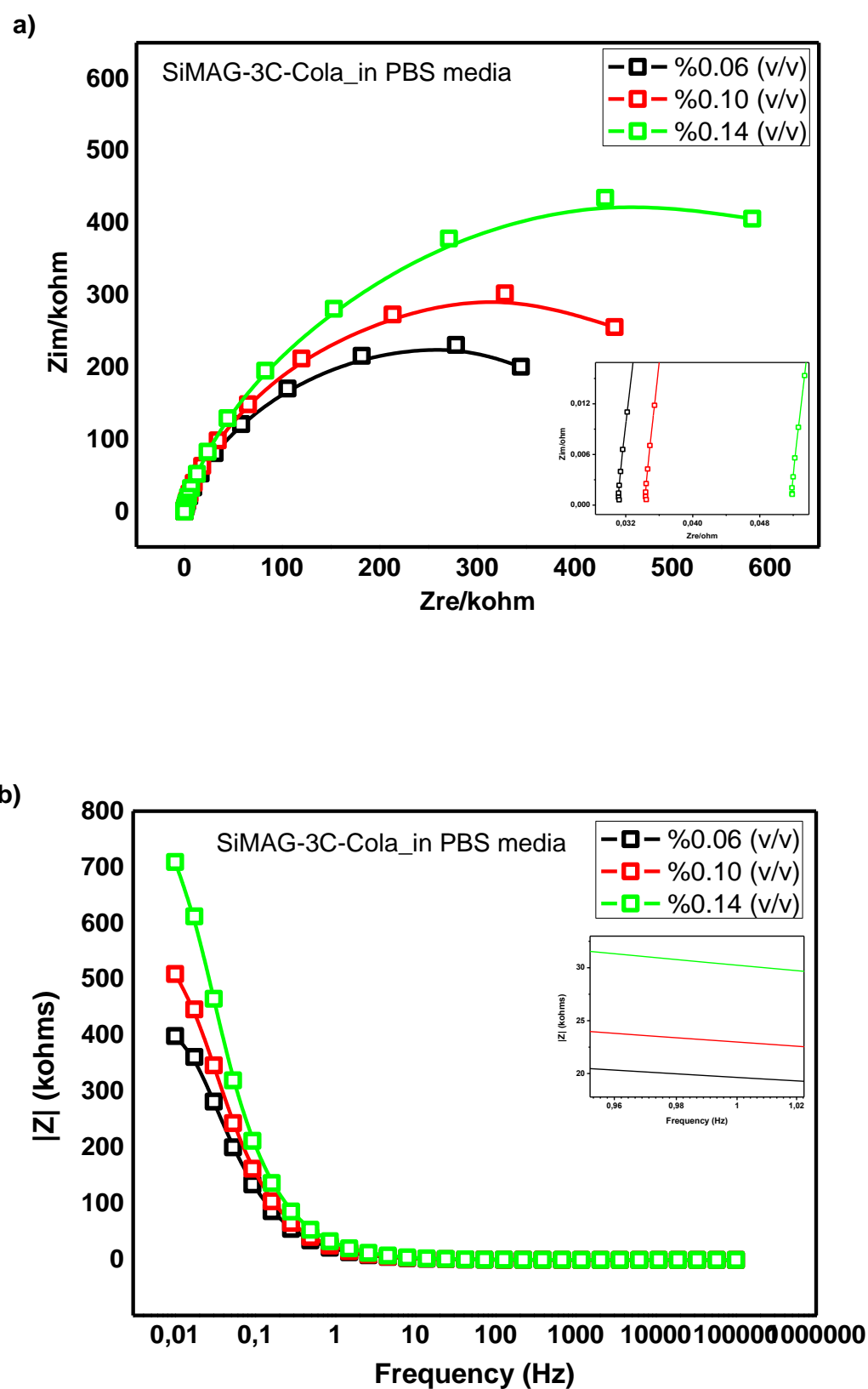


**Figure 4.19** : Nyquist (a) and Bode-Magnitude (b) plots of SiMAG-3C-Cola nanoparticle at %0.06, %0.10, and %0.14 (v/v) dilution ratios.

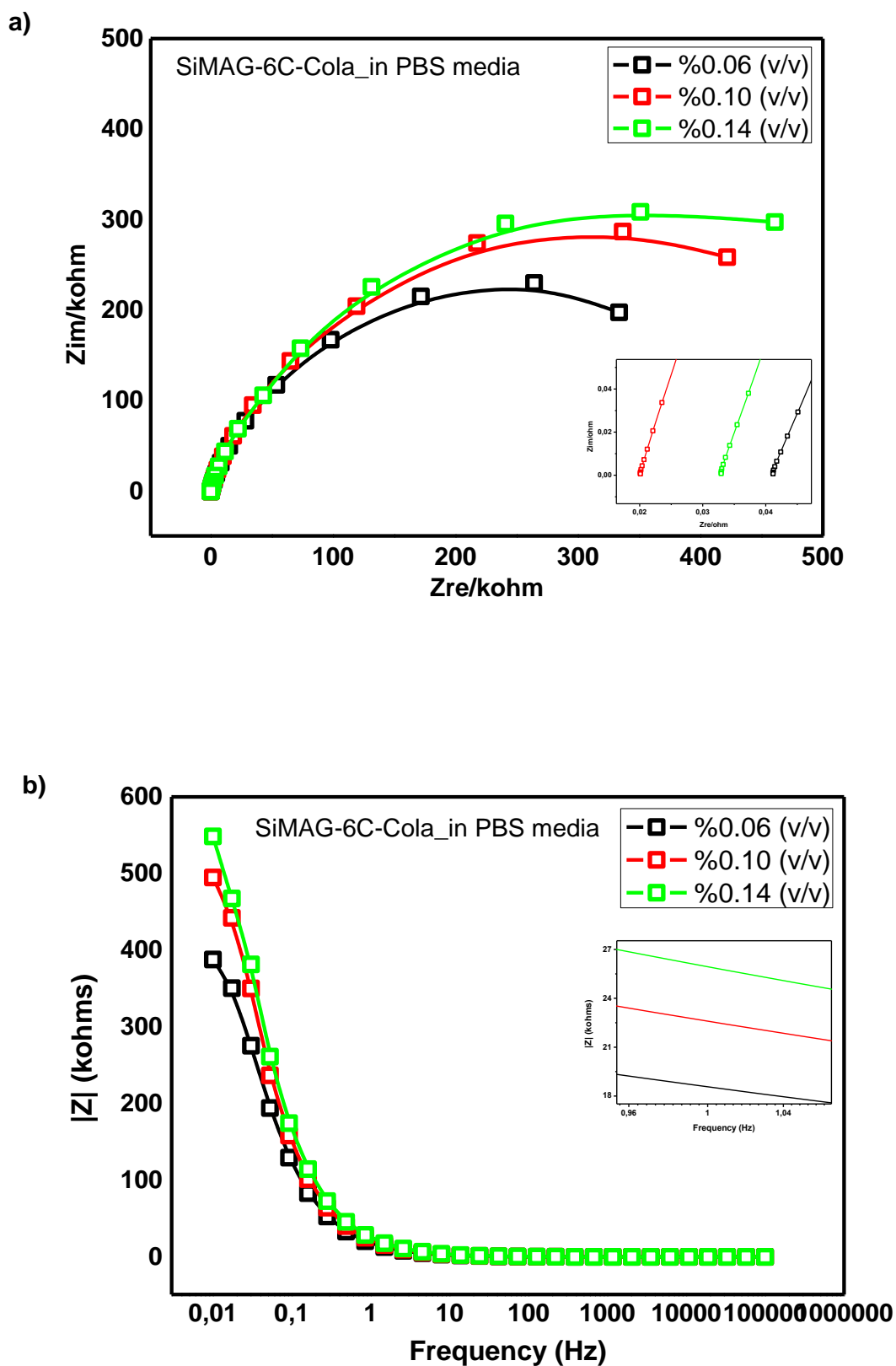


**Figure 4.20** : Nyquist (a) and Bode-Magnitude (b) plots of SiMAG-6C-Cola nanoparticle at %0.06, %0.10, and %0.14 (v/v) dilution ratios.

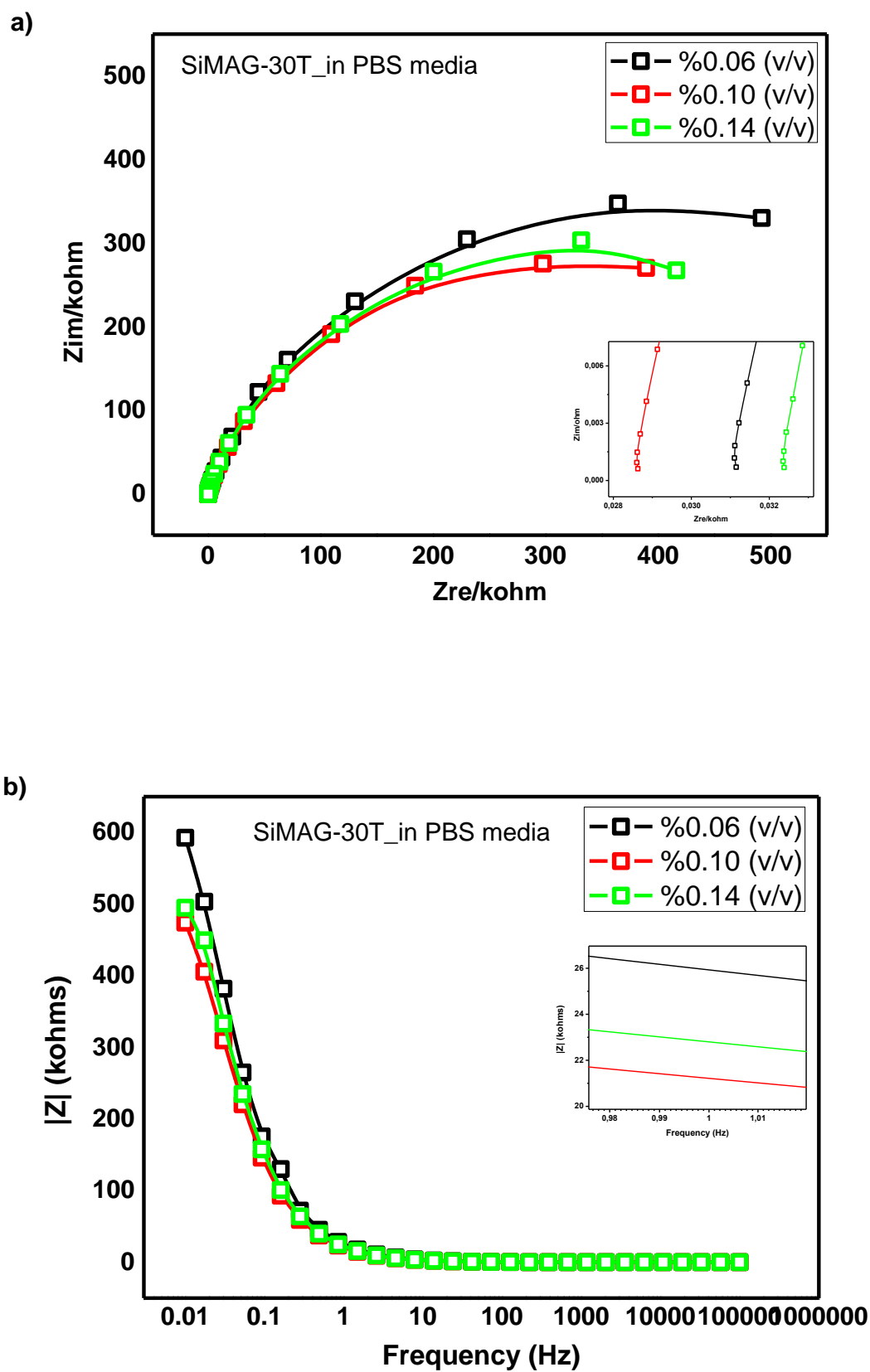


**Figure 4.21 :** Nyquist (a) and Bode-Magnitude (b) plots of SiMAG-30T nanoparticle at %0.06, %0.10, and %0.14 (v/v) dilution ratios.

The  $|Z|$  values for 0.01Hz,  $C_{dl}$  values for 1Hz, and  $C_{LF}$  values for 0.01Hz belonging to MNP samples which are SiMAG without DNA binding, SiMAG-Cola, SiMAG-3C-Cola, SiMAG-6C-Cola, and SiMAG-30T are given in Table 4.1.

**Table 4.1 :** Impedance and Capacitance values obtaining from Nyquist and Bode-Magnitude plots and belonging to SiMAG without DNA binding, SiMAG-Cola, SiMAG-3C-Cola, SiMAG-6C-Cola, and SiMAG-30T at %0.06, %0.10, and %0.14 (v/v) dilution ratios.

Dilution percentage	Impedance & Capacitance values	SiMAG	SiMAG-Cola	SiMAG-3C-Cola	SiMAG-6C-Cola	SiMAG-30T
%0.06 (v/v)	$ Z $ (kohm)	726.7	467.6	397.6	388.1	592.7
	$C_{dl}$ (mF)	0.033	0.041	0.051	0.053	0.039
	$C_{LF}$ ( $\mu$ F)	0.167	0.280	0.310	0.320	0.190
%0.10 (v/v)	$ Z $ (kohm)	664.8	568.5	509.4	494.6	474.0
	$C_{dl}$ (mF)	0.032	0.041	0.043	0.044	0.047
	$C_{LF}$ ( $\mu$ F)	0.213	0.200	0.240	0.240	0.232
%0.14 (v/v)	$ Z $ (kohm)	835.0	741.9	709.8	549.1	495.0
	$C_{dl}$ (mF)	0.027	0.031	0.033	0.038	0.044
	$C_{LF}$ ( $\mu$ F)	0.155	0.160	0.150	0.210	0.235

SiMAG magnetic nanoparticles have a structure form as  $\gamma\text{-Fe}_2\text{O}_3\text{@SiO}_2$ .  $\text{Fe}_2\text{O}_3$  magnetic nanoparticle has low resistive property. However, resistive contribution of silica to the system is the dominant factor in the overall impedance [120]. Moreover, the modification of the metallic surface with an organic layer is an important effect to the system due to decrease the double layer capacitance [119]. As an other point, biofunctionalization layers are physical barriers with a resistance to ionic transfer and diffusion, especially at very low frequencies [121].

Table 4.1 illuminates that SiMAG without DNA binding, SiMAG-Cola, SiMAG-3C-Cola, SiMAG-6C-Cola, and SiMAG-30T exhibited different impedance values; however they exhibit the same characteristic impedance and capacitance behavior associated with increasing of concentration. Therefore it means that  $|Z|$  values increased; nevertheless  $C_{dl}$  and  $C_{LF}$  values diminished while the MNP (SiMAG) concentration was increased.

## 4.7 Interaction Amongst UV Absorbance/Impedance/Concentration

Figure 4.22 demonstrates that concentration increasing of ttr4 DNA oligonucleotide was in direct proportion to UV absorbance at 260nm and impedance value ( $|Z|$ ) for 0.01Hz. However, that concentration increasing was inversely proportional to  $C_{dl}$  and  $C_{LF}$  values (Figure 4.23).

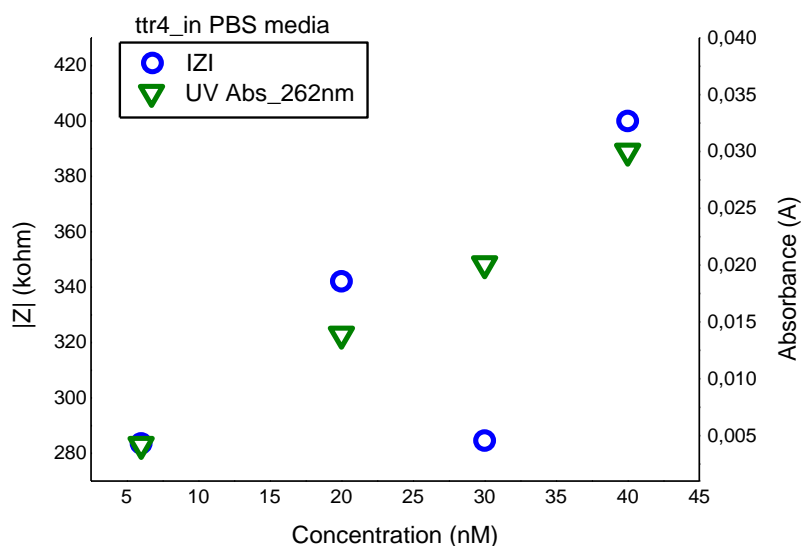


**Figure 4.22 :**  $|Z|$ -Concentration % (v/v) & Absorbance-Concentration % (v/v) plot for ttr4 DNA oligonucleotide.

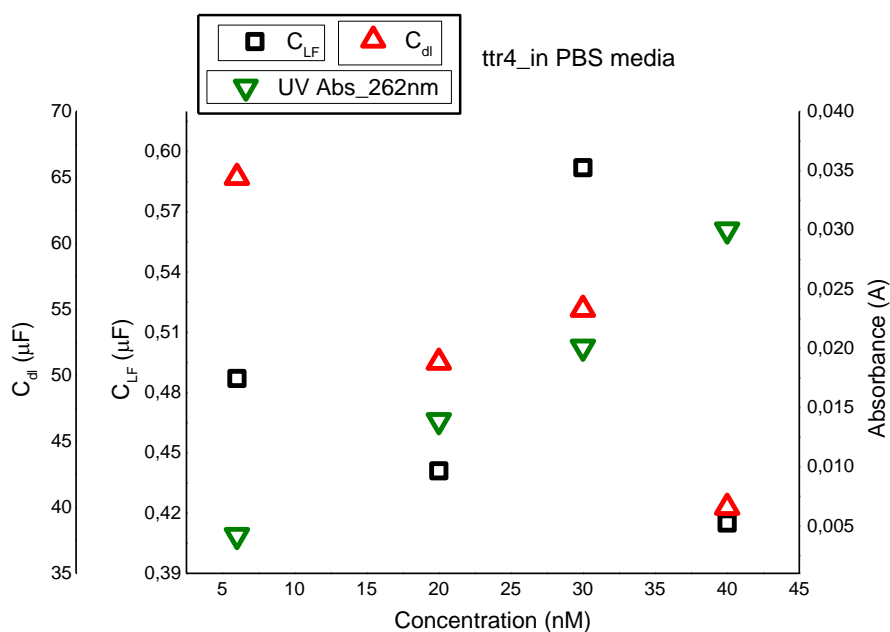


**Figure 4.23 :**  $C_{dl}$ -Concentration % (v/v),  $C_{LF}$ -Concentration % (v/v) & Absorbance-Concentration % (v/v) plot for ttr4 DNA oligonucleotide.

Figure 4.24 expresses the relationship amongst concentration,  $|Z|$ ,  $C_{dl}$ , and  $C_{LF}$  for the other DNA oligonucleotide which is called as dT20. It was observed that when the concentration of the dT20 was increased,  $C_{dl}$ , and  $C_{LF}$  values decreased while  $|Z|$  values ascended.

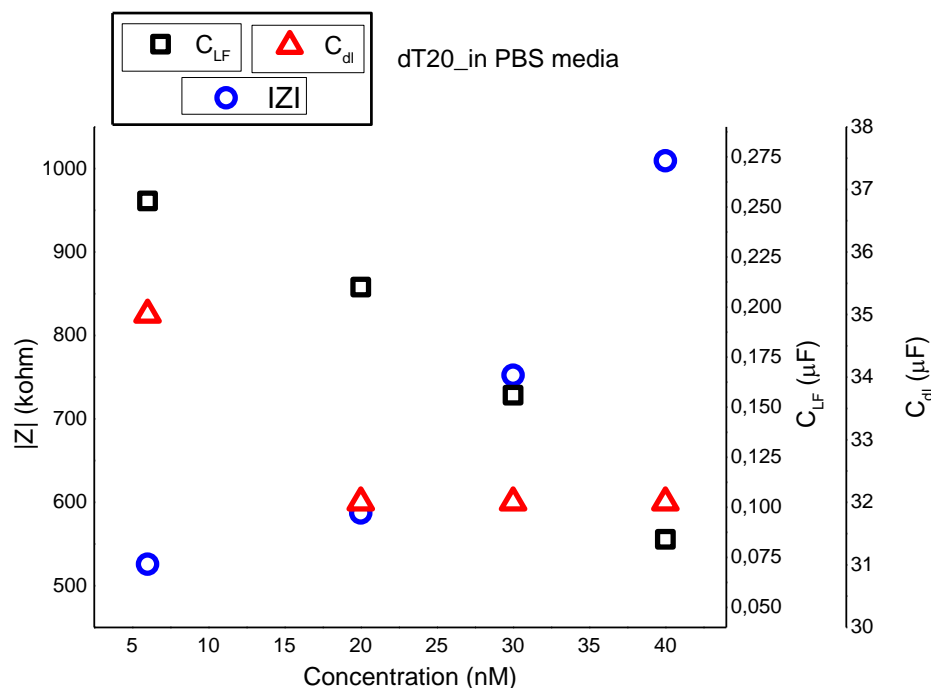


**Figure 4.24 :**  $|Z|$ -Concentration % (v/v),  $C_{LF}$ -Concentration % (v/v), &  $C_{dl}$  Concentration % (v/v) plot for dT20 DNA oligonucleotide.

That comparison related with concentration, absorbance, and impedance was also performed for SiMAG nanoparticles. Three different UV absorbance wavelengths and their absorbance amounts belonging to each concentration value and  $|Z|$  values were displayed at Figure 4.25. These UV absorbance values at different wavelengths and concentrations changed regularly and proportionally.

As it is seen on Figure 4.26, SiMAG without DNA binding exhibited that when the concentration was increased,  $C_{dl}$ , and  $C_{LF}$  values decreased while  $|Z|$  and UV absorbance values increased.

Alteration of UV absorbance associated with concentration increment was observed for three different wavelengths and for each SiMAG with DNA binding. Moreover,  $|Z|$ ,  $C_{dl}$ , and  $C_{LF}$  values were calculated, and then they were compared with UV absorbance values and concentration alterations. The results can be compared with different multiple arrangements on figures belonging to SiMAG-Cola (Figure 4.27,

Figure 4.28), SiMAG-3C-Cola (Figure 4.29, Figure 4.30), SiMAG-6C-Cola (Figure 4.31, Figure 4.32), and SiMAG-30T (Figure 4.33, Figure 4.34).

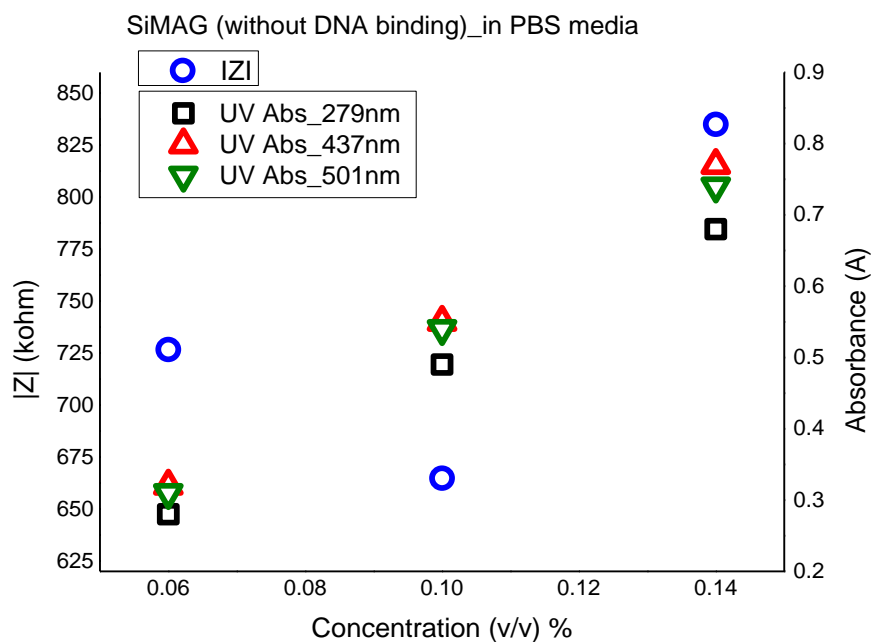


**Figure 4.25 :**  $|Z|$ -Concentration % (v/v) & Absorbance-Concentration % (v/v) plot for SiMAG nanoparticle.

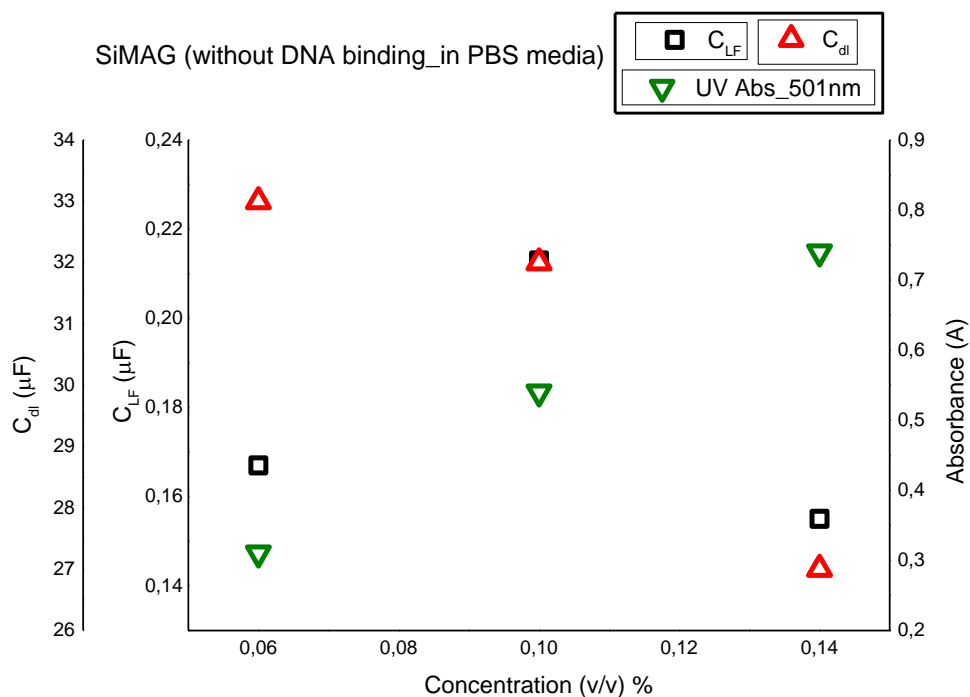


**Figure 4.26 :**  $C_{dl}$ -Concentration % (v/v),  $C_{LF}$ -Concentration % (v/v) & Absorbance-Concentration % (v/v) plot for SiMAG nanoparticle.

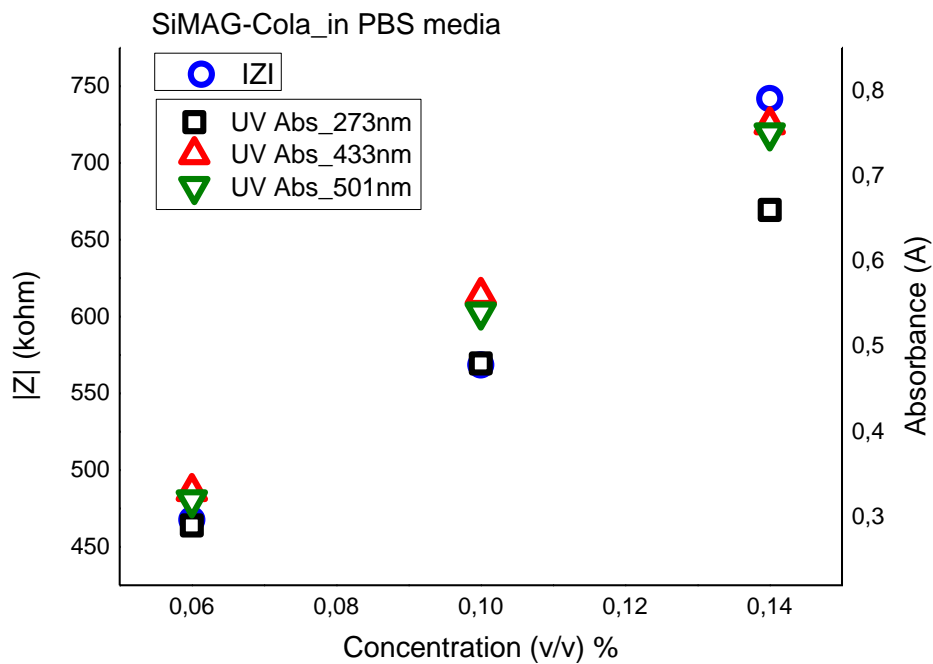


**Figure 4.27 :**  $|Z|$ -Concentration % (v/v) & Absorbance-Concentration % (v/v) plot for SiMAG-Cola nanoparticle.

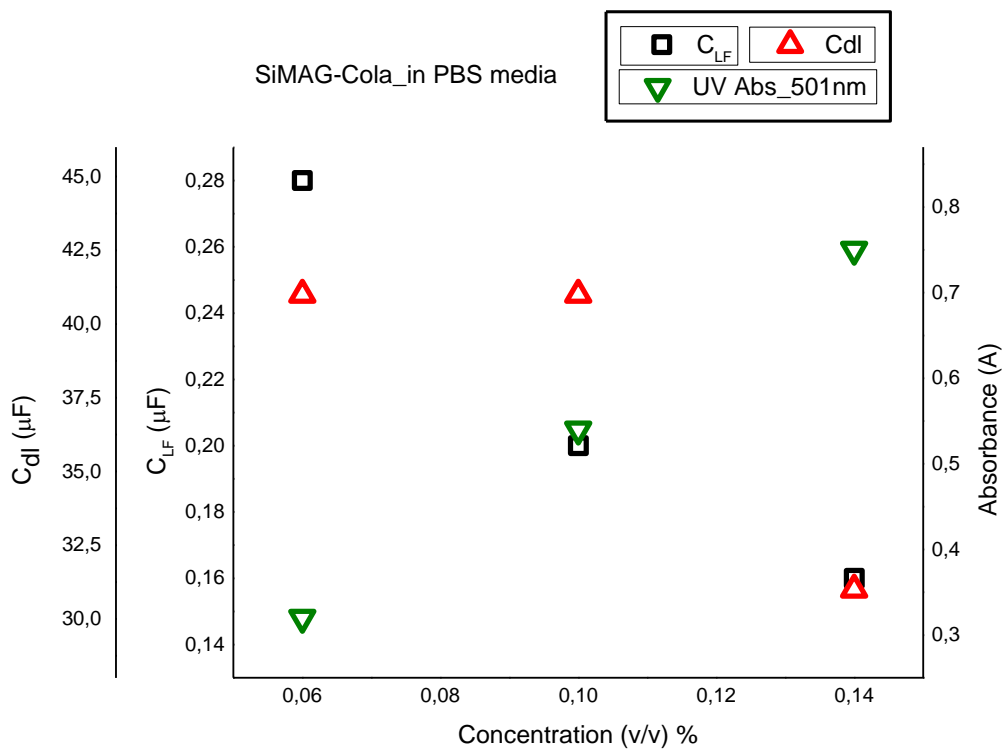


**Figure 4.28 :**  $C_{dl}$ -Concentration % (v/v),  $C_{LF}$ -Concentration % (v/v) & Absorbance-Concentration % (v/v) plot for SiMAG-Cola nanoparticle.



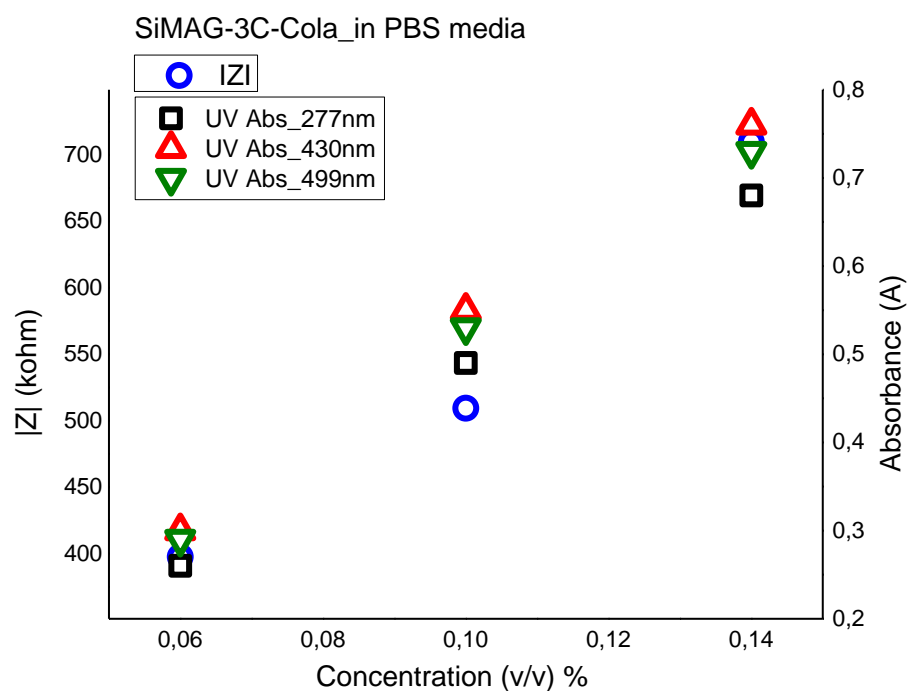


**Figure 4.29 :**  $|Z|$ -Concentration % (v/v) & Absorbance-Concentration % (v/v) plot for SiMAG-3C-Cola nanoparticle.

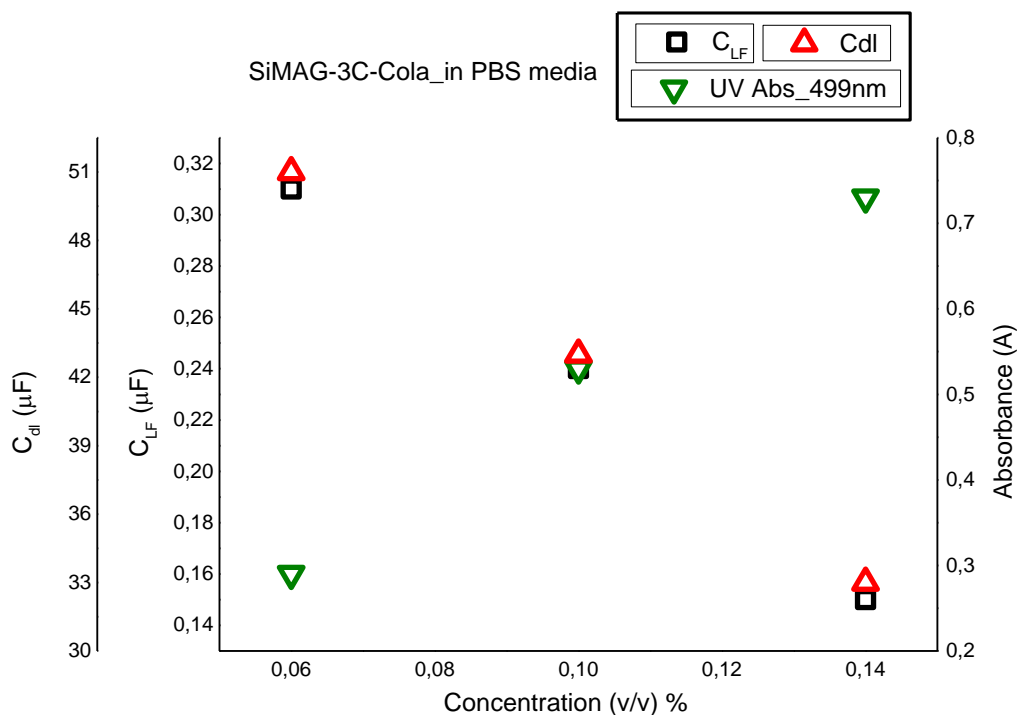


**Figure 4.30 :**  $C_{dl}$ -Concentration % (v/v),  $C_{LF}$ -Concentration % (v/v) & Absorbance-Concentration % (v/v) plot for SiMAG-3C-Cola nanoparticle.

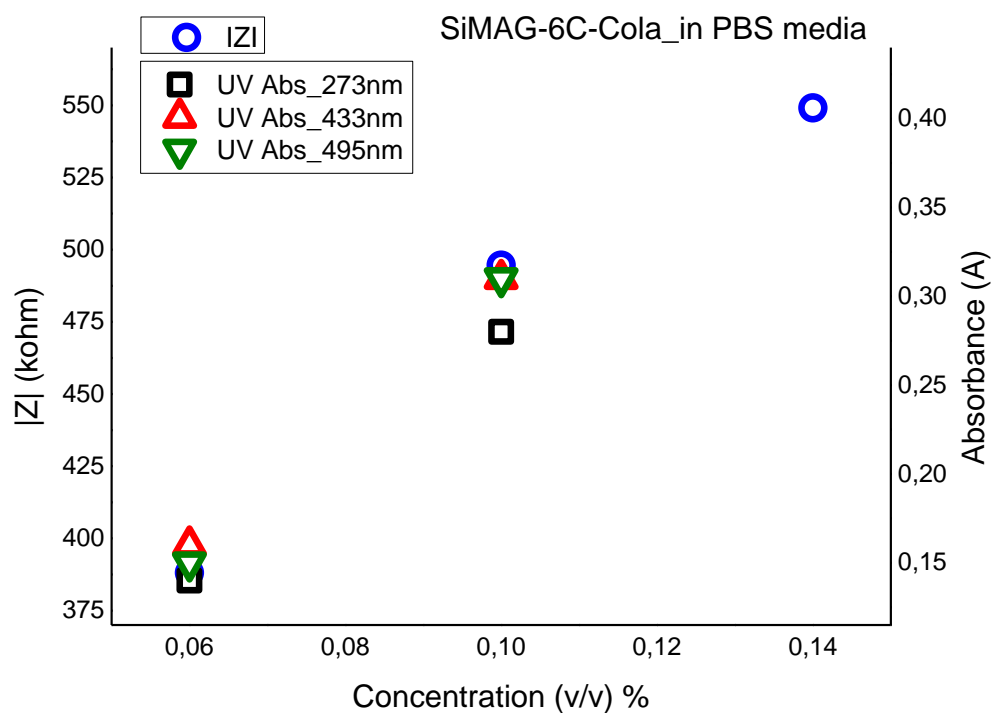


**Figure 4.31 :**  $|Z|$ -Concentration % (v/v) & Absorbance-Concentration % (v/v) plot for SiMAG-6C-Cola nanoparticle.

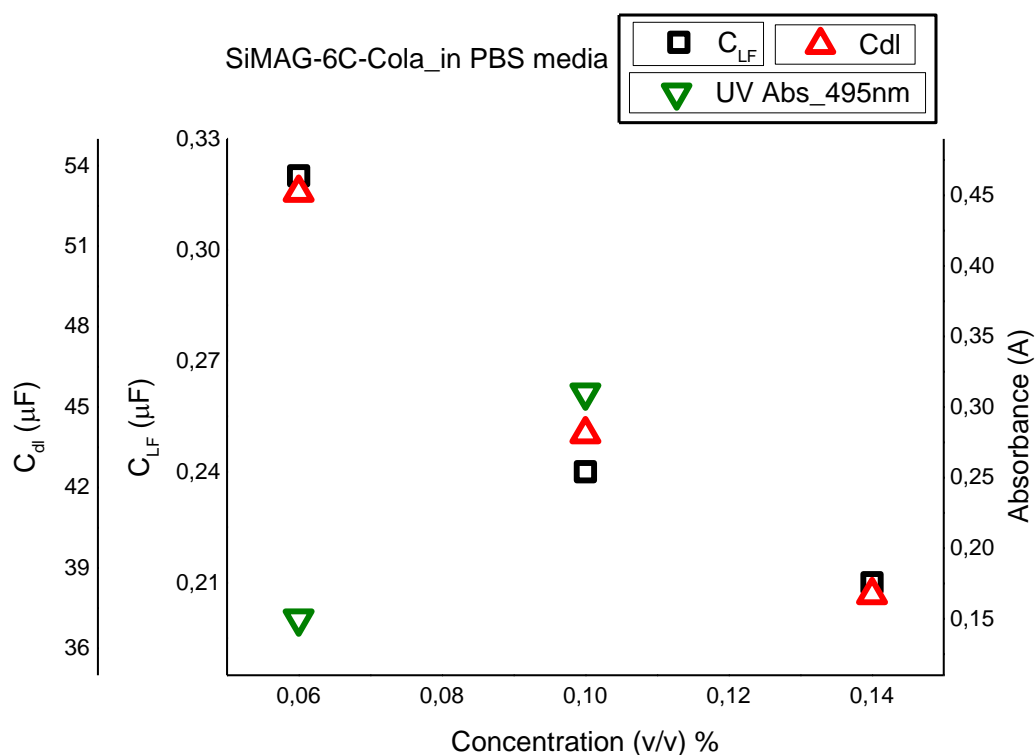


**Figure 4.32 :**  $C_{dl}$ -Concentration % (v/v),  $C_{LF}$ -Concentration % (v/v) & Absorbance-Concentration % (v/v) plot for SiMAG-6C-Cola nanoparticle.

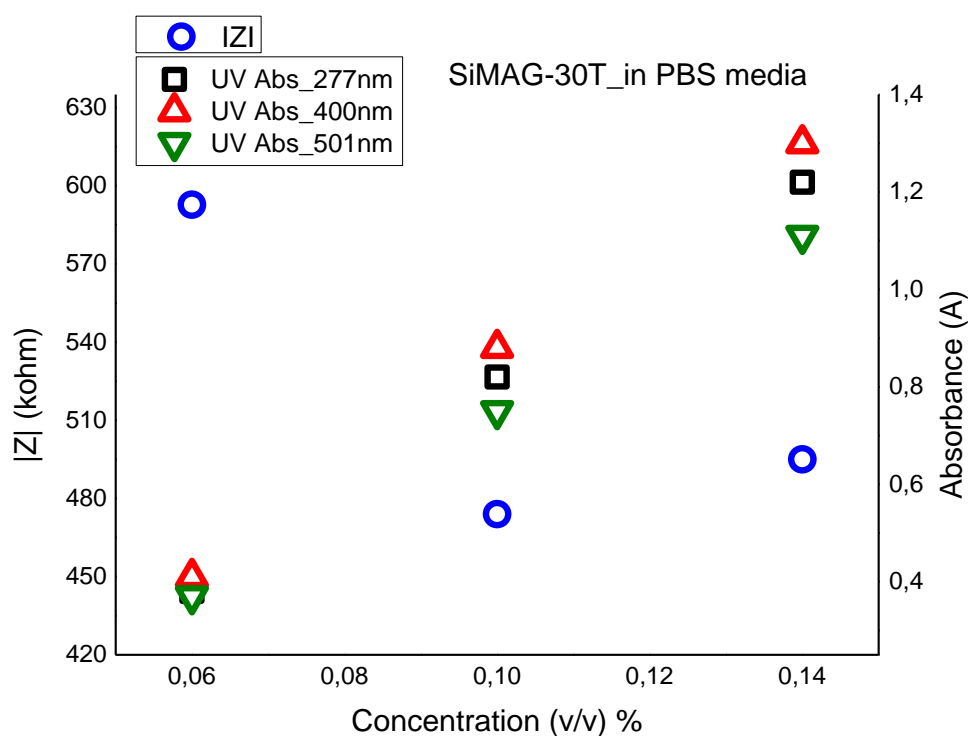


**Figure 4.33 :**  $|Z|$ -Concentration % (v/v) & Absorbance-Concentration % (v/v) plot for SiMAG-30T nanoparticle.

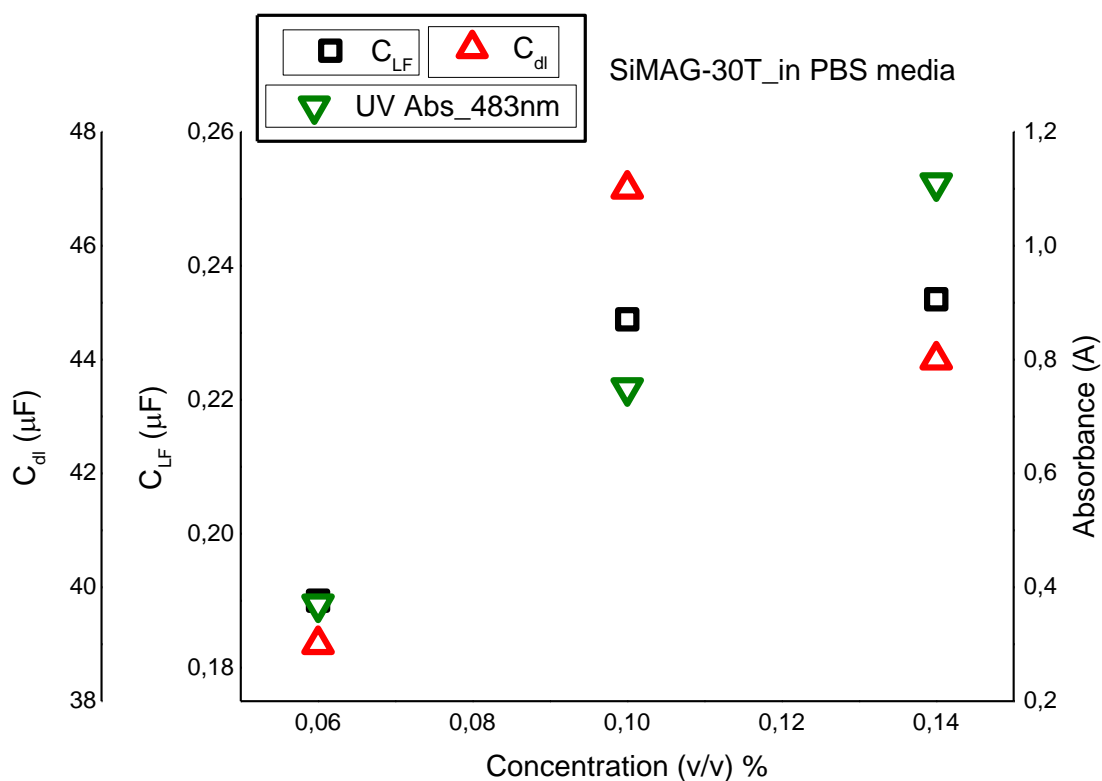


**Figure 4.34 :**  $C_{dl}$ -Concentration % (v/v),  $C_{LF}$ -Concentration % (v/v) & Absorbance-Concentration % (v/v) plot for SiMAG-30T nanoparticle.

It was deduced that increasing at UV absorbance value was very responsive to increasing of MNPs concentration. Not only UV absorbance value, but also reply of  $|Z|$ ,  $C_{dl}$ , and  $C_{LF}$  were very responsive to concentration changing. According to the common response obtaining from the figures, when the concentration of MNPs were increased in solution,  $C_{dl}$  and  $C_{LF}$  values diminished while  $|Z|$  and UV absorbance value increased as similarly results of the comparison graphs belonging to SiMAG without DNA binding.

When DNA bound sample is used as working electrode on system, the Nyquist plot consists of both semi-circle and linear part which represent charge transfer resistance and ion diffusion. However, when impedance of solution which includes sample such as metal nanoparticles coated with organic or polymer is measured and Platinum wire is used as working electrode, the Nyquist plot exhibits only semi-circle [122]. Therefore, Nyquist plots of SiMAG samples exhibited a semi-circle behavior due to the similarity of system.

According to the research, Golshaei et al. [122] reported impedance results of Au/PANA core/shell nanocomposites measured in solution impedance system. The report expresses that when the concentration of Au/PANA core/shell nanocomposites was increased, the semi-circle diameter became smaller, so while charge transfer resistance decreased, double layer capacitance ( $C_{dl}$ ) increased. Furthermore, according to the our research, the semi-circle diameter became larger, impedance values increased; nevertheless  $C_{dl}$  and  $C_{LF}$  values diminished while the MNP (SiMAG) concentration was increased. The reason of that variance is different core-shell compound of nanoparticles. While Au/PANA has low resistive and conductive core-shell (PANA), SiMAG nanoparticle has high resistive core-shell (silica). Consequently, it leads to increase on impedance and decrease on capacitance while concentration of SiMAG is increased.

Once the system was investigated, the double layer capacitance ( $C_{dl}$ ) located along Pt working electrode, the resistance arose from between SiMAG (with and without DNA binding) nanoparticles and Pt electrode [122]. The decrease in  $C_{dl}$  was attributed to increase in thickness of electronic double layer between SiMAG (with and without DNA binding) nanoparticles and Pt electrode. Besides, the increase of charge transfer resistance was attributed to the formation of layer on the Pt electrode–nanoparticles interphase [123].

#### 4.8 Comparative EIS Results of Magnetic Nanoparticles

Figure 4.35 includes concentration values and  $|Z|$  values which were measured by changing the concentration for each sample. According to the results, it was observed that when the concentration of the nanoparticles was increased in solution,  $|Z|$  values increased regularly. Additionally the other inference from the figure was that when the DNA oligonucleotide was bound to the magnetic nanoparticle and the length of DNA oligonucleotide was elongated from 12 base to 30 base, the  $|Z|$  values diminished for each concentration value.

$C_{dl}$  values of magnetic nanoparticles were compared at Figure 4.36. The concentration of magnetic nanoparticles was increased, then as a result of increasing concentration, the influence was observed on  $C_{dl}$  values. Figure 4.36 demonstrated that once the concentration of the samples was increased, the  $C_{dl}$  values of magnetic nanoparticles decreased. Moreover, it can be expressed that binding of DNA to magnetic nanoparticle and enlarging of the DNA oligonucleotide length which was bound to the magnetic nanoparticle were increased the  $C_{dl}$  values for each concentration value.

Figure 4.37 illustrated the relationship among concentration and  $C_{LF}$  values. Once the concentration of magnetic nanoparticles was increased, it was seen that  $C_{LF}$  values diminished in overview. Besides, the other significant point obtaining from the Figure 4.37 was that the  $C_{LF}$  values increased for each concentration value similarly to the  $C_{dl}$  values when the DNA oligonucleotide was bound to the magnetic nanoparticle and the length of DNA oligonucleotide was elongated from 12 base to 30 base.

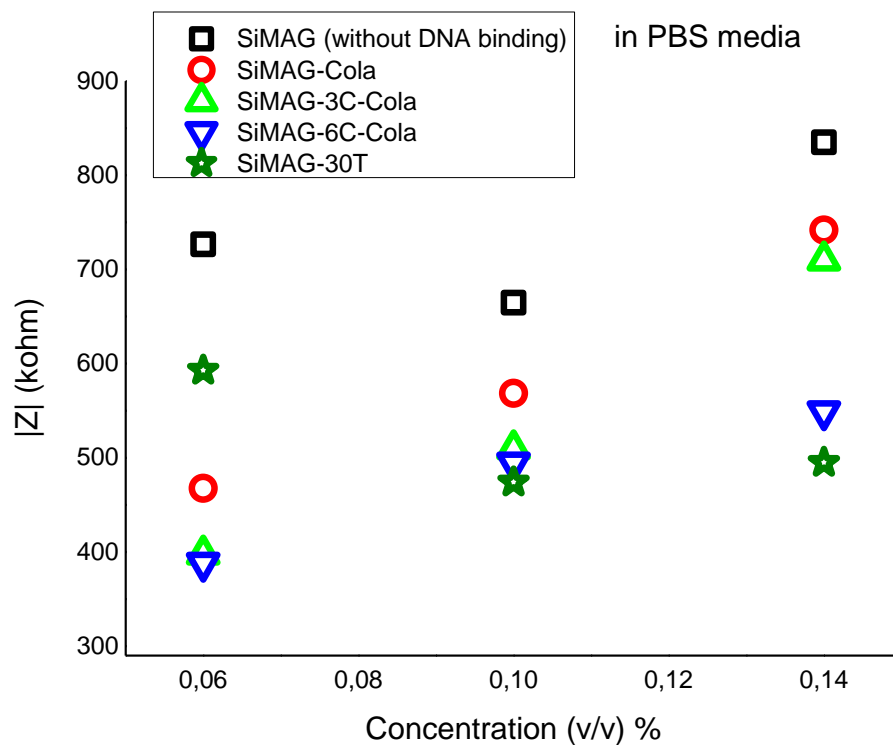


**Figure 4.35 :**  $|Z|$ -Concentration % (v/v) plot for SiMAG without DNA binding, SiMAG-Cola, SiMAG-3C-Cola, SiMAG-6C-Cola, and SiMAG-30T at %0.06, %0.10, and %0.14 (v/v) dilution ratios.

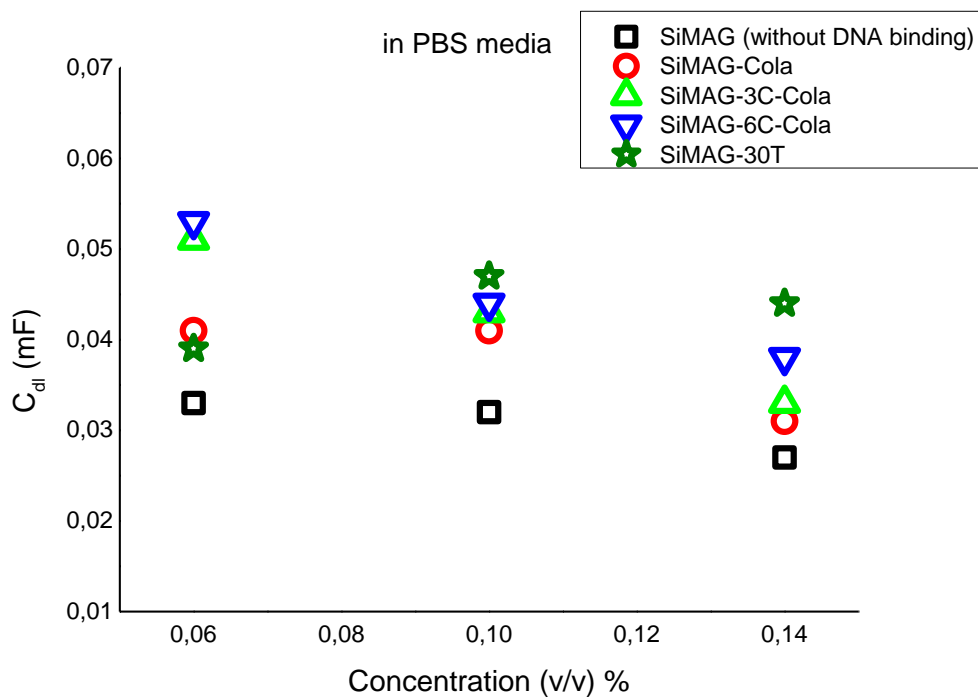


**Figure 4.36 :**  $C_{dl}$ -Concentration % (v/v) plot for SiMAG without DNA binding, SiMAG-Cola, SiMAG-3C-Cola, SiMAG-6C-Cola, and SiMAG-30T at %0.06, %0.10, and %0.14 (v/v) dilution ratios.

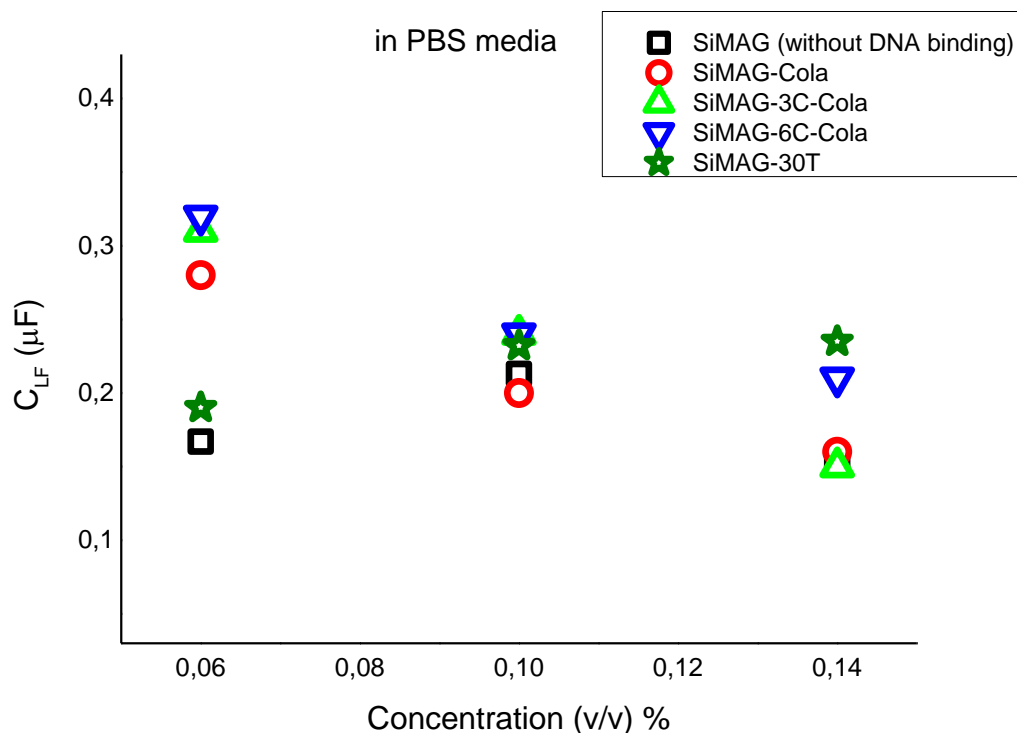


**Figure 4.37 :**  $C_{LF}$ -Concentration % (v/v) plot for SiMAG without DNA binding, SiMAG-Cola, SiMAG-3C-Cola, SiMAG-6C-Cola, and SiMAG-30T at %0.06, %0.10, and %0.14 (v/v) dilution ratios.

#### 4.9 Morphological Characterization of Magnetic Nanoparticles

Surface morphology of the MNPs and ttr4 DNA oligonucleotide were investigated by atomic force microscopy (AFM) at various scales as 1 $\mu$ m, 500nm, and 300nm. The two and three dimensional surface images of the samples were exhibited at Figure 4.38, Figure 4.39, and Figure 4.40. The roughness values of these samples are measured via Nanosurf Easy-scan software and presented at Table 4.2.

**Table 4.2 :** Roughness values of SiMAG without DNA binding, SiMAG-Cola, SiMAG-3C-Cola, SiMAG-6C-Cola, and SiMAG-30T nanoparticles.

Name of Samples	1 $\mu$ m	500 nm	300 nm
SiMAG	4.10 nm	2.79 nm	12.53 nm
SiMAG-3C-Cola	6.40 nm	5.72 nm	2.92 nm
SiMAG-6C-Cola	5.24 nm	3.41 nm	3.30 nm
SiMAG-30T	7.97 nm	5.51 nm	4.54 nm
ttr4	2.42 nm	1.36 nm	-

Name of the Sample	1 $\mu$ m	500nm	300nm
<b>SiMAG</b>			
<b>SiMAG-3C-Cola</b>			
<b>SiMAG-6C-Cola</b>			
<b>SiMAG-30T</b>			

**Figure 4.38 :** AFM images of SiMAG without DNA binding, SiMAG-Cola, SiMAG-3C-Cola, SiMAG-6C-Cola, and SiMAG-30T nanoparticles on two dimensional (2D).



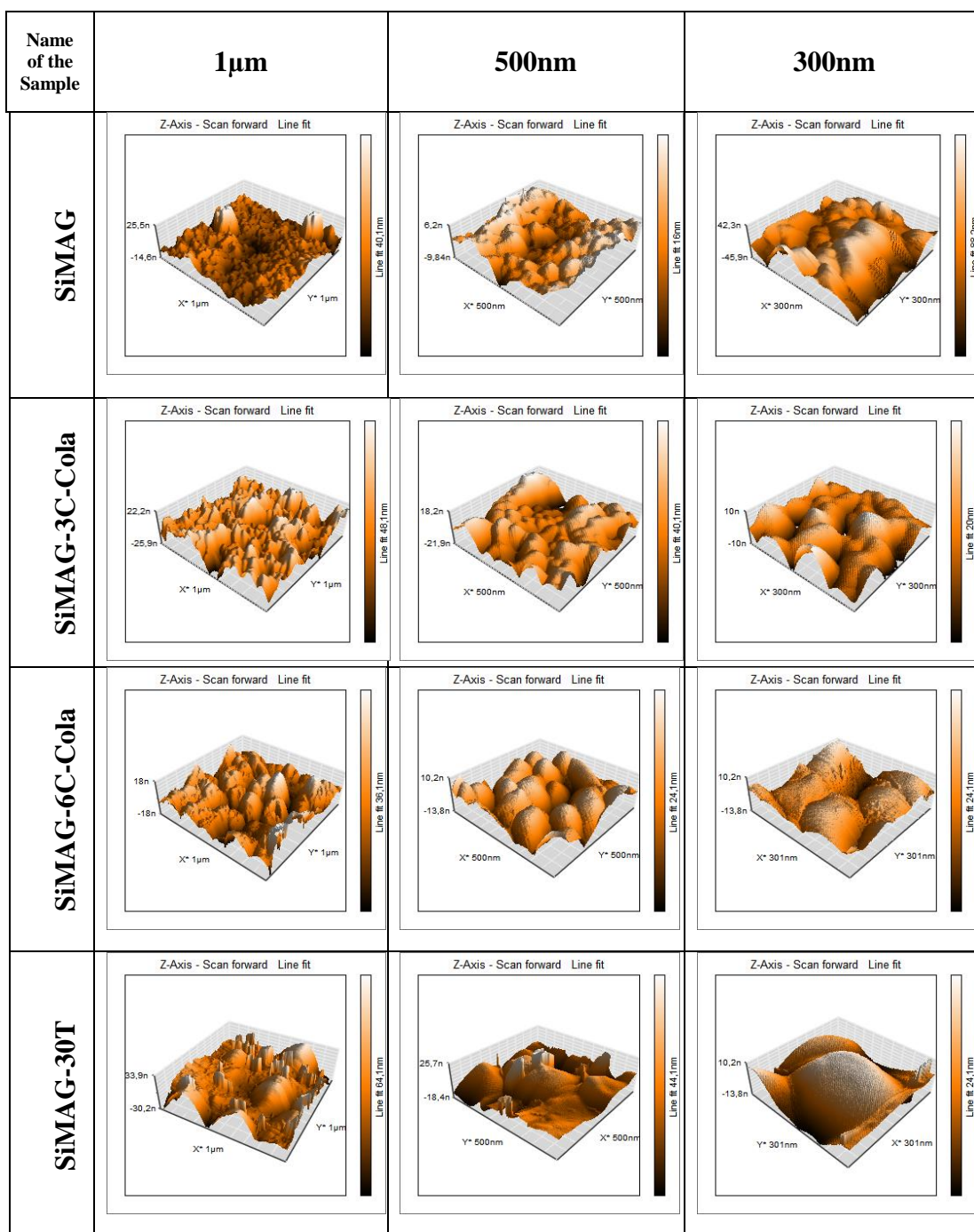


**Figure 4.39 :** AFM images of SiMAG without DNA binding, SiMAG-Cola, SiMAG-3C-Cola, SiMAG-6C-Cola, and SiMAG-30T nanoparticles on three dimensional (3D).

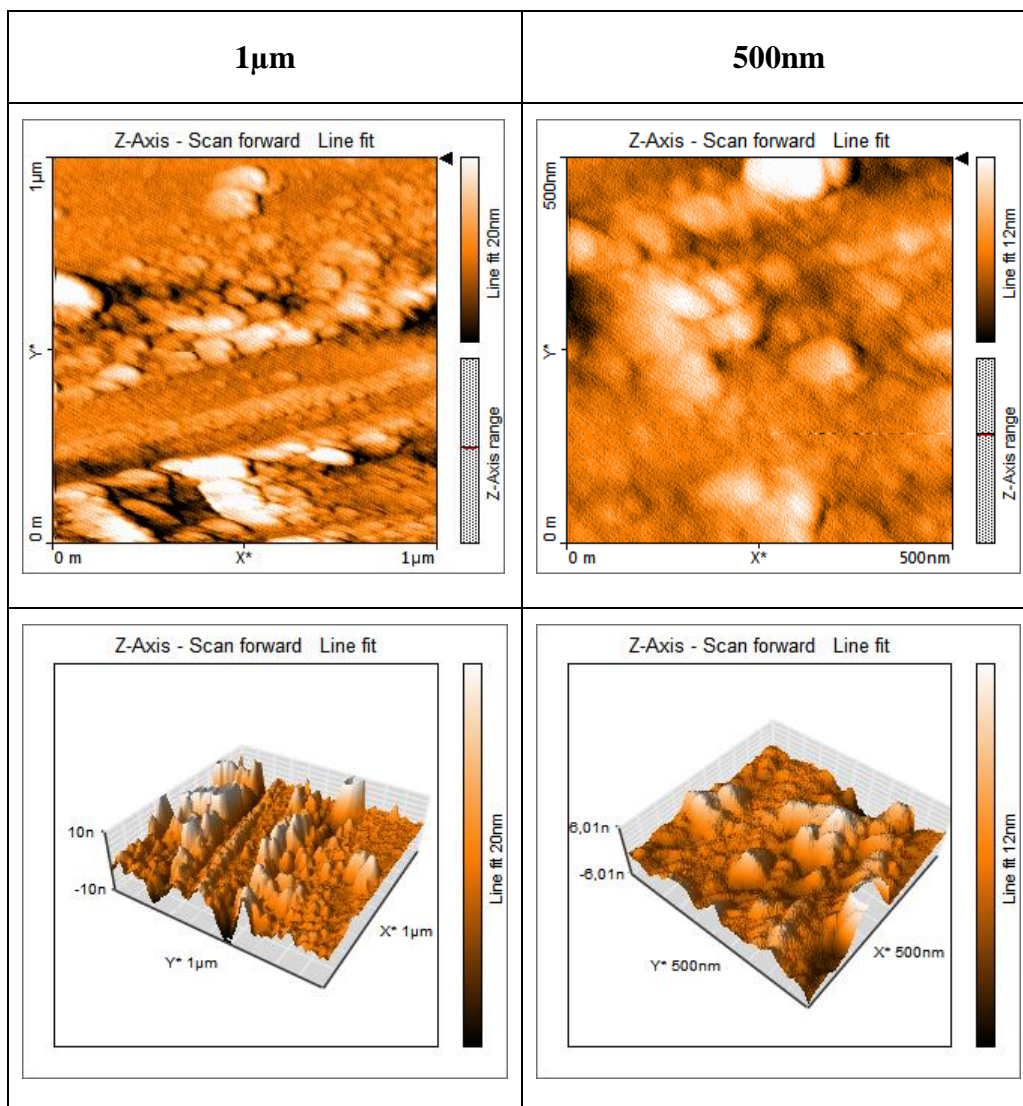


**Figure 4.40 :** AFM images of ttr4 DNA oligonucleotide at 1 $\mu$ m and 500nm scales, and on 2D and 3D.

Figure 4.41 and Figure 4.42 belong to the SEM (Scanning Electron Microscope) images of ttr4 and dT20 DNA oligonucleotides, respectively. Figure 4.43 consists of SEM images of SiMAG-Cola, SiMAG-3C-Cola, SiMAG-6C-Cola, and SiMAG-30T DNA bound nanoparticles. The granule diameters of samples were measured via ImageJ software. The diameter values of samples are exhibited at Table 4.3. According to the results taken place at the Table 4.3, granule diameters were expanded while DNA oligonucleotides were bound to the MNPs and while DNA strand length was got increase.

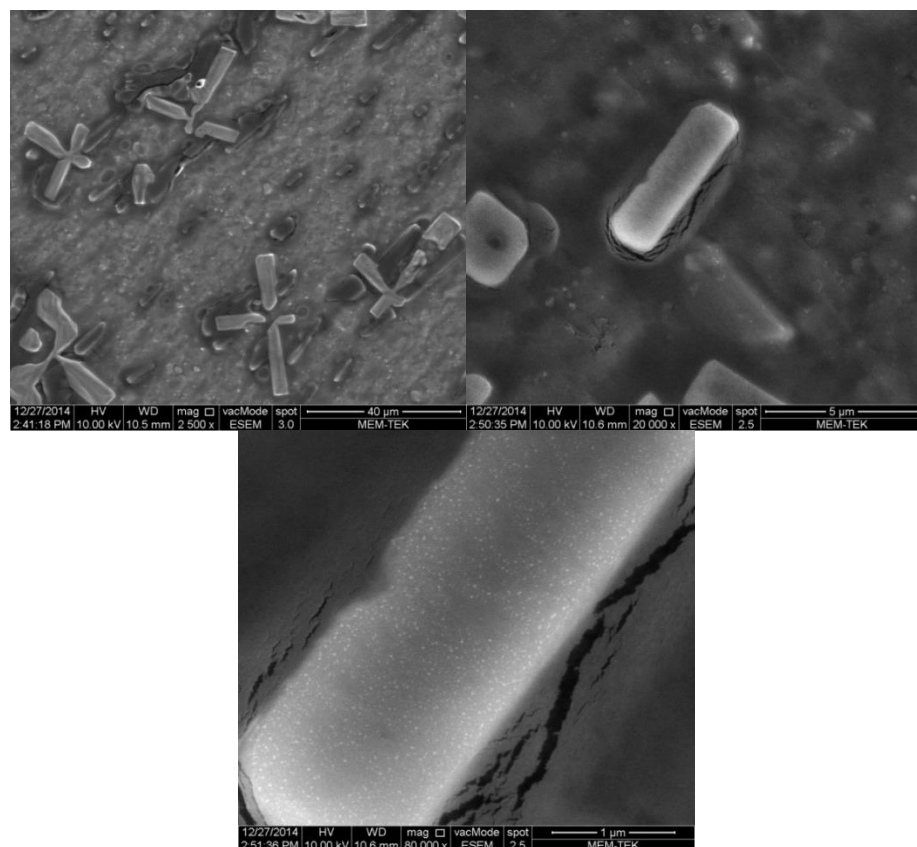


**Figure 4.41 :** SEM images of ttr4 DNA oligonucleotide at 40μm, 5μm, and 1μm scales.

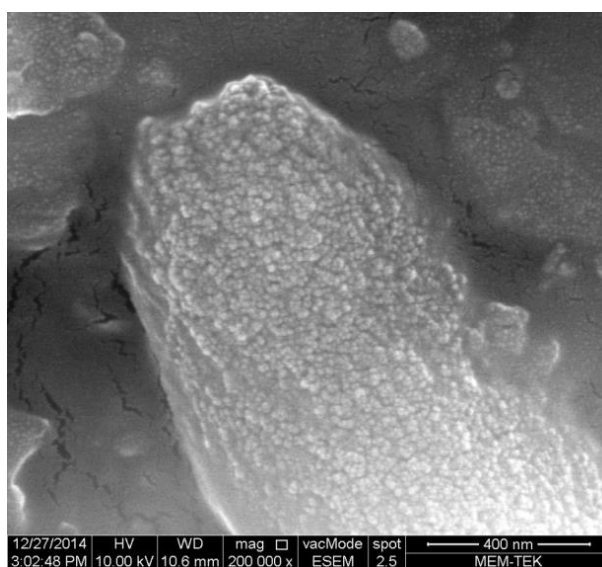


**Figure 4.42 :** SEM images of dt20 DNA oligonucleotide at 400nm scale.

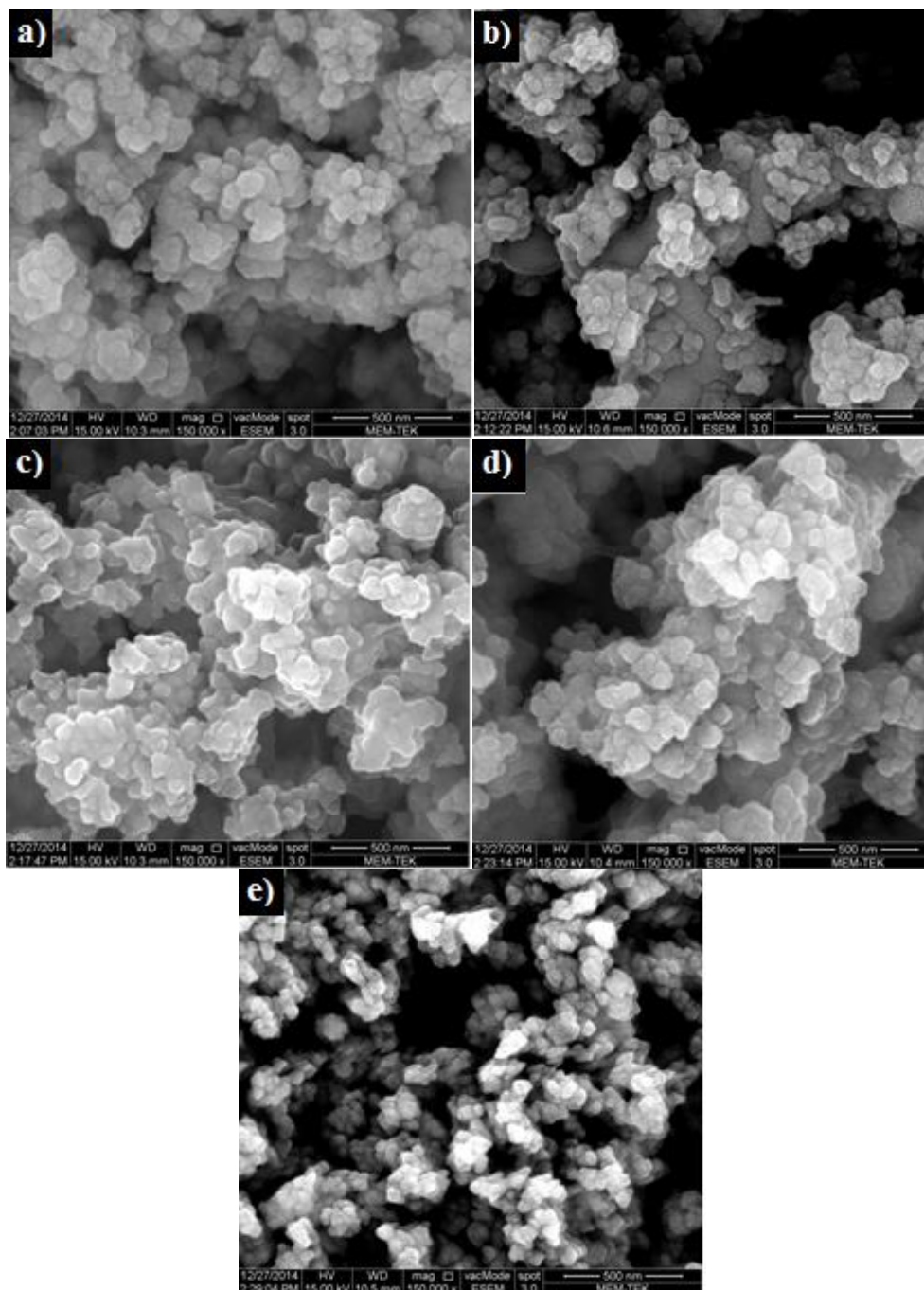


**Figure 4.43 :** SEM images of a) SiMAG without DNA binding, b) SiMAG-Cola, c) SiMAG-3C-Cola, d) SiMAG-6C-Cola, and e) SiMAG-30T nanoparticles at 500nm scale.

**Table 4.3:** Measured granule diameters from SEM images belonging to SiMAG without DNA binding, SiMAG-Cola, SiMAG-3C-Cola, and SiMAG-6C-Cola nanoparticles and ttr4 and dT20 DNA oligonucleotides.

Name of Samples	Granule diameter
SiMAG	70 nm ( $\pm 8$ )
SiMAG -Cola	74 nm ( $\pm 8$ )
SiMAG -3C-Cola	77 nm ( $\pm 7$ )
SiMAG -6C-Cola	80 nm ( $\pm 13$ )
ttr4	23 nm ( $\pm 9$ )
dT20	14 nm ( $\pm 2$ )

Figure 4.44 and Figure 4.45 show roughness- $|Z|$  and roughness- $C_{dl}$  relationships amongst samples which were ttr4 DNA oligonucleotide, SiMAG, SiMAG-3C-Cola, SiMAG-6C-Cola, SiMAG-30T. As it is seen on figures, when the DNA oligonucleotide was bound to the magnetic nanoparticle and the length of DNA oligonucleotide was elongated from 12 base to 30 base, the  $|Z|$  values diminished; however,  $C_{dl}$  values increased for each concentration value.

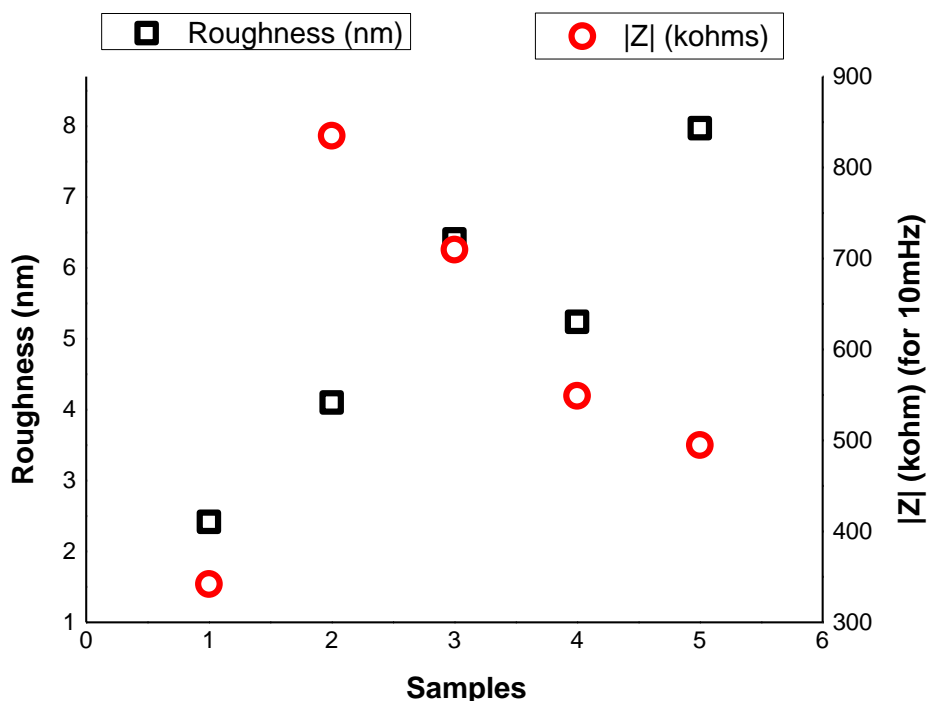


**Figure 4.44 :** Roughness- $|Z|$  relationship amongst samples which were enumerated as 1) ttr4 DNA oligonucleotide, 2) SiMAG, 3) SiMAG-3C-Cola, 4) SiMAG-6C-Cola, 5) SiMAG-30T.

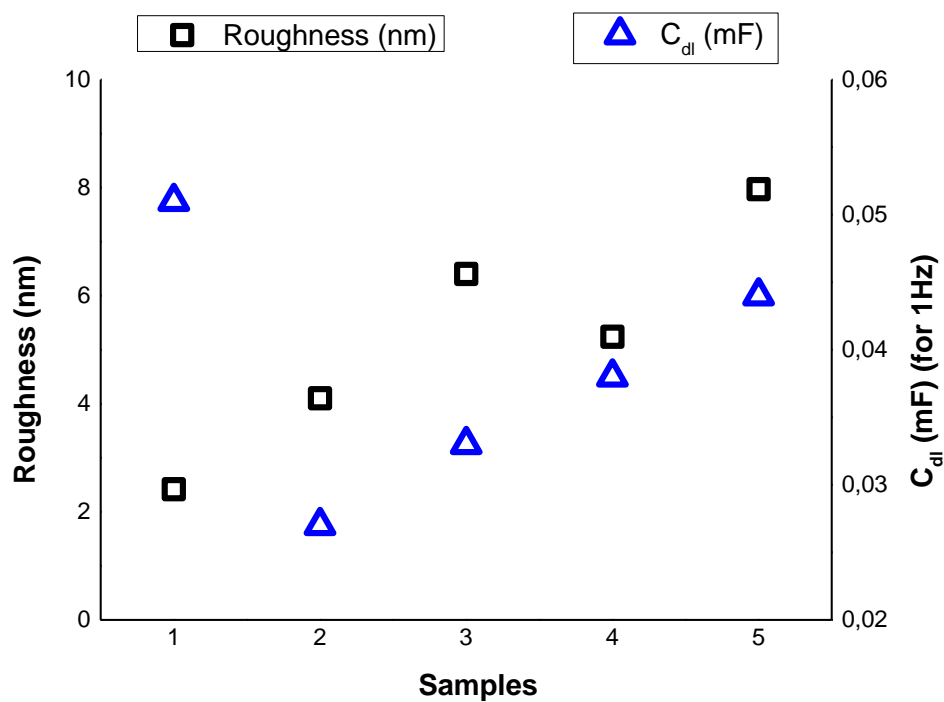


**Figure 4.45 :** Roughness- $C_{dl}$  relationship amongst samples which were enumerated as 1) ttr4 DNA oligonucleotide, 2) SiMAG, 3) SiMAG-3C-Cola, 4) SiMAG-6C-Cola, 5) SiMAG-30T

## 5. CONCLUSION

Iron oxide magnetic nanoparticles were synthesized on magnetite form ( $\text{Fe}_3\text{O}_4$ ). Then, magnetite iron oxide nanoparticles were converted to maghemite form ( $\gamma\text{-Fe}_2\text{O}_3$  NPs) by calcination proces at  $300^\circ\text{C}$ . After that,  $\gamma\text{-Fe}_2\text{O}_3$  NPs were coated with silica. Therefore, silica coated  $\gamma\text{-Fe}_2\text{O}_3$  NPs have same structural form as SiMAG, which were obtained commercially. Both synthesized silica coated  $\gamma\text{-Fe}_2\text{O}_3$  NPs and SiMAG nanoparticles were characterized spectroscopically with FTIR-ATR Spectrometer, Raman Spectrophotometer, and UV-Vis Spectrophotometer, and results were compared in each other. It was observed that both of magnetic nanoparticles had same structure and formation owing to exhibition same characteristic bands. Additionally, DNA oligonucleotides (ttr4, and dT20) and magnetic nanoparticles with and without DNA binding (SiMAG, SiMAG-Cola, SiMAG-3C-Cola, SiMAG-6C-Cola, and SiMAG-30T) were investigated spectroscopically (UV-Vis Spectrophotometer), morphologically (AFM and SEM), and electrochemically (Electrochemical Impedance Spectroscopy (EIS)). The effect of parameters such as concentration, presence of bound DNA, length of DNA on impedance, capacitance, UV absorbance and granule size were investigated. As a result of the measurements, it was observed that when the concentration was increased,  $C_{dl}$  (double layer capacitance) and  $C_{LF}$  (Low frequency capacitance) values decreased while  $|Z|$  (impedance) and UV absorbance values increased. Moreover, when the DNA oligonucleotide was bound to the magnetic nanoparticle and the length of DNA oligonucleotide was elongated from 12 base to 30 base, it was observed that granule diameters were expanded, the  $|Z|$  values diminished,  $C_{dl}$  and  $C_{LF}$  values increased for each concentration value.





## REFERENCES

- [1] Nikam, A. P., Mukesh, P. R. & Chaudhary, S. P. (2014). Nanoparticles – an overview. *Int. J. Res. Dev. Pharm. L. Sci.*, 3(5), 1121- 1127.
- [2] Gupta, A. K. & Gupta, M. (2005). Synthesis and surface engineering of iron oxide nanoparticles for biomedical applications. *Biomaterials*, 26, 3995–4021. doi:10.1016/j.biomaterials.2004.10.012
- [3] Patel, D., Moon, J. Y., Chang, Y., Kim, T. J. & Lee, G. H. (2008). *Colloid Surf. A*, 313–314, 91. doi:10.1016/j.colsurfa.2007.04.078.
- [4] Zhao, M., Josephson, L., Tang, Y. & Weissleder, R. (2003). *Angew. Chem. Int. Ed.*, 42, 1375. doi:10.1002/anie.200390352.
- [5] Mornet, S., Vasseur, S., Grasset, F., Veverka, P., Goglio, G., Demourgues, A., et al. (2006). *Prog. Solid State Chem.*, 34, 237. doi:10.1016/j.progsolidstchem.2005.11.010.
- [6] Stevens, P. D., Fan, J., Gardimalla, H. M. R., Yen, M. & Gao, Y. (2005). *Org. Lett*, 7, 2085. doi:10.1021/ol050218w.
- [7] Jun, Y., Choi, J. & Cheon, J. (2007). *Chem. Commun. (Camb)*, 1203. doi:10.1039/b614735f.
- [8] Pham, T. A., Kumar, N. A. & Jeong, Y. T. (2010). *Colloids Surf., A*, 370 95–101.
- [9] Anirudhan, T. S., Dilu, D. & Sandeep, S. (2013). *J. Magn. Magn. Mater*, 343 149–156.
- [10] Lai, B. H., Yeh, C. C. & Chen, D. H. (2012). *Process Biochem*, 47 799–805.
- [11] Crosswhite, M., et al. (2013). *ACS Catal*, 3, 1318–1323.
- [12] Gu, X., Zhang, Y., Sun, H., Song, X., Fu, C. & Dong, P. (2015). Mussel-Inspired Polydopamine Coated Iron Oxide Nanoparticles for Biomedical Application. *Journal of Nanomaterials*, 12. <http://dx.doi.org/10.1155/2015/154592>.
- [13] Laurent, S., et al. (2008). *Chem. Rev.*, 108 2064–2110.
- [14] Wu, W., He, Q. & Jiang, C. (2008). Magnetic Iron Oxide Nanoparticles: Synthesis and Surface Functionalization Strategies. *Nanoscale Res Lett*, 3, 397–415. DOI 10.1007/s11671-008-9174-9.
- [15] Guo, C., Yunhui, M., Pengfei, S. & Baishan, F. (2012). Direct binding glucoamylase onto carboxyl-functioned magnetic nanoparticles. *Biochemical Engineering Journal*, 67, 120– 125. <http://dx.doi.org/10.1016/j.bej.2012.06.002>.

- [16] Sun, S. & Zeng, H. (2002). Size-controlled synthesis of magnetite nanoparticles. *Journal of the American Chemical Society*, 124 (28), 8204–8205.
- [17] Sousa, M. H., Rubim, J. C., Sobrinho, P. G. & Tourinho, F. A. (2001). *J. Magn. Magn. Mater.* 225, 67. doi:10.1016/S0304-8853(00)01229-4.
- [18] Sahoo, Y., Goodarzi, A., Swihart, M. T., Ohulchanskyy, T. Y., Furlani, E. P. & Prasad, P. N. (2005). *J. Phys. Chem. B*, 109, 3879. doi:10.1021/jp045402y.
- [19] Morais, P. C., Oliveira, A. C., Tronconi, A. L., Goetze, T. & Buske, N. (2003). *IEEE Trans. Magn.* 39, 2654. doi:10.1109/TMAG.2003.815544.
- [20] Mornet, S., Vasseur, S., Grasset, F. & Duguet, E. (2004). *J. Mater. Chem.* 14, 2161. doi:10.1039/b402025a.
- [21] Xie, J. & Wang, C. H. (2005). *Pharm. Res.* 22, 2079. doi:10.1007/s11095-005-7782-y.
- [22] Banerjee, S. S. & Chen, D. (2007). *Chem. Mater.* 19, 6345. doi:10.1021/cm702278u.
- [23] Hou, Y., Kondoh, H., Shimojo, M., Sako, E. O., Ozaki, N., Kogure T., et al. (2005). *J. Phys. Chem. B*, 109, 4845. doi:10.1021/jp0476646.
- [24] Bonacchi, D., Caneschi, A., Dorignac, D., Falqui, A., Gatteschi, D., Rovai, D., et al. (2004). *Chem. Mater.* 16, 2016. doi:10.1021/cm034948e.
- [25] Xia, H., Yi, J., Foo, P., Liu, B. (2007). *Chem. Mater.* 19, 4087. doi:10.1021/cm070918q.
- [26] Chen, Z. P., Zhang, Y., Zhang, S., Xia, J. G., Liu, J. W., Xu, K., et al. (2008). *Colloid Surf. A*, 316, 210. doi:10.1016/j.colsurfa.2007.09.017.
- [27] Lattuada, M. & Hatton, T. A. (2007). *Langmuir*, 23, 2158. doi:10.1021/la062092x.
- [28] Shen, X., Fang, X., Zhou, Y. & Liang, H. (2004). *Chem. Lett.* 33, 1468. doi:10.1246/cl.2004.1468.
- [29] Ma, M., Zhang, Y., Yu, W., Shen, H., Zhang, H & Gu, N. (2003). *Colloid Surf. A*, 212, 219. doi:10.1016/S0927-7757(02)00305-9.
- [30] Can, K., Ozmen, M. & Ersoz, M. (2009). Immobilization of albumin on aminosilane modified superparamagnetic magnetite nanoparticles and its characterization. *Colloids and Surfaces B: Biointerfaces*, 71, 154–159. doi:10.1016/j.colsurfb.2009.01.021.
- [31] Arales, B. (1977). *Chemtechnology*, 7, 766.
- [32] Berry, C. C., Wells, S., Charles, S. & Curtis, A. S. G. (2003). *Biomaterials*, 24, 4551. doi:10.1016/S0142-9612(03)00237-0.
- [33] Bautista, M. C., Bomati-Miguel, O., Morales, M. P., Serna, C. J. & Veintemillas-Verdaguer, S. (2005). *J. Magn. Magn. Mater.* 293, 20. doi:10.1016/j.jmmm.2005.01.038.
- [34] Kim, D. K., Maria, M., Wang, F. H., Jan, K., Bo'rje, B., Zhang Y., et al. (2003). *Chem. Mater.* 15, 4343. doi:10.1021/cm031104m.

- [35] Gaihre, B., Aryal, S., Khil, M. S. & Kim, H. Y. (2008). *J. Microencapsul*, 25, 21. doi:10.1080/02652040701737697.
- [36] Li, G., Huang, K., Jiang, Y., Ding, P. & Yang, D. (2008). *Biochem. Eng. J.* doi:10.1016/j.bej.2008.01.018.
- [37] Castelló, J., Gallardo, M., Busquets, M. A. & Estelrich, J. (2015). Chitosan (or alginate)-coated iron oxide nanoparticles: A comparative study. *Colloids and Surfaces A: Physicochem. Eng. Aspects*, 468, 151–158. <http://dx.doi.org/10.1016/j.colsurfa.2014.12.031>.
- [38] Herea, D. D., Chiriac, H., Lupua, N., Grigorasa, M., Stoiana, G., Stoica, B. A. & Petreus, T. (2015). Study on iron oxide nanoparticles coated with glucose-derived polymers for biomedical applications. *Applied Surface Science*, 352, 117–125. <http://dx.doi.org/10.1016/j.apsusc.2015.03.137>.
- [39] Ma, H. L., Xu, Y. F., Qi, X. R., Maitani, Y. & Nagai, T. (2006). *Int. J. Pharm.*, 354, 217. doi:10.1016/j.ijpharm.2007.11.036.
- [40] Morales, M. A., Finotelli, P. V., Coaquira, J. A. H., Rocha-Leaño, M. H. M., Diaz-Aguila, C., Baggio-Saitovitch, E. M., et al. (2007). *Mater. Sci. Eng. C*, 28, 253. doi:10.1016/j.msec.2006.12.016.
- [41] Shan, G., Xing, J., Luo, M., Liu, H. & Chen, J. (2003). *Biotechnol. Lett.* 25, 1977. doi:10.1023/B:BILE.0000004388.15751.8c.
- [42] Arbab, A. S., Bashaw, L. A., Miller, B. R., Jordan, E. K., Lewis, B. K., Kalish, H., et al. (2003). *Radiology*, 229, 838. doi:10.1148/radiol.2293021215
- [43] Chen, F., Gao, Q., Hong, G. & Ni, J. (2008). *J. Magn. Magn. Mater.* 320, 1921. doi:10.1016/j.jmmm.2008.02.132.
- [44] Chastellain, M., Petri, A. & Hofmann, H. J. (2004). *Colloid Interface Sci.* 278, 353. doi:10.1016/j.jcis.2004.06.025.
- [45] D'Souza, A. J. M., Schowen, R. L. & Topp, E. M. (2004). *J Control Release*, 94, 91. doi:10.1016/j.jconrel.2003.09.014.
- [46] Zhu, D. M., Wang, F., Han, M., Li, H. B. & Xu, Z. (2007). *Chin. J. Inorg. Chem*, 23, 2128.
- [47] Singh, H., Laibinis, P. E. & Hatton, T. A. (2005). *Langmuir*, 21, 11500. doi:10.1021/la0517843.
- [48] Demchenko, P., Nedelko, N., Mitina, N., Lewińska, S., Dłużewski, P., Greneche, J. M., Ubizskii, S., Navrotskyi, S., Zaichenko, A. & Ślowska-Waniewska, A. (2015). Collective magnetic behavior of biocompatible systems of maghemite particles coated with functional polymer shells. *Journal of Magnetism and Magnetic Materials*, 379, 28–38. <http://dx.doi.org/10.1016/j.jmmm.2014.12.002>.
- [49] Mondini, S., Cenedese, S., Marinoni, G., Molteni, G., Santo, N., Bianchi, C.L., et al. (2008). *J. Colloid Interface Sci.* 322, 173. doi:10.1016/j.jcis.2008.03.008.

- [50] Yanga, J., Zoua, P., Yanga, L., Caoa, J., Suna, Y., Hanc, D., Yangc, S., Wang, Z., Chena, G., Wang, B. & Kong, X. (2014). A comprehensive study on the synthesis and paramagnetic properties of PEG-coated Fe<sub>3</sub>O<sub>4</sub> nanoparticles. *Applied Surface Science*, 303, 425–432. <http://dx.doi.org/10.1016/j.apsusc.2014.03.018>.
- [51] Halupka-Bryl, M., Bednarowicz, M., Dobosz, B., Krzyminiewski, R., Zalewski, T., Wereszczyńska, B., Nowaczyk, G., Jarek, M. & Nagasaki, Y. (2015). Doxorubicin loaded PEG-b-poly(4-vinylbenzylphosphonate) coated magnetic iron oxide nanoparticles for targeted drug delivery. *Journal of Magnetism and Magnetic Materials*, 384, 320–327. <http://dx.doi.org/10.1016/j.jmmm.2015.02.078>.
- [52] Yang, G., Zhang, B., Wang, J., Xie, S. & Li, X. (2015). Preparation of polylysine-modified superparamagnetic iron oxide nanoparticles. *Journal of Magnetism and Magnetic Materials*, 374, 205–208. <http://dx.doi.org/10.1016/j.jmmm.2014.08.040>.
- [53] Hutchings, G. J., Hall, M. S., Carley, A. F., Landon, P., Solsona, B. E., Kiely, C. J., et al. (2006). *J. Catal.*, 242, 71. doi:10.1016/j.jcat.2006.06.001.
- [54] Li, J., Zhan, Y., Zhang, F., Lin, X. & Zheng, Q. (2008). *Chinese J. Catal.*, 29, 346.
- [55] Andreeva, D., Tabakova, T., Idakiev, V., Christov, P. & Giovanoli, R. (1998). *Appl. Catal. A Gen.*, 169, 9. doi:10.1016/S0926-860X(97)00302-5.
- [56] Wang, Z., Shen, B., Aihua, Z. & He, N. (2005). *Chem. Eng. J.*, 113, 27. doi:10.1016/j.cej.2005.08.003.
- [57] Yao, K. M., Lee, S. I., Lee, Y. T., Chung, Y. K. & Lee, I. S. (2008). *Chem. Lett.* 37, 116. doi:10.1246/cl.2008.116.
- [58] Zhang, D. H., Li, G. D., Li, J. X. & Chen, J. S. (2008). *Chem. Commun. (Camb)*, 3414. doi:10.1039/b805737k.
- [59] Wang, Z., Guo, H., Yu, Y. & He, N. (2006). *J. Magn. Magn. Mater.* 302, 397. doi:10.1016/j.jmmm.2005.09.044.
- [60] Liu, Z., Zhang, D., Han, S. & Li, C. (2005). *J. Am. Chem. Soc.* 127, 6. doi:10.1021/ja0445239.
- [61] Castro, R. H. R., Hidalgo, P., Coaquira, J. A. H., Bettin, J., Zanchet, D. & Gouve, D. (2005). *Eur. J. Inorg. Chem.* 11, 2134. doi:10.1002/ejic.200400879.
- [62] Decker, S. & Klabunde, K. J. (1996). *J. Am. Chem. Soc.* 118, 12465. doi:10.1021/ja962371e.
- [63] Natile, M. M. & Glisenti, A. (2003). *Chem. Mater.* 15, 2502. doi:10.1021/cm031019e.
- [64] Chen, C. T. & Chen, Y. C. (2008). *Anal. Chem.* 77, 5912. doi:10.1021/ac050831t.
- [65] Chen, C. T. & Chen, Y. C. (2008). *Biomed. Nanotechnol.* 4, 73. doi:10.1166/jbn.2008.008.

- [66] **Chen, W. J., Tsai, P. J. & Chen, Y. C.** (2008). *Small* 4, 485. doi:10.1002/sml.200701164.
- [67] **Habibi, N.** (2014). Immobilization of bacterial S-layer proteins from *Caulobacter crescentus* on iron oxide-based nanocomposite: Synthesis and spectroscopic characterization of zincite-coated Fe<sub>2</sub>O<sub>3</sub> nanoparticles. *Spectrochimica Acta Part A: Molecular and Biomolecular Spectroscopy*, 125, 359–362. <http://dx.doi.org/10.1016/j.saa.2014.01.084>.
- [68] **Hu, J., Chen, G. & Lo, I. M. C.** (2005). Removal and recovery of Cr (VI) from electroplating waste water by maghemite nanoparticles. *Water Res.* 39, 4528–4536. <http://dx.doi.org/10.1016/j.watres.2005.05.051>.
- [69] **Mayo, J. T., Yavuz, C., Yean, S., Cong, L., Shipley, H., Yu, W., Falkner, J., Kan, A., Tomson, M. & Colvin, V. L.** (2007). The effect of nanocrystalline magnetite size on arsenic removal. *Sci. Technol. Adv. Mater*, 8, 71–75, <http://dx.doi.org/10.1016/j.stam.2006.10.005>.
- [70] **Xu, L., Guo, C., Wang, F., Wang, S. & Liu, C. Z.** (2011). A simple and rapid harvesting method for microalgae by in situ magnetic separation. *Bioresour Technol.* 102 10047–10051. <http://dx.doi.org/10.1016/j.biortech.2011.08.021>.
- [71] **Rivas, J., Bañobre-López, M., Piñeiro-Redondo, Y., Rivas, B. & López-Quintela, M. A.** (2012). Magnetic nanoparticles for application in cancer therapy. *J. Magn. Magn. Mater.* 324 (21), 3499–3502. <http://dx.doi.org/10.1016/j.jmmm.2012.02.075>.
- [72] **Sahu, S. K., Chakrabarty, A., Bhattacharya, D., Ghosh, S. K. & Pramanik, P.** (2011). Single step surface modification of highly stable magnetic nanoparticles for purification of his-tag proteins. *J. Nanoparticle Res.* 13, 2475–2484. <http://dx.doi.org/10.1007/s11051-010-0140-y>.
- [73] **Fellenza, N. A., Pérez De Bertib, I. O., Soldatic, A. L., Stewart, S. J., Marchetti, S. G. & Bengoa, J. F.** (2015). Changes on structural and magnetic properties of maghemite nanoparticles during their coverage with MCM-41. *Ceramics International*, 41, 15057–15066.
- [74] **Ali, L. I. A., Ibrahim, W. A. W., Sulaiman, A., Kamboh, M. A. & Sanagi, M. M.** (2016). New chrysin-functionalized silica-core shell magnetic nanoparticles for the magnetic solid phase extraction of copper ions from water samples. *Talanta*, 148, 191–199. <http://dx.doi.org/10.1016/j.talanta.2015.10.062>.
- [75] **Ma, D., Guan, J., Normandin, F., De'nomme'e, S., Enright, G., Veres T., et al.** (2006). *Chem. Mater.* 18, 1920. doi:10.1021/cm052067x.
- [76] **Ashtari, P., He, X., Wang, K. & Gong, P.** (2005). *Talanta*, 67, 548. doi:10.1016/j.talanta.2005.06.043.
- [77] **Chen, F., Shi, R., Xue, Y., Chen, L. & Wan, Q.** (2010). Templated synthesis of monodisperse mesoporous maghemite/silica microspheres for magnetic separation of genomic DNA. *Journal of Magnetism and Magnetic Materials*, 322, 2439–2445. doi:10.1016/j.jmmm.2010.02.053.

- [78] Liua, J. W., Zhanga, Y., Chenc, D., Yanga, T., Chena, Z. P., Panc, S. Y. & Gu, N. (2009). Facile synthesis of high-magnetization  $\gamma$ -Fe<sub>2</sub>O<sub>3</sub>/alginate/silica microspheres for isolation of plasma DNA. *Colloids and Surfaces A: Physicochem. Eng. Aspects*, 341, 33–39. doi:10.1016/j.colsurfa.2009.03.033.
- [79] Shi, R., Wang, Y., Hu, Y., Chen, L. & Wan, Q. (2009). Preparation of magnetite-loaded silica microspheres for solid-phase extraction of genomic DNA from soy-based foodstuffs. *Journal of Chromatography A*, 1216, 6382–6386. doi:10.1016/j.chroma.2009.07.016.
- [80] Medina-Llamas, J. C., Chávez-Guajardo, A. E., Andrade, C. A. S., Alves, K. G. B. & Pinto de Melo, C. (2014). Use of magnetic polyaniline/maghemite nanocomposite for DNA retrieval from aqueous solutions. *Journal of Colloid and Interface Science*, 434, 167–174. <http://dx.doi.org/10.1016/j.jcis.2014.08.002>.
- [81] He, H., Liu, H., Zhou, K., Wang, W., Rong, P. & Cent, J. (2006). *South Univ. Technol.* 13, 6. doi:10.1007/s11771-006-0097-2.
- [82] Mikhaylova, M., Kim, D. K., Berry, C. C., Zagorodni, A., Toprak, M., Curtis, A. S. G., et al. (2004). *Chem. Mater.* 16, 2344. doi:10.1021/cm0348904.
- [83] Lewin, M., Carlesso, N., Tung, C., Tang, X., Cory, D., Scadden, D. T., et al. (2000). *Nat. Biotechnol.* 18, 410. doi:10.1038/74464.
- [84] Tiefenauer, L. X., Kuhne, G. & Andres, R. Y. (1993). *Bioconjug. Chem.* 4, 347. doi:10.1021/bc00023a007.
- [85] Nam, J. M., Stoeva, S. I. & Mirkin, C. A. (2004). *J. Am. Chem. Soc.* 126, 5932. doi:10.1021/ja049384?.
- [86] Weizmann, Y., Patolsky, F., Lioubashevski, O. & Willner, I. (2004). *J. Am. Chem. Soc.* 126, 1073. doi:10.1021/ja038257v.
- [87] Zhou, H., Li, W., Shou, Q., Gao, H., Xu, P., Deng, F. & Liu, H. (2012). Immobilization of penicillin G acylase on magnetic nanoparticles modified by ionic liquids. *Chinese Journal of Chemical Engineering*, 20(1) 146–151.
- [88] Sulek, F., Drofenik, M., Habulin, M. & Knez, Z. (2010). Surface functionalization of silica-coated magnetic nanoparticles for covalent attachment of cholesterol oxidase. *Journal of Magnetism and Magnetic Materials*, 322, 179–185. doi:10.1016/j.jmmm.2009.07.075.
- [89] Zhang, C., Cao, J., Yin, D., Wang, Y., Feng, Y. & Tan, J. (2004). *Appl. Radiat. Isot.* 61, 1255. doi:10.1016/j.apradiso.2004.03.114.
- [90] Rosi, N. L. & Mirkin, C. A. (2005). *Chem. Rev.* 105, 1547. doi:10.1021/cr030067f.
- [91] Lee, C., Huang, K., Wei, P. & Yao, Y. (2006). *J. Magn. Magn. Mater.* 304, e412. doi:10.1016/j.jmmm.2006.01.213.

- [92] Cornell, R. M. & Schwertmann, U. (2003). The iron oxides: structure, properties, reactions, occurrences and uses. *John Wiley & Sons*.
- [93] Kovalenko, M. V., Bodnarchuk, M. I., Lechner, R. T., Hesser, G., Schäffler, & Heiss, W. (2007). Fatty acid salts as stabilizers in size-and shape controlled nanocrystal synthesis: the case of inverse spinel iron oxide. *Journal of the American Chemical Society*, 129(20), 6352- 6353.
- [94] Saravanan, P., Hsu, J. H., Sivaprahasam, D. & Kamat, S. V. (2013). Structural and magnetic properties of  $\gamma$ -Fe<sub>2</sub>O<sub>3</sub> nanostructured compacts processed by spark plasma sintering. *Journal of Magnetism and Magnetic Materials*, 346, 175-177.
- [95] Sugimoto, M. (1999). The past, present, and future of ferrites. *Journal of the American Ceramic Society*, 82(2), 269-280.
- [96] Bate, G. (1999). *J. Magn. Mater.* 100, 413–424.
- [97] Alivisatos, A. P., Johnsson, K. P., Peng, X., Wilson, T. E., Loweth, C. J., Bruchez, M. P. & Schultz, P. G. (1996). Organization of nanocrystal molecules' using DNA.
- [98] Colvin, V. L., Schlamp, M. C. & Alivisatos, A. P. (1994). Light-emitting diodes made from cadmium selenide nanocrystals and a semiconducting polymer. *Nature*, 370 (6488), 354-357.
- [99] Guo, H. & Barnard, A. S. (2013). Naturally occurring iron oxide nanoparticles: morphology, surface chemistry and environmental stability. *J. Mater. Chem. A*, 1, 27-42. DOI: 10.1039/C2TA00523A.
- [100] Sharrock, M. P. (1989). Measurement and interpretation of magnetic time effects in recording media. *IEEE Trans. Magn.*, 25, 4374–4389.
- [101] Ennas, G., Musinu, A., Piccaluga, G., Zedda, D., Gatteschi, D., Sangregorio, C. & Spano, G. (1998). Characterization of iron oxide nanoparticles in an Fe<sub>2</sub>O<sub>3</sub>-SiO<sub>2</sub> composite prepared by a sol-gel method. *Chemistry of materials*, 10(2), 495-502.
- [102] Monte, F. D., Morales, M. P., Levy, D., Fernandez, A., Ocana, M., Roig, A., Molins, E. & Ogrady, K. (1997). *Langmuir*, 13, 3627– 3634.
- [103] Borelli, M. F., Morse, D. L. & Schreurs, J. W. H. (1983). *J. Appl. Phys.*, 54, 3344.
- [104] Ziolo, R. F., Giannelis E. P., Weinstein B. A., Ohoro M. P., Gangul B. N., Mehrotra, V., Russell, M. W. & Huffman, D. R. (1992). *Science*, 257, 219–222.
- [105] Yousufa, S., Enocha, I. V. M. V., Selvalumara, P. M. & Premnath, D. (2015). Chromenone-conjugated magnetic iron oxide nanoparticles toward conveyable DNA binders. *Colloids and Surfaces B: Biointerfaces*, 135, 448–457. <http://dx.doi.org/10.1016/j.colsurfb.2015.07.049>.
- [106] Dey, T. & O'Connor, C. J. (2005). Synthesis of polymer-coated magnetic nanoparticles. *NSTI-Nanotech*, 2, 1-4.

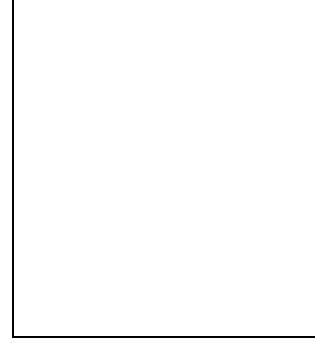
- [107] **Aliahmad, M. & Moghaddam, N. N.** (2013). Synthesis of maghemite ( $\gamma$ -Fe<sub>2</sub>O<sub>3</sub>) nanoparticles by thermal-decomposition of magnetite (Fe<sub>3</sub>O<sub>4</sub>) nanoparticles. *Materials Science-Poland*, 31 (2), 264-268.
- [108] **Liberman, A., Mendez, N., Trogler, W. C., Kummel, A. C.** (2014). Synthesis and surface functionalization of silica nanoparticles for nanomedicine. *Surface ScienceReports*, 69, 132–158. <http://dx.doi.org/10.1016/j.surfrep.2014.07.001>.
- [109] **Chemicell**, geneMAG-DNA / Meat, the magnetic DNA purification kit for isolation of genomic DNA from meat with magnetic beads. Retrieved November 22, 2015, Available from <http://www.chemicell.com/products/purification/docs/geneMAG-DNAMeat.pdf>
- [110] **Pereira, C., Pereira, A. M. & Quaresma, P.** (2010). Superparamagnetic  $\gamma$ -Fe<sub>2</sub>O<sub>3</sub>@SiO<sub>2</sub> nanoparticles: a novel support for the immobilization of [VO(acac)<sub>2</sub>]. *Dalton Trans.*, 39, 2842–2854.
- [111] **Lovell, E. C., Scott, J. & Amal, R.** (2015). Ni-SiO<sub>2</sub> catalysts for the carbon dioxide reforming of methane: varying support properties by flame spray pyrolysis. *Molecules*, 20, 4594-4609. doi:10.3390/molecules20034594.
- [112] **Colomban, P.** (2011). Potential and drawbacks of raman (micro)spectrometry for the understanding of iron and steel corrosion, new trends and developments in automotive system engineering. Prof. Marcello Chiaberge (Ed.), ISBN: 978-953-307-517-4, InTech.
- [113] **Zhang, X., Niu, Y., Meng, X., Li, Y. & Zhao, J.** (2013). Structural evolution and characteristics of the phase transformations between  $\alpha$ -Fe<sub>2</sub>O<sub>3</sub>, Fe<sub>3</sub>O<sub>4</sub> and  $\gamma$ -Fe<sub>2</sub>O<sub>3</sub> nanoparticles under reducing and oxidizing atmospheres. *Cryst Eng Comm*, 15, 8166-8172.
- [114] **Lia, Y., Church, J. S. & Woodhead, A. L.** (2012). Infrared and Raman spectroscopic studies on iron oxide magnetic nano- particles and their surface modifications. *Journal of Magnetism and Magnetic Materials*, 324 (8), 1543-1550. doi: 10.1016/j.jmmm.2011.11.065.
- [115] **Archer, R. D.** (2004). *Inorganic and Organometallic Polymers*. John Wiley & Sons, 154.
- [116] **Spizzirri, P. G., Fang, J. H., Rubanov, S., Gauja, E. & Prawer, S.** (2010). Nano-Raman spectroscopy of silicon surfaces. Retrieved from <http://arxiv.org/ftp/arxiv/papers/1002/1002.2692.pdf>
- [117] **Brescia, P.** (2012). Micro-volume purity assessment of nucleic acids using A260/A280 ratio and spectral scanning. *BioTek Instruments, Inc.*, Winooski, VT.
- [118] **Sherman, D. M. & Waite, T. D.** (1985). Electronic spectra of Fe<sup>3+</sup> oxides and oxide hydroxides in the near IR to near UV. *American Mineralogist*, 70, 1262-1269.
- [119] **Long, Y., Li, C., Kraatz, H. & Lee, J. S.** (2003). AC impedance spectroscopy of native DNA and M-DNA. *Biophysical Journal* , 84, 3218–3225. doi:0006-3495/03/05/3218/08.



- [120] Cai, W., Peck, J. R., van der Weide, D. W. & Hamers, R. J. (2004). Direct electrical detection of hybridization at DNA-modified silicon surfaces. *Biosensors and Bioelectronics*, 19, 1013–1019. doi:10.1016/j.bios.2003.09.009.
- [121] Espinosa, N., Schwarz, S. U., Cimalla, V., Podolska, A. & Ambacher, O. (2015). Impedance characterization of DNA-functionalization layers on AlGaN/GaN high electron mobility transistors. *Procedia Engineering*, 120, 912 – 915. doi: 10.1016/j.proeng.2015.08.790.
- [122] Golshaei, R., Guler, Z., Ünsal, C. & Sarac, A. S. (2015). In situ spectroscopic and electrochemical impedance study of gold/poly (anthranilic acid) core/shell nanoparticles. *European Polymer Journal*, 66, 502–512. <http://dx.doi.org/10.1016/j.eurpolymj.2015.03.009>.
- [123] Sophia, I. A., Gopu, G. & Vedhi, C. (2012). Synthesis and characterization of poly anthranilic acid metal nanocomposites. *Open J Synth Theory Appl*, 1(01):1–8. <http://dx.doi.org/10.4236/ojsta.2012.11001>.



## **CURRICULUM VITAE**



**Name Surname:** Burcu SAYINLI  
**Place and Date of Birth:** İstanbul, 22.10.1990  
**E-Mail:** sayinlib@itu.edu.tr  
**B.Sc.:** Chemistry, ITU